Electroproduction of Hadrons at 6 GeV using the CEBAF Large Acceptance Spectrometer

Collaboration List

D.S. Carman, R.A. Schumacher
Carnegie Mellon University, Pittsburgh, PA 15213

E. Anciant, G. Audit, N. D'Hose, M. Garcon, P. Guichon, J.M. Laget, C. Marchand
CEA/Saclay, DAPNIA/SPhn, Gif-sur-Yvette Cedex, France F-91191

H. Funsten
The College of William and Mary, Williamsburg, VA 23187

L.H. Kramer, B.A. Raue
Florida International University, Miami, FL 33199

S.P. Barrow, L. Dennis
Florida State University, Tallahassee, FL 32306

I. Strakovsky
The George Washington University, Washington, DC 20052

M. Ripani, M. Taiuti
INFN-Sezione di Genova, Genova, Italy I-16146

J.P. Didelez, M. Guidal, E. Hourany
Institut de Physique Nucléaire, Orsay, France F-91406

S.V. Boiarinov
ITEP, Moscow, Russia 117259

W. Brooks, V.D. Burkert, D. Cords, A.P. Freyberger, F.J. Klein,
M.D. Mestayer, B.B. Niczyporuk, E.S. Smith, A. Yegneswaran
Jefferson Lab, Newport News, VA 23606

K.H. Hicks, G. Niculescu
Ohio University, Athens, OH 45701

A. Empl, P. Stoler
Rensselaer Polytechnic Institute, Troy, NY 12180

M. Vanderhaeghen
University of Mainz, Mainz, Germany D-55099

J.A. Mueller
University of Pittsburgh, Pittsburgh, PA 15260

K. Joo, R. Minehart
University of Virginia, Charlottesville, VA 22901

I. Aznauryan, S. Stepanyan
Yerevan Physics Institute, Yerevan, Armenia 375036

*and the CLAS collaboration

Contents

1 Physics Motivation - Experiment Overview **5**
1.1 Introduction 5
1.2 Deeply Virtual Meson Electroproduction 7
1.3 The N^* 6 GeV Program 8
1.4 Exclusive Kaon Electroproduction 8
1.5 High Q^2 ϕ-Meson Production 9
1.6 Search for $J^{PC} = 1^{-+}$ Exotic Mesons 9
1.7 Forward Pseudoscalar Meson Electroproduction Above the Resonance Region 10

2 Beam Time Request **12**

3 Performance of CLAS at 6 GeV **13**
3.1 CLAS Kinematic Acceptances 13
3.2 Charged-Particle Identification 15
3.3 Separation of Exclusive Channels 17
3.3.1 $ep \rightarrow e'n\pi^+$ 17
3.3.2 $ep \rightarrow e'p\pi^0, e'p\eta$ 18
3.3.3 $ep \rightarrow e'KY$ 18
3.4 Electron/Pion Separation 20
3.5 Luminosity Considerations 21

4 Deeply Virtual Meson Electroproduction **23**
4.1 Introduction 23
4.2 The Physics Case 24
4.3 Deeply Virtual Electroproduction of Vector Mesons 28
4.4 Deeply Virtual Electroproduction of Pseudoscalar Mesons 28
4.4.1 $ep \rightarrow e'\pi^+n$ 29
4.4.2 $ep \rightarrow e'(\pi^0, \eta)p$ 38

5 The N^* 6 GeV Program **44**
5.1 Introduction 44
5.2 Physics of the N^* Program with the CLAS 44
5.3 N^* Excitations at High Q^2 in the $p\pi^0$, $p\eta$, and $n\pi^+$ Channels 47
5.3.1 Preliminary CLAS Results at Lower Q^2 47
5.3.2 Preliminary Results at High Energy 49
5.3.3 Proposed Measurements 51
5.3.4 Expected Statistical Accuracy 52
5.3.5 Data Analysis 52
5.3.6 Summary 53
5.4 N^* Excitations at High Q^2 in the Two-Pion Channel 53
5.4.1 CLAS Data from the 1998 4 GeV Electron Run 55
5.4.2 CLAS Data from the 1999 5.56 GeV Electron Run 55
5.4.3 Data Analysis 57
5.4.4 Summary 58
5.5 Measurement of η' Electroproduction 58

5.5.1 Physics Motivation . . . 58
5.5.2 Baryon Resonances Coupling to η' . . . 59
5.5.3 Previous Experiments . . . 59
5.5.4 Experimental Method . . . 61
5.5.5 Identifying η' in the e1 data at 4.0 GeV . . . 62
5.5.6 Backgrounds . . . 64
5.5.7 Angular Distributions . . . 64
5.5.8 Expected Rates . . . 68
5.5.9 Summary of η' Proposal . . . 68

6 Exclusive Kaon Electroproduction 74
6.1 Introduction . . . 74
6.2 Physics Analyses . . . 75
6.2.1 Structure Function Extraction . . . 75
6.2.2 Σ^0/Λ Production Ratios . . . 76
6.2.3 Λ Polarization Measurements . . . 76
6.2.4 Missing N^* Resonances . . . 78
6.2.5 Excited-State Hyperon Production . . . 79
6.2.6 Neutral Kaon Production . . . 81
6.3 Theoretical Approaches . . . 81
6.3.1 Hadrodynamical Models . . . 81
6.3.2 Quark Models . . . 82
6.3.3 Regge-Exchange Models . . . 83
6.4 Monte Carlo Studies . . . 84
6.5 Statistical Errors . . . 85
6.6 Systematic Errors . . . 86
6.7 Summary . . . 88

7 High Q^2 ϕ-Meson Production 91
7.1 Vector Meson Electroproduction . . . 91
7.2 Models of Transverse-Size Shrinkage with Q^2 . . . 91
7.3 Data Analysis Techniques . . . 92
7.4 Existing Data . . . 92
7.5 Extension of ϕ Electroproduction to 6 GeV . . . 93
7.6 Estimation of Measurement Uncertainties . . . 93
7.7 Possible Future Additional Measurements . . . 94
7.7.1 L,T ϕ Polarization Measurements . . . 94
7.7.2 Semi-Exclusive 6 GeV Measurements . . . 94
7.7.3 Gluon Condensation . . . 94

8 Search for $J^{PC} = 1^{-+}$ Exotic Mesons 96
8.1 Introduction . . . 96
8.2 Theoretical Predictions and Existing Data . . . 96
8.2.1 Theory . . . 96
8.2.2 Existing Data . . . 97
8.3 Proposed Experiment . . . 98
8.4 Acceptance Simulations . . . 98
8.5 Cross Section and Counting Rates . . . 99

8.6 Background 99
8.7 Summary 100

9 Forward Pseudoscalar Meson Electroproduction Above the Resonance Region 102
9.1 Introduction 102
9.2 Physics Motivations 103
9.3 Cross Section 104
9.4 Simulation 105
9.5 Particle Identification 106
9.6 Analysis of Reconstructed Events 106
9.7 Summary 107
9.8 Conclusions 108

1 Physics Motivation - Experiment Overview

This section contains a summary of the physics motivation for each of the individual contributions contained in this package, with references to the already approved or conditionally approved proposals, extensions of already approved experiments to 6 GeV, and the list of new proposals.

1.1 Introduction

For decades electron scattering has been utilized as the major tool for probing the structure of nucleons in inclusive reactions. Unpolarized and polarized quark and gluon structure functions have been studied in these experiments over many years. Studies of exclusive reactions are needed to understand the dynamics of production processes through resonance decays, quark fragmentation, or hard processes. Unfortunately, little is known about exclusive hadron production in inelastic electron scattering. One of the main reasons for this lack of knowledge has been technical in nature. The low production rates and the need to cover a large phase space in the final state, made it necessary to employ large-acceptance detectors with sufficient resolution to isolate exclusive channels. Furthermore, these detectors had to operate in an electron beam environment with high luminosity. These requirements could not be met at electron accelerators with low-duty cycles. As a consequence, only the simplest reactions were studied, often in a very limited kinematical regime, and most often with insufficient statistics.

The CLAS detector, operated at the CEBAF CW electron machine for the past 18 months, has quickly proven that these technical obstacles have been overcome. Large acceptance, combined with good resolution and particle identification capabilities, and the ability to operate at luminosities of 10^{34} cm^{-2}s^{-1} in an electron beam environment, have opened up many new avenues leading to detailed investigations of hadron structure in exclusive reactions.

This proposal package has been developed based on the experience of operating CLAS for the study of exclusive reactions at lower energies and momentum transfers. Moreover, a short test run at 5.56 GeV was carried out and analyzed. The results of this run give us full confidence that the performance of CLAS is adequate to to carry out the program put forward in this proposal package.

On the theoretical side, it is now becoming more apparent that the elementary quark and gluon fields are likely not the relevant, or at the least, not the dominant degrees of freedom for many exclusive reactions in the energy domain of CEBAF. Constituent quarks, gluon flux tubes, and pions may be much more relevant for the interpretation of the data. Theoretical models based on these degrees of freedom have been developed in many areas, such as N^*-resonance transitions, the production of strange mesons in hyperon excitations, and the production of gluonic mesons ("hybrids"), and are able to make predictions in the large kinematic regime that is currently covered at CEBAF and beyond.

Having said that, we hasten to stress that new theoretical developments during the past few years have shown that there are windows available for the study of exclusive reactions at high momentum transfer. These bear on the interpretation in terms of elementary parton fields. A theoretical framework has emerged for the study of a new set of generalized parton distribution functions, the "skewed parton distributions" (SPDs), that can only be accessed in deeply virtual exclusive reactions at sufficiently high momentum transfer, and in the deep-

Physics Category	Exp. #	Sect. #	Reaction $ep\ \rightarrow$	PAC Status	Main Physics Focuses
Deeply Virtual Meson Production	1	4.3	$e'p\rho$ $e'p\omega$	E98-107 (C)	-Study transition to asymptotic regime to probe unpolarized SPDs.
	2	4.4	$e'n\pi^+$	New	-Study transition to asymptotic regime to probe polarized SPDs. -Measure cross sections for Q^2 <5.5 (GeV/c)^2 and σ_L,σ_T response for Q^2 <3.2 (GeV/c)^2
			$e'p\pi^0$ $e'p\eta$	New	-Measure cross sections for Q^2 <5.5 (GeV/c)^2
N^* Physics at High Q^2	3	5.3	$e'p\pi^0$	E91-002 (E)	-Study $\Delta(1232)$ and $S_{11}(1535)$ up to Q^2 <5.5 (GeV/c)^2
			$e'p\eta$		-Study transition regime between CQM and pQCD
			$e'n\pi^+$		-Study I=1/2 resonance excitations e.g. $D_{13}(1510)$ and $F_{15}(1680)$
	4	5.4	$e'p\pi^+\pi^-$	E93-006 (E)	-Study higher mass resonances e.g. $S_{31}(1620)$ and $D_{33}(1700)$ -Study transition to $[70,1^-]$ supermultiplet at high Q^2 -Test validity of CQM at high Q^2
	5	5.5	$e'p\eta'^{(\dagger)}$	New	-Study resonances above 1.9 GeV and search for missing resonances -Study quark content of η' and $U_A(1)$ anomaly
Strangeness Production	6	6	$e'KY$	E89-043 (E) E93-030 (E) E95-003 (E) E99-006 (E)	-Measure cross sections, single and double polarization observables -Search for strange decays of missing N^* resonances -Study reaction mechanism
	7	7	$e'p\phi$	E93-022 (E)	-Test QCD-predicted shrinkage of longitudinal photons with Q^2
Exotic Meson	8	8	$e'\pi\eta X^{(\dagger)}$ $e'\pi\eta' X^{(\dagger)}$	E94-119 (C)	-Search for J^{PC}=1^{-+} exotic mesons
Forward Pseudoscalar Meson Production	9	9	$e'n\pi^+$ $e'p\pi^0$ $e'K^+\Lambda$	New	-Study transition to asymptotic regime -Extract structure functions σ_T, σ_L, σ_{TT}, and σ_{TL}

Table 1: Summary of all experiments in this package. Those reactions highlighted with a (†) require CLAS operation at $B = -50\% B_0$. All other will run CLAS at $B = 90\% B_0$. In the *PAC Status* column, (C) indicates experiments that have been conditionally approved by PAC for running at 6 GeV and (E) indicates an extension of a PAC-approved lower-energy experiment.

inelastic regime. Rapid theoretical development in this new area of electromagnetic physics is underway, and needs to be nurtured by the prospect of data coming from CLAS in a timely fashion. While it is quite clear that 6 GeV will not allow us to fully reach the asymptotic regime, mapping out the transition into this regime will be of great importance as corrections due to higher-twist contributions can be evaluated. Evaluating these contributions is now becoming the main focus of the theoretical activity in this area.

In the following sections we present brief motivations and experimental summaries related to the nine individual contributions to the package. Table 1 gives an overview of the full proposal package and the main physics goals for each of the contributions.

1.2 Deeply Virtual Meson Electroproduction

The possibility of operating JLab at high luminosity and momentum transfers greater than a few (GeV/c)^2 has influenced the theoretical community into making a concerted effort to deal with exclusive reactions in this kinematic regime. Very recently, several theoretical groups have made ground-breaking progress. The techniques involve a combination of soft and hard physics. It was proven, for the case of longitudinal photons, that at high enough Q^2, exclusive reactions can be factorized into parts containing the soft and hard physics involved. For non-longitudinal cross sections, the transverse higher-twist mechanisms would have to be modeled.

The hard physics can be treated separately by pQCD techniques, and the soft physics of the hadronic states can be parameterized in terms of skewed parton distribution functions. These SPDs are generalizations of the deep-inelastic scattering (DIS) distribution functions $q(x)$ and $\Delta q(x)$ that are accessed in non-polarized and polarized inclusive DIS electron experiments, respectively. For the prototype deeply virtual Compton scattering, the SPDs are said to be *diagonal*, while for single-meson production, the SPDs are of a different, newly accessible, *non-diagonal* type. Vector and pseudoscalar meson production are complementary in that vector meson production is sensitive to the unpolarized quark distribution functions, while pseudoscalar meson production, which is proposed here, is sensitive to the polarized structure functions relating to the nucleon spin distribution.

This proposal is to measure pseudoscalar meson production cross sections, and is complementary to experiment E98-107, which will measure vector meson production. The intent is to obtain cross sections at W above the resonance region at the highest Q^2 possible. For a 6 GeV electron beam, we estimate the maximum Q^2 attainable for π^0 production is about 5.5 (GeV/c)^2, and for η production, is somewhat lower. The momentum transfer t will be in the range t_{min} up to several (GeV/c)^2. The connection with the DIS structure functions are closest near t_{min}. For $n\pi^+$ production, the focus is on isolating the longitudinal part of the cross section. By combining measurements at 2 or 3 different energies in a Rosenbluth separation of the cross sections, we can reach a maximum Q^2 of about 3 (GeV/c)^2. Moreover, the experiment would produce high quality cross section data for $n\pi^+$ with Q^2 up to 5.5 (GeV/c)^2 and a maximum $-t$ of 6 (GeV/c)^2. No such data has been measured before.

It is expected that the mechanisms that will be accessible at potential JLab energies, and moderate Bjorken x_B, are those involving quark currents, as opposed to those involving gluonic currents that can only be accessed at much higher energies. Specific to pseudoscalar mesons, there is currently considerable theoretical activity to calculate the possible experimental manifestations. Among the important questions that need to be addressed is how to handle the hard kernel. The simplest approach would be to treat it in terms of valence pQCD. The question is, at what Q^2 does this become valid? For the reaction proposed here, this is related to the question of where hard processes become important for the pseudoscalar meson form factors. The lower the Q^2, the more higher-twist effects need to be considered. The Q^2 dependence is expected to signal whether we are approaching the regime of strict factorizability. In any case, we expect that the rapid current theoretical progress in this field will make it possible to include higher-order effects.

1.3 The N^* 6 GeV Program

Finding the relevant degrees of freedom for the interpretation of results at energies and momentum transfers accessible at CEBAF remains one of the main motivations for studying electromagnetic form factors through elastic or inelastic electron scattering. These areas are currently under intense theoretical scrutiny using a variety of quark-model approaches, flux-tube models, QCD sum-rule methods, chiral models, etc. Much is being contributed to this field from the data collected with CLAS during the past 18 months of operation. However, it has also become more apparent that in the low momentum transfer region, symmetry properties often mask genuine features due to the internal nucleon structure. This has been recently pointed out with respect to the study of N^* excitations in photoproduction experiments, whose relationship to each other is largely controlled by symmetry properties of the electromagnetic current operator. For this reason the evolution to high Q^2 is an important aspect in these studies. Another motivation is to study the transition to pQCD behavior in a 3-quark system with considerable inelasticity for the higher-mass states.

A wealth of information can be obtained from measuring transition form factors for higher-mass states. While past experiments have concentrated on the "easy" $p\pi^0$ or $p\eta$ channels, the $n\pi^+$ channel is more sensitive to the isospin-1/2 resonances. Moreover, the two-pion channels, such as $p\pi^+\pi^-$, are very sensitive to several higher-mass states that nearly decouple from the $N\pi$ channel. They are also predicted to couple strongly to many of the so-called "missing" quark-model states that are predicted to populate the mass region from 1.9 to 2.2 GeV/c^2. Due to the isospin selectivity of η', the reaction $ep \rightarrow ep\eta'$ may provide an excellent probe to the structure of isospin-1/2 baryon resonances in this mass range. Recent photoproduction data from SAPHIR has claimed evidence for S_{11} and P_{11} excitations. Born term contributions are likely to be small since the threshold for this reaction lies at W=1.896 GeV. η' has never been investigated in electroproduction because of the low cross section and the difficult channel identification. CLAS gives the unique opportunity to surmount both impediments.

Initiated to a large degree by the CLAS N^* program, theoretical models have been developed that make predictions over a larger range in momentum transfer than have been possible previously. It is our expectation that new data, covering a considerably larger range in Q^2 than has been available for energies up to 4 GeV, will put these models to the test and help create a better understanding of hadron structure.

1.4 Exclusive Kaon Electroproduction

We propose to extend the CLAS kaon electroproduction program to a beam energy of 6 GeV, significantly enlarging the Q^2 and W ranges covered in current proposals. The $ep \rightarrow eKY$ reaction will be studied over a range of Q^2 from roughly 1.5 to 6 (GeV/c)^2 and W from 1.6 to 3.0 GeV using CLAS at maximum magnetic field. This will allow study of the elementary production of strangeness at kinematics well above the resonance region while providing substantial overlap with phase space coverage at 4 GeV, which spans Q^2 from 0.5 to 3 $(\mathrm{GeV/c})^2$ and W from 1.6 to 2.4 GeV. This proposal is based on the Letter of Intent LOI-99-002 that received favorable review by PAC-15.

The proposed program encompasses all of the current Hall B experiments focusing on the $ep \to e'KY$ reaction. This proposal includes extensions of E89-043 to study the different reaction-channel contributions to Λ(gnd) and $\Lambda(1520)$ production, E93-030 to extract the KΛ response functions σ_T, σ_L, σ_{LT}, and σ_{TT} over a broad kinematic range, E95-003 to study the reaction mechanism for K^0 electroproduction, and E99-006 to provide sensitivity to a number of response functions through Λ polarization measurements. Another important aim of this program is to continue the search for missing N^* resonances predicted by constituent quark models to decay through strange final states. The data acquired will allow for tests of Regge-exchange models, the constituent quark model, hadrodynamical models, and other quark models of the nucleon, which will ultimately help to better understand the reaction mechanism for open strangeness production.

1.5 High Q^2 ϕ-Meson Production

QCD predicts that longitudinal photons transform into smaller size $q\bar{q}$ pairs with increasing momentum transfer. This is a non-trivial prediction of QCD and reflects the space-time structure of hadronic matter. This prediction can be tested in the production of vector mesons if the longitudinal and transverse response functions are separated. A separation is possible by studying the decay distribution of vector mesons. Here we propose to measure the reaction $ep \to e'p\phi$, $\phi \to K^+K^-$. The angular distribution of the K^+K^- final state is sensitive to the transverse/longitudinal nature of the high-energy photon. A measurement of the t-dependence of the longitudinal component of ϕ production from a proton target will determine the slope parameter b in the production cross section $\mathrm{d}\sigma/\mathrm{dt} \sim \exp -b|t|$. This slope contains information on the size of the $q\bar{q}$ pair involved in the process. Shrinkage is evident in a hardening of the slope parameter b, or in other words, a decrease in magnitude of b. Two of the most successful models, the quark model and the VMD model, make very different predictions for this effect. A 40 day run at 6 GeV, combined with existing CLAS photoproduction data, can readily distinguish between prediction of these models.

1.6 Search for $J^{PC} = 1^{-+}$ Exotic Mesons

Gluon self coupling in QCD suggests the existence of hadrons with explicit gluon degrees of freedom, e.g. gg, $gqqq$, and $gq\bar{q}$. Since the gluon carries color charge it can act as a particle and experience a binding force to quarks. QCD-based models predict the masses of the lightest states to be below or near 2 GeV/c^2, with widths in the range of 50 to 300 MeV. Predicted dominant decays are to an S-wave and P-wave pair of mesons, such as πf_1 and πb_1, although there are suggestions that decays to two pseudoscalar particles may not be negligible.

The discovery of hybrids would be a strong confirmation of QCD, and important for understanding the non-perturbative structure of hadrons. The most promising approach for finding hybrids is to look for exotic quantum numbers, like $J^{PC} = 1^{-+}$, forbidden for $q\bar{q}$ meson states. Since the predicted mass range for light hybrids is densely populated by conventional $q\bar{q}$ mesons, this could be the only way of identifying a hybrid. Decays to two pseudoscalars in a relative P-wave is a unique signature of the $J^{PC} = 1^{-+}$ state.

Several experiments using pion beams have been performed to search for hybrid states in the $\pi\eta$ and $\pi\eta'$ channels in the mass range from 1 to 2 GeV/c^2. Decay angular distributions of final-state mesons have been examined in order to detect the $J^{PC} = 1^{-+}$ state. Although the results of these studies have not been conclusive, there is some general indication of the existence of exotic states around a mass of 1.4 GeV/c^2.

A promising place to look for hybrids could be electromagnetic production of t-channel mesons since there is an indication that hybrids may have significant coupling to vector mesons and photons. There are only two reported experiments on photoproduction of possible hybrid states that are not necessarily J^{PC} exotics. Due to the lack of the statistics, no partial wave analyses have been made for these data. At present there are no reported data on the electroproduction of exotic states.

In this experiment we are proposing to search for exotic hybrids in electroproduction reactions on hydrogen using the 6 GeV CEBAF electron beam. Exotic hybrids will be identified by their decay to $\pi^0\eta$, $\pi^+\eta$, $\pi^0\eta'$, and $\pi^+\eta'$ in the detected final states $e'\ p\ \gamma\ \gamma\ \gamma\ \gamma$, $e'\ \pi^+\ \gamma\ \gamma$, $e'\ \pi^+\ \pi^+\ \pi^-\ \gamma$, and $e'\ p\ \pi^+\ \pi^-\ \gamma\ \gamma\ \gamma$, respectively.

The CLAS detector is an excellent tool for detection and identification of the multi-particle final states. Running CLAS with reversed-field polarity for the main torus will allow us to cover the mass range of the t-channel mesons up to 2 GeV/c^2. A search will be done in the range of hadronic mass $W > 2.5$ GeV, and $Q^2 \approx 0.6$ GeV/c^2.

Detailed studies of the acceptances and the resolutions have been performed. Cross section estimates have been done based on a_2 photoproduction cross sections and the given upper limit of the branching ratios of exotic hybrid decays from Primakoff production. The largest yield was found for the $\pi^+\eta$ final state. This gives 1000 $\pi^+\gamma\gamma$ states per day at a luminosity 1×10^{34} cm^{-2}s^{-1}. In order to get sufficient statistics for a detailed partial wave analysis, 15 days of running at a luminosity 1×10^{34} cm^{-2}s^{-1} will be required. The estimated signal to noise ratio for the above reactions will be about 4:1.

1.7 Forward Pseudoscalar Meson Electroproduction Above the Resonance Region

A principal motivation for studying exclusive reactions is that they provide a new class of observables, called off-diagonal parton distributions, for the internal structure of the nucleon. The internal structure of the nucleon has been studied through inclusive scattering of high-energy leptons in the deep inelastic scattering (DIS) limit. Polarized DIS measurements of $g_1(x, Q^2)$, or the relevant helicity densities $\Delta q(x, Q^2)$, have revealed that only about 30% of the nucleon's spin is carried by the quark's intrinsic spin. The quark helicity densities, $\Delta q(x, Q^2)$, are not only accessible through polarized DIS measurements, but also via exclusive electroproduction of pseudoscalar mesons. It has been shown that exclusive meson production at large Q^2 and small t factorizes into a hard scattering coefficient, a quark-antiquark distribution amplitude of the meson, and an off-diagonal quark (or gluon) distribution that describes the "soft" physics in the nucleon. Hence, the polarized parton densities can be probed in unpolarized exclusive reactions. It is clear that we should study exclusive reactions at low t, and at high Q^2 and W, in the region of validity of QCD factorization theorems, and also in the transition region where off-diagonal parton distributions provide important information about the non-perturbative structure of the nucleon. The comparison of the reactions $ep \to ep\pi^0$ and $ep \to en\pi^+$ is vital for better understanding of the soft part of a proton structure, since these reactions may proceed via different production mechanisms.

We propose to study exclusive electroproduction of π^+, π^0, and K^+ mesons at low t, for $Q^2 > 1.4$ (GeV/c)^2, and $W > 2.0$ GeV. In order to properly and fully carry out the physics program described in this proposal, we plan on acquiring data at several different beam energies between 4 and 6 GeV. Our W, Q^2, and t kinematical regions were chosen to obtain sufficient acceptance for at least four of these beam energies in order to extract the Q^2 and t dependence of the structure functions: σ_T, σ_L, σ_{TT}, and σ_{LT} in a model independent way.

As part of the overall proposal package we ask here *only* for the required beam time at 6 GeV. We assume that data at beam energies of 4.0, 4.5, and 5.0 GeV are going to be taken within the approved beam time of the current e1 program. In case no data are taken at a fifth beam energy of 5.5 GeV, we will require beam time for that energy in a future update of this proposal.

2 Beam Time Request

This experimental package requests a total of 55 days of new beam time at 6 GeV electron beam energy with the highest possible electron-beam polarization. Of these 55 days, 40 days are for running CLAS at maximum magnetic field and 15 days are for running CLAS at 50% reversed field. The experiments in this package that will rely mainly on the reversed-field running conditions of CLAS are highlighted in Table 1 and in their corresponding sections of this document.

The high-field operation will serve the extended high Q^2 portion of the program. The reversed-field running will provide the high W and low Q^2 needed for statistically significant measurements of η' production and the search for exotic mesons. It will also serve to obtain high statistics at lower Q^2 for the remaining program and provide sufficient overlap with the already accumulated data at lower energies.

The program uses the standard CLAS electron beam detector system and data acquisition system, along with the standard Hall B liquid-hydrogen target. The individual measurements of this new run group have been designed to run concurrently with identical beam and trigger conditions.

The analysis of several experiments in this proposal package will ultimately rely on combining data sets at several different beam energies, including 4, 5, and 6 GeV. However this proposal package is only seeking new beam time at 6 GeV beam energy. The complete set of 4 GeV data will be acquired as part of the existing Hall B e1 run period. As well, the spokesmen of the current e1 run group have recently agreed to include up to 20 days of 5 GeV running as part of the beam time that they already have approved for running with electrons on a hydrogen target with CLAS. In the subsequent sections in this package, all references to 5 GeV running are referring to this time that will come out of the currently approved e1 beam hours.

3 Performance of CLAS at 6 GeV

The proposed physics program requires the selection of exclusive hadronic channels such as $ep \to en\pi^+$, $ep \to ep\pi^0$, and $ep \to eKY$. CLAS relies on precise time-of-flight (TOF) measurements and good momentum resolution to identify charged particles and to isolate exclusive channels using missing-mass techniques. While these methods have been demonstrated to work well at energies up to 4 GeV, at higher energies they will become increasingly more difficult. Particle identification using time-of-flight information alone will become more ambiguous, leading to larger backgrounds in our missing-mass distributions. Moreover, the missing-mass resolution will also become increasingly poorer at the higher energies.

In order to address these questions, a short test run was carried out with CLAS at an incident electron beam energy of 5.56 GeV, the highest energy available at CEBAF at that time. Data were taken with an electron trigger with low energy threshold in the electromagnetic calorimeter to provide the least-biased event selection. To maximize resolution, the torus magnetic field was at 90% of maximum. The results of this run show that the performance of CLAS at 5.56 GeV is sufficient to carry out the program described in this 6 GeV proposal.

To understand the performance of CLAS at 6 GeV, there are a number of important issues, common to all experiments, that must be considered. For the present discussion this list includes:

- CLAS kinematic acceptances
- Identification of charged hadrons with TOF techniques as $\beta \to 1$
- Separation of exclusive reaction channels
- Identification of hadrons through missing-mass techniques
- Electron/pion separation
- Luminosity

In the following sections we address these issues from study of the data accumulated during the 5.56 GeV test run.

3.1 CLAS Kinematic Acceptances

The accepted Q^2 and W ranges of CLAS at 5.56 GeV are shown in Fig. 1. The kinematic coverage extends to Q^2 of 6.5 (GeV/c)^2 at the mass of the $\Delta(1232)$ resonance, and to nearly 5 (GeV/c)^2 at W of 2 GeV, which marks the beginning of the deep inelastic regime. The angular acceptances for electrons, protons, and pions are shown in Fig. 2. Note that the ϕ acceptance is shown for one 60° sector only. The electron acceptance is limited by the Ĉerenkov counters, while the other charged-hadron acceptances are limited by the geometry of the drift chambers and the sign and magnitude of the magnetic field. In this test run, the magnetic field was such that electrons were bent towards the beam line. Positive particles were accepted from 9° to 130°, and π^- were accepted from 20° to 140°.

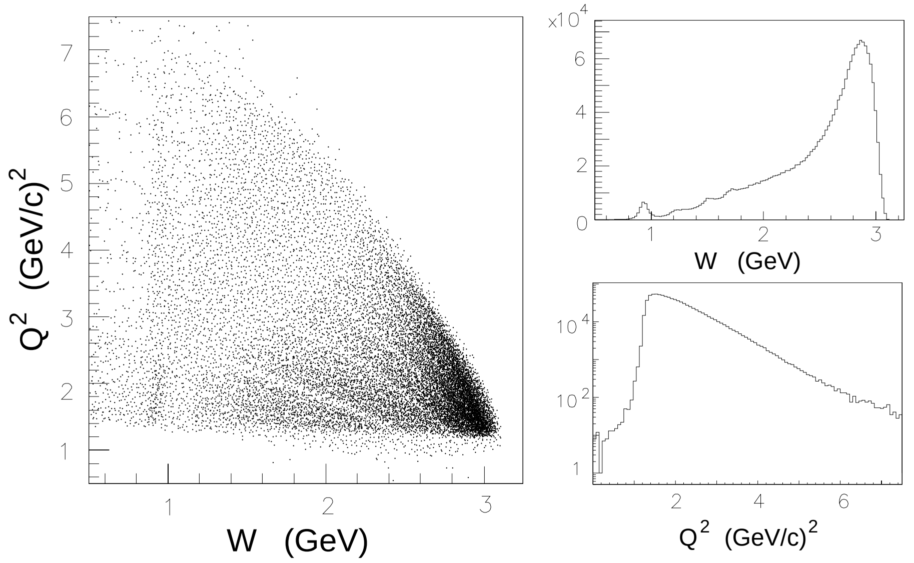

Figure 1: CLAS kinematic coverage in Q^2 and W from analysis of 5.56 GeV data. At 6 GeV the corresponding kinematic boundaries will be slightly more extended.

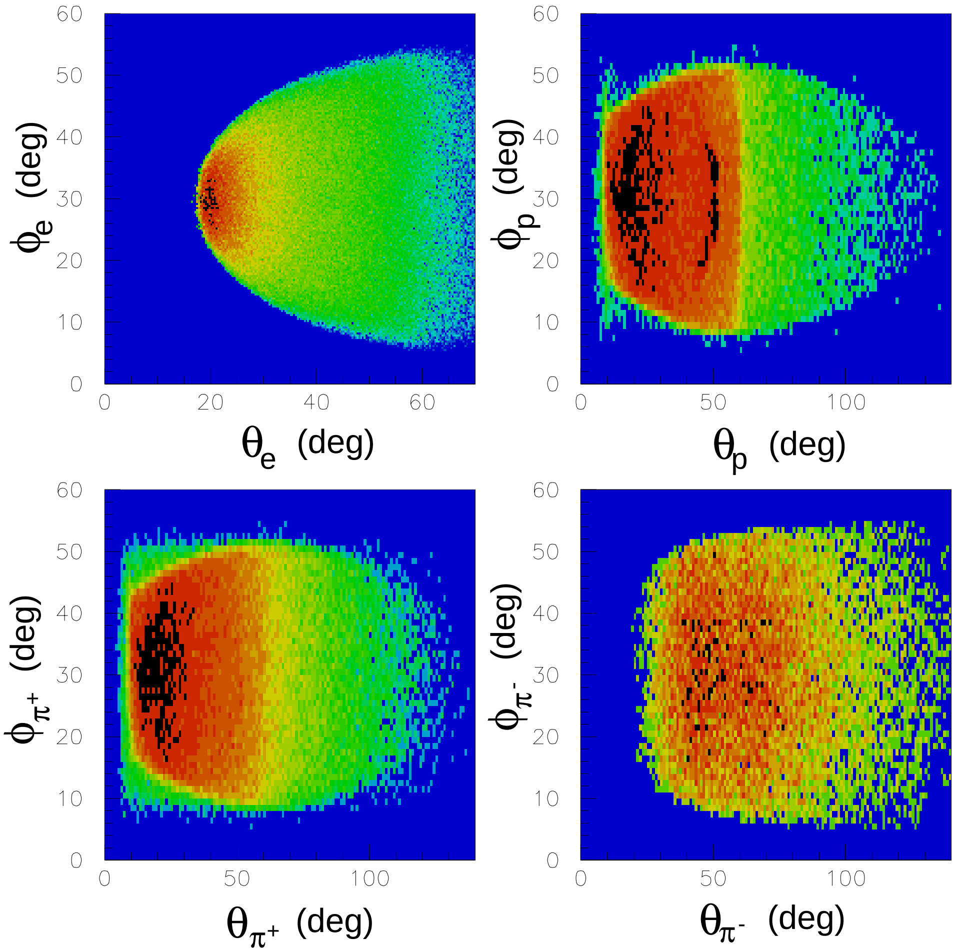

Figure 2: Laboratory angular acceptances in terms of ϕ and θ for electrons, protons, and pions. The distributions are shown for one sector only.

3.2 Charged-Particle Identification

Charged hadrons (π, K, p) are identified from their reconstructed mass by combining TOF information with momentum information from the drift chambers. Charged hadrons must traverse all three Regions of the drift chambers and strike the outer scintillation counters in order to be identified. Those with low momentum are curled up by the magnetic field and fail to reach the scintillators, while those with too small a production angle go down the forward hole between the coils of the torus magnet. Fig. 3, from analysis of the 5.56 GeV data, shows the mass spectrum of hadrons created in the $ep \to e'X$ reaction. A cut on this spectrum is typically used to select the scattered hadrons during event reconstruction. The ratio of the pion and proton peaks to the kaon peak in this spectrum is quantitatively the same as for the corresponding 4 GeV spectrum.

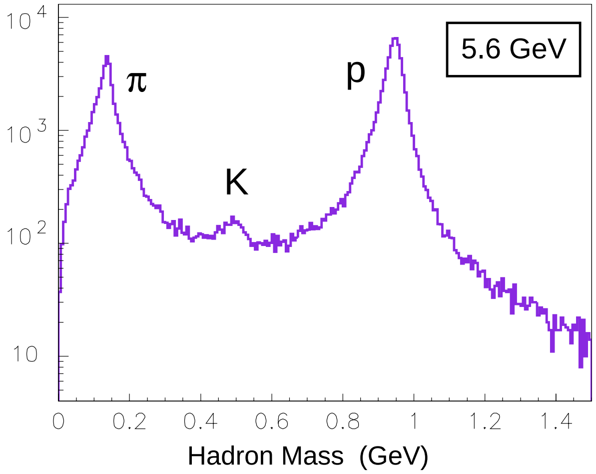

Figure 3: Hadron mass distribution for positively charged particles produced in $ep \to e'X$ from analysis of 5.56 GeV CLAS data.

The quality of the charged-particle separation as a function of the momentum and velocity of the particles is shown in Fig. 4. From this figure, the pion, kaon, and proton bands are all clearly visible. This data sample includes a loose selection of kaons that enhances this band relative to the others. Although the bands get quite close at the highest momenta, so that complete separation becomes more difficult, there is still sufficient mass resolution for a nearly complete separation of pions from protons up to the highest momenta. Kaon production proceeds in a kinematic regime where momenta remain relatively low. However, using only time-of-flight techniques, a complete separation of kaons from pions and protons is not possible. The use of kinematical constraints and energy cuts is required to isolate channels containing kaons in the final state. Additionally, our analysis and simulation studies have shown that the signal to noise ratio in our reconstructed exclusive final-state spectra can be further improved by taking advantage of the very different dE/dX characteristics and energy-deposition patterns of the hadrons within the calorimeters.

The highest momentum hadrons are going forward in the lab, where the flight path to the scintillators is about 5 m. For small angles, the expected timing resolution of the scintillators is about 120 ps. With the current CLAS timing resolution and particle identification techniques, pions, kaons, and protons can be distinguished up to ≈2 GeV/c. Fig. 5 shows the expected separation between the different hadron bands as a function of the hadron momentum. The separation is defined in terms of the σ-difference between the calculated flight times for the particles using the expected timing resolution.

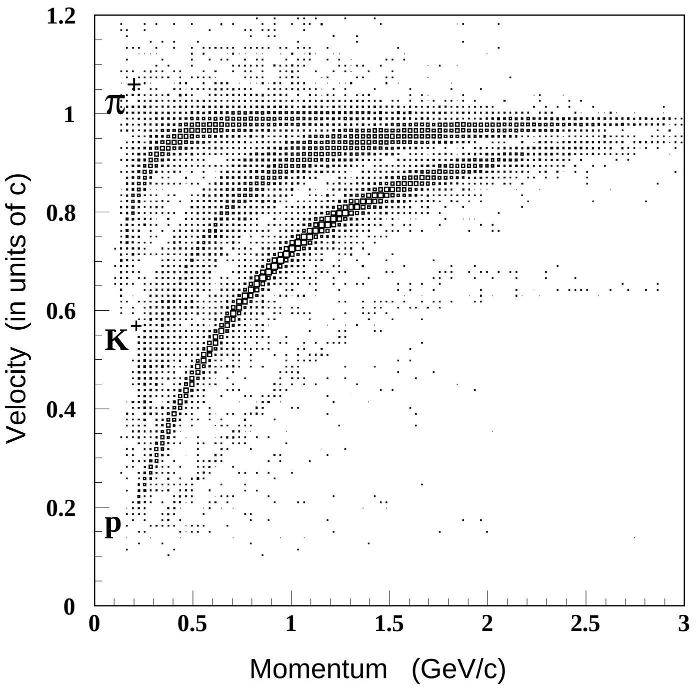

Figure 4: Charged-particle velocity versus momentum showing the separation of the pion, kaon, and proton bands. The data sample includes a loose cut on kaons to enhance their appearance.

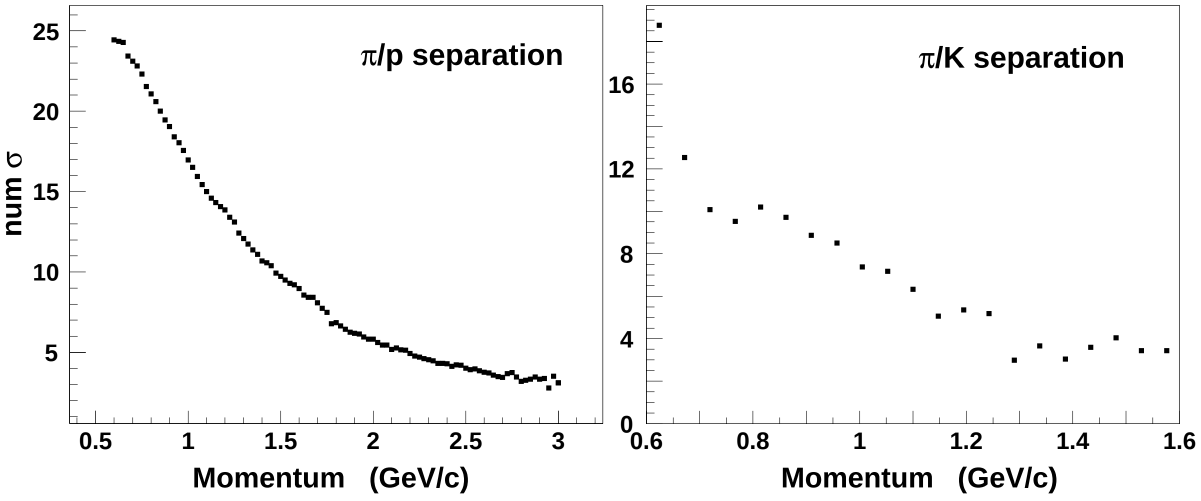

Figure 5: Calculation of the number of σ separation between (a) the calculated pion and proton flight times, and (b) the calculated pion and kaon flight times, as a function of the hadron momentum using the expected timing resolution of the scintillators. It is expected that reasonable hadron separations can be achieved in the analysis down to $\approx 2\sigma$.

3.3 Separation of Exclusive Channels

3.3.1 $ep \to e'n\pi^+$

The pion-production data were analyzed using the standard CLAS analysis chain. The kinematic coverage for single π^+-production events can be shown clearly through a correlation of the reconstructed $ep \to e'\pi^+$ missing mass and the hadronic invariant mass W. This is shown in Fig. 6 after selecting the reconstructed π^+ events. The neutron band is quite distinct indicating that single π^+ production can be isolated up to high invariant masses. The additional constraint from missing mass significantly helps to isolate the relevant process. Fig. 7a shows the missing-mass distribution for all identified pions, and Fig. 7b shows the same distribution for pion momenta >3 GeV/c. The neutron mass peak is still clearly visible.

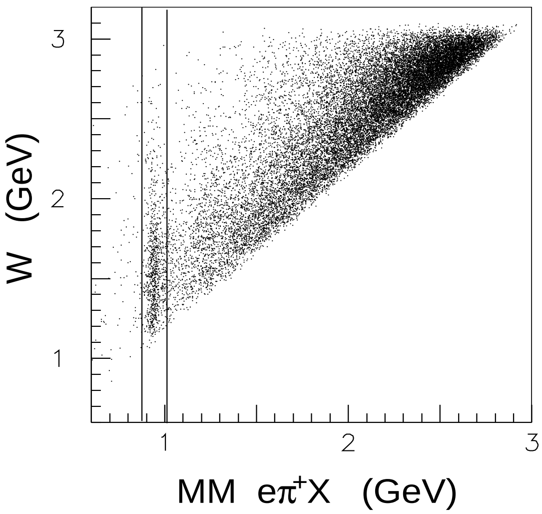

Figure 6: Missing mass for $ep \to e'\pi^+X$ vs. the invariant hadronic mass W from 5.56 GeV data. The vertical band marks the location of the missing neutron peak.

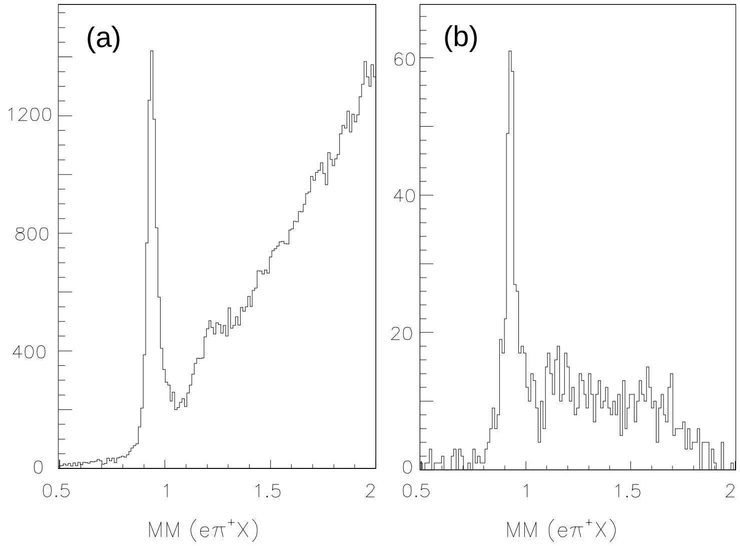

Figure 7: Missing-mass distribution for $ep \to e'\pi^+X$ from analysis of 5.56 GeV data for (a) all pion momenta and (b) pion momenta >3 GeV/c. The neutron mass peak is still well identified at high momentum.

3.3.2 $ep \to e'p\pi^0, e'p\eta$

Fig. 8 shows the missing-mass distribution for the $ep \to e'pX$ reaction from 5.56 GeV CLAS data. The pion peak is wide due to the contribution from the elastic radiative tail. For full separation of single γ and π^0 events, kinematic cuts or subtractions are required as the radiative photons are strongly peaked along the electron direction. Further analysis results are shown in section 5.3.2.

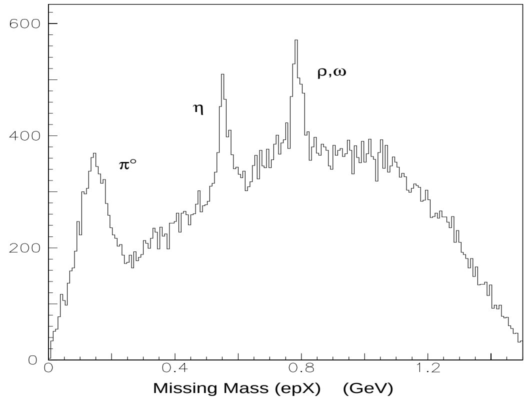

Figure 8: Missing-mass distribution for $ep \to e'pX$ from analysis of 5.56 GeV data showing peaks for $X = \pi^0, \eta, \rho,$ and ω production. The spectrum has been cut on W<2.5 GeV to remove the elastic radiative tail and requires Q^2 >1.5 (GeV/c)^2.

3.3.3 $ep \to e'KY$

Reconstruction of exclusive reactions leading to production of hyperons in the final state relies heavily on time-of-flight hadron identification and missing-mass techniques. Fig. 9 highlights the reconstruction of the charged-kaon final state $ep \to e'K^+\Lambda, \Sigma$ from 5.56 GeV CLAS data, cutting on the kaon peak in the hadron-mass spectrum of Fig. 3. Fig. 9a shows clear evidence of the Λ and Σ^0 peaks after reconstruction of the scattered electron and electro-produced kaon. The main source of background beneath the hyperon peaks comes from pions misidentified as kaons. These pions are believed to come from the reaction $ep \to e'\pi^+\Delta^0$. This background can be effectively removed with further kinematic cuts. Fig. 9c shows the hyperon spectrum after cutting on the π^- peak in the $ep \to e'K^+pX$ spectrum of Fig. 9b. The width of the Λ peak from this data summed over all Q^2 and W subtended by CLAS is about 14 MeV. From analysis of 4 GeV CLAS data, the reconstructed Λ peak width is about 12 MeV.

The reconstruction of the $K^0\Sigma^+$ final state is highlighted in Fig. 10. The electro-produced K^0 is reconstructed from the invariant mass of its $\pi^+\pi^-$ decay mode as shown in Fig. 10a, although no clear signature of the K^0 is present as no cuts on the detached K^0 event vertex have been made. Fig. 10b shows a clear signature of the missing Σ^+ peak from the missing-mass distribution for $ep \to e'K^0X$. By cutting on the missing π^0 from the Σ^+ decay, as shown in Fig. 10c, the charged-hyperon spectrum results. This distribution is wide as the K^0 identification algorithm has not been optimized.

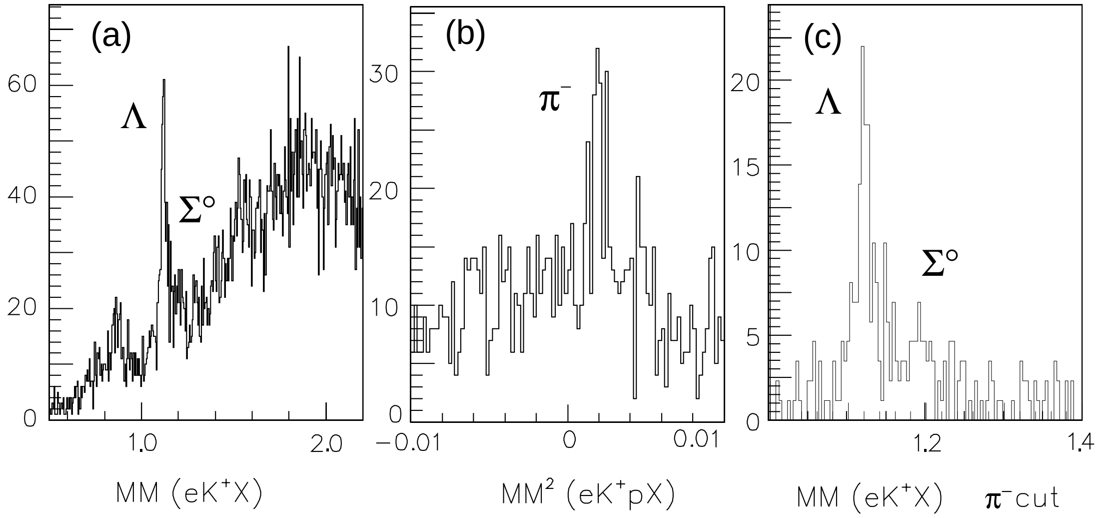

Figure 9: Analysis of the K^+Y final state from the 5.56 GeV data showing (a) the missing-mass spectrum for $p(e, e'K^+)X$, (b) the missing π^- from the $p(e, e'K^+p)X$ reaction, and (c) the final, nearly background-free, hyperon distribution after cutting on the missing π^- peak.

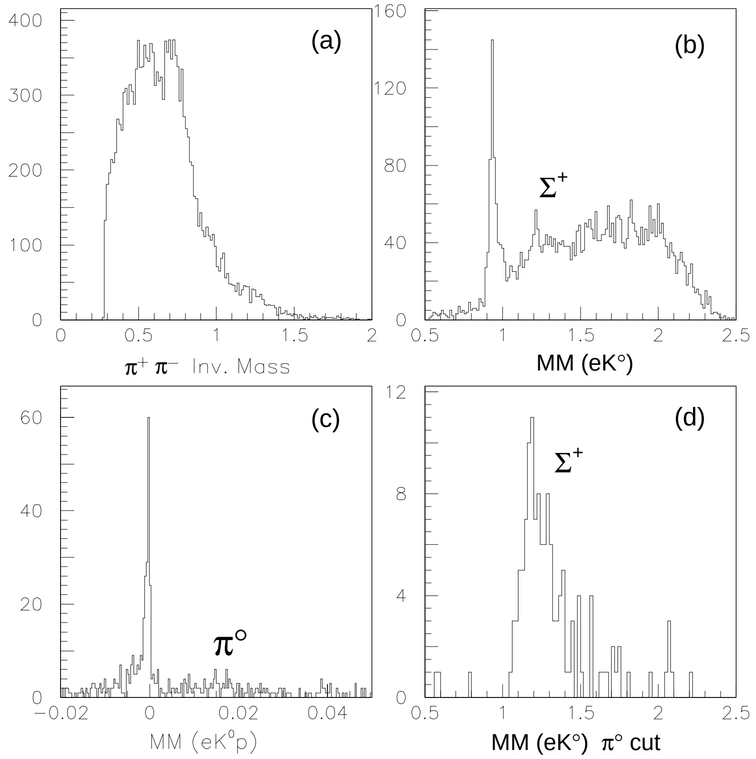

Figure 10: Analysis of the $K^0\Sigma^+$ final state from the 5.56 GeV data showing (a) the $\pi^+\pi^-$ invariant-mass distribution used to select K^0 production, (b) the resultant spectrum for $ep \rightarrow e'K^0X$, (c) the reconstructed π^0 spectrum from $\Sigma^+ \rightarrow p\pi^0$, and (d) the charged-hyperon distribution after cutting on the missing π^0 peak.

3.4 Electron/Pion Separation

Electron identification in CLAS relies on the combination of a signal from the Ĉerenkov detectors (sensitive to particles with $\beta \geq 0.998$), and the energy deposition in the electromagnetic calorimeters matching the momentum as determined by the drift chambers. This technique is fully efficient for momenta below 2.7 GeV/c since the Ĉerenkov counters start becoming efficient for pions above this limit. A possible solution to move above this momentum limit is to include information from the electromagnetic calorimeters whose relative resolution improves with increasing energy. We can make use of the fact that the longitudinal and transverse energy deposition patterns in the calorimeter layers are different for electrons and pions.

Fig. 11 shows the electron acceptance from analysis of 5.56 GeV high magnetic field CLAS data. The plot shows reconstructions of the polar scattering angle versus the laboratory momentum. The minimum electron angle subtended by CLAS with the employed trigger configuration (EC·CC) was 13°. However, for the smallest angles spanned, there is a background present as the Ĉerenkov detectors are quite efficient for firing on pions. But the background does not dominate as a clear signature of the elastic scattering events is visible at the highest reconstructed electron momenta. The minimum electron angle of CLAS determines the smallest Q^2 values that can be probed. Maintaining good electron identification in the low Q^2 range of the 6 GeV data (*i.e.* down to 1.5 (GeV/c)^2) is quite important. Accepted electrons at these angles have high momenta and the contamination from π^- would only slowly increase the background under the signal in the missing-mass distributions used in the analyses.

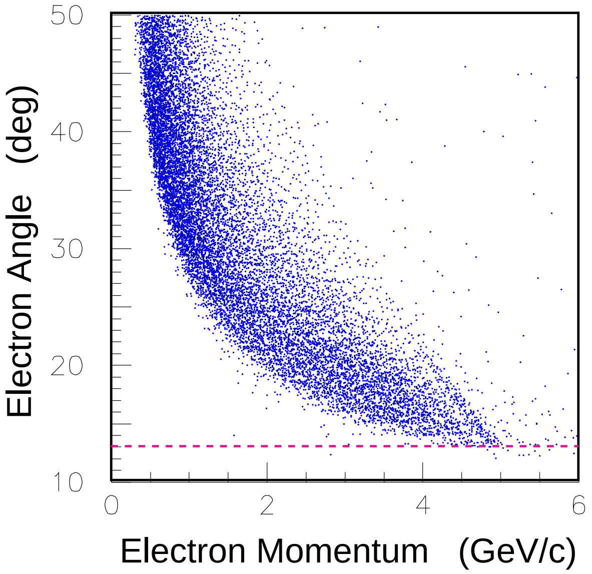

Figure 11: Electron scattering angle vs. laboratory momentum from analysis of 5.56 GeV high-field CLAS data. The minimum electron angle subtended by CLAS is about 13°. Above momenta of 2.7 GeV/c, the Ĉerenkov detectors begin to become very efficient for pions, and other techniques are required to positively identify electrons.

3.5 Luminosity Considerations

CLAS has recently been operating at luminosities close to or even exceeding design values of 1×10^{34} cm^{-2}s^{-1}. While design luminosities have been surpassed for light nuclear targets, as well as for the polarized-target operation during the eg1 run period, hydrogen target operation has been limited to about 2/3 of this value. While polarized-target operation is a rather special case with a 2 T·m longitudinal magnetic field around the target, nuclear targets have been operated in the same way as the liquid-hydrogen target. The difference in operating luminosities is simply due to the fact that much of the background originates from Møller electrons in the target. The amount of Møller background per luminosity unit is Z/A, which for most light nuclei is ≈0.5, while for hydrogen Z/A = 1.

During the e1 and e2 run periods it was found that the number of accidental hits in the drift-chamber system was proportional to luminosity per Z, which indicates that much of this background was due to X-rays from secondary interaction of Møller electrons with the lead shield in the mini-torus area. For hydrogen-target operation, track reconstruction efficiencies depend only slightly on the beam current for luminosities up to about 70% of the design luminosity. Beyond that, a drop of up to 10% is observed for operation at luminosities up to 1×10^{34} cm^{-2}s^{-1}. These results are highlighted below.

The average hit occupancies are shown as a function of luminosity in Fig. 12 for the Region 1 and Region 3 drift chambers. From these data it is clear that the average accidental occupancies are well below 5% at full design luminosity. Fig. 13 shows this information in a slightly different manner through the correlation of the average CLAS event size as a function of luminosity. At 1×10^{34} cm^{-2}s^{-1}, the average event size is <7 kbytes, which allows for operation with our current data acquisition system at live times >90%. Finally, Fig. 14 shows the calculated tracking efficiency for recoil protons from e-p elastic scattering, plotted as a function of the Region 1 hit occupancy for the sector where the recoil proton is expected. The tracking efficiency remains >95% for chamber hit occupancies up to 4%. At higher occupancies the tracking efficiency begins to fall off.

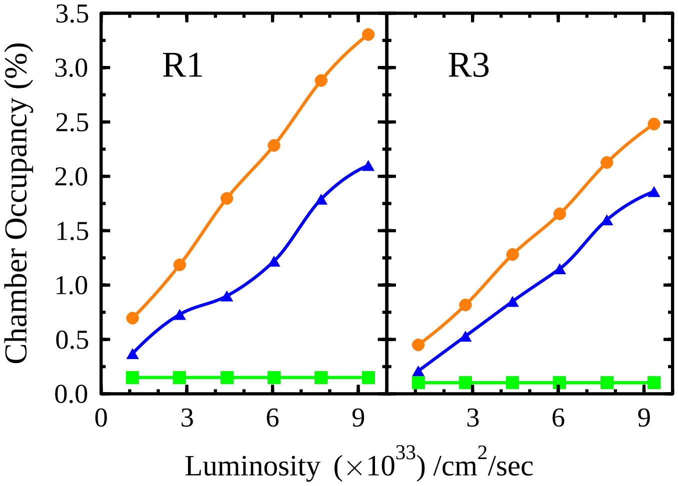

Figure 12: Drift-cell hit occupancy in the Region 1 and Region 3 drift chambers averaged over all six sectors as a function of luminosity. The circles correspond to the occupancy including all chamber hits, triangles represent hits unrelated to tracks, and squares represent the cosmic-ray contribution.

The 5.56 GeV test run was carried out with a luminosity of 6.6×10^{33} cm^{-2}s^{-1}. For the upcoming run periods with the hydrogen target, e5 and e1, additional shielding will be added in the target region to further reduce the Møller-related backgrounds. With these modifications, which are also needed for the next e1 run period, we expect that the full design luminosity can be utilized in a manner that will lead to track reconstruction efficiencies >95%.

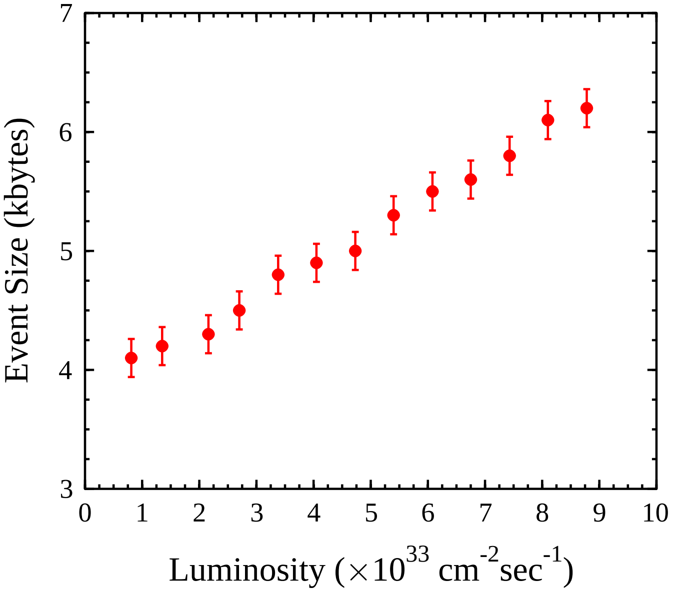

Figure 13: Average CLAS event size as a function of luminosity. The target material in the electron beam consisted of 50 mm of liquid hydrogen, 220 μm of aluminum, and 30 μm of mylar.

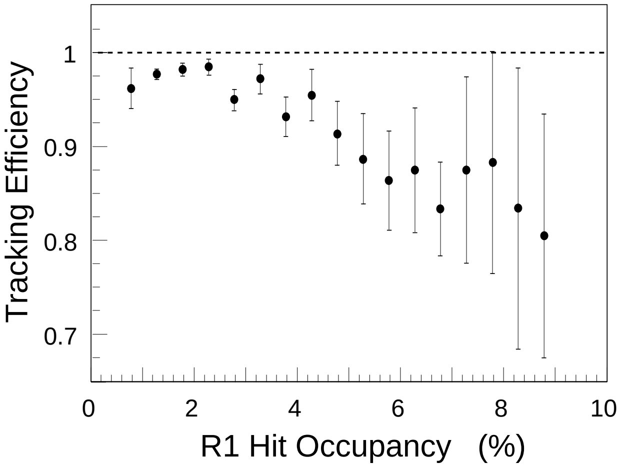

Figure 14: Tracking efficiency plotted as a function of the Region 1 hit occupancy (%) for recoil protons from elastic scattering where the corresponding electron track has been reconstructed.

4 Deeply Virtual Meson Electroproduction

4.1 Introduction

Much of the internal structure of the nucleon has been revealed during the last two decades through the inclusive scattering of high-energy leptons on the nucleon in the Bjorken -or "Deep Inelastic Scattering" (DIS)- regime ($Q^2, \nu \gg$ and $x_B = \frac{Q^2}{2M\nu}$ finite). Simple theoretical interpretations of the experimental results and quantitative conclusions can be reached in the framework of QCD when one sums over all possible hadronic final states. For instance, *unpolarized* DIS brought us evidence of the quark and gluon substructure of the nucleon, with the quarks carrying about half of the nucleon momentum. Furthermore, *polarized* DIS revealed that about 25% of the spin of the nucleon is carried by the quarks' intrinsic spin. Now, with the advent of the new generation of high-energy, high-luminosity lepton accelerators, combined with large-acceptance spectrometers, a wide variety of exclusive processes in the Bjorken regime can be envisioned to become accessible experimentally. Until recently, very few exclusive processes could be treated in the framework of pQCD and compared to experimental data (typical examples are the $\pi^0\gamma\gamma^*$ transition form factor and the elastic form factors of the pion and the nucleon). Fundamental information on the structure of the nucleon has been learned from such analyses, from the shape of light-cone meson wave functions (or distribution amplitudes) to the scale of the intrinsic transverse momentum of the partons in the nucleon (or Fermi motion), Sudakov effects, etc.

The recently developed formalism of "Off-Forward Parton Distributions" [1, 2] (OFPDs) -also called "Skewed Parton Distributions"- allows us to enlarge these types of exclusive processes and analyses to the broad class of exclusive electroproduction of mesons and photons. These OFPDs are generalized parton distributions that provide a unifying picture between a whole set of fundamental quantities of hadronic structure such as: (vector and axial) nucleon form factors, (polarized and unpolarized) parton distributions, (orbital) spin content of the nucleon, etc. In this framework, we propose to investigate the following exclusive meson electroproduction reactions up to the highest Q^2 attainable with the CLAS detector and a 6 GeV incident electron beam energy:

- $ep \to e'(\rho, \omega)p$
- $ep \to e'\pi^+n$
- $ep \to e'(\pi^0, \eta)p$

From the Q^2 and t dependence (at fixed x_B) of these reactions, and from the ratios of the cross sections of these various channels, we expect to learn: fundamental information about the notions of factorization between "soft" and "hard" physics and their relative contributions as a function of Q^2, the domains of validity and onset of pQCD techniques, pre-asymptotic effects related to the transverse momentum of the quarks in hadrons, etc.

These reactions have been grouped here following the nature of the outgoing meson (vector vs. pseudoscalar mesons) and experimental detection concerns (neutral vs. charged channels). After a brief review of the OFPD formalism, we present the feasibility studies for these 3 groups of processes with the CLAS detector, including kinematical domains attainable, count rates estimates, observables to measure, etc.

In a general fashion, the goal of this package of experiments is to measure these reactions up to the highest Q^2 values attainable with the CEBAF 6 GeV electron beam. The Q^2,

x_B, and t dependence will be investigated to help distinguish between "soft" and "hard" mechanisms, *i.e.* the transition from meson-exchange mechanisms at low Q^2 to quark-exchange processes at larger Q^2. At high values of Q^2, one will test the onset of the $1/Q^6$ scaling behavior of the cross section predicted by the OFPD/pQCD formalism.

For the different channels, we want to separate the longitudinal parts of the cross sections as much as possible to make the connection with the OFPD formalism that relies on the factorization of the longitudinal part. Also, ratios of the cross sections of these various channels have to be investigated, as they might show some "precocious" scaling.

We want to emphasize at this point that the actual determination of the OFPDs will require a more extended and ambitious experimental program (that might be reached in the near future with the perspective of the rise in energy of CEBAF in the next decade). Our goal is to make a first step in this direction, which is clearly a prerequisite to the development of this field.

These experiments are the first ones to explore this new OFPD domain of hadronic physics. This subject is currently in full expansion on the theoretical side. Other experimental facilities, such as COMPASS and HERMES, are currently considering a similar study of the OFPDs. In spite of the relatively "low" energy of the incident beam, the high luminosity and the better resolution that one can achieve with CLAS, will allow equivalent count rates to the two other facilities in the same kinematical range (but sooner and in a shorter period). Also, in the case of COMPASS and HERMES, the ability to perform truly exclusive measurements is questionable [9]. The perspective of a rich experimental program opens up for the coming decade.

4.2 The Physics Case

We briefly review in this section the formalism of the Off-Forward Parton Distributions. The OFPDs are generalized parton distributions that parameterize the structure of the nucleon in leading-order pQCD. In recent years, Ji [1] and Radyushkin [2] have shown that the leading-order pQCD deeply virtual Compton scattering (DVCS) amplitude in the forward direction can be factorized into a hard-scattering part (exactly calculable in pQCD), and a non-perturbative nucleon structure part as illustrated in Fig. 15a. In these so-called "handbag" diagrams, the lower blob represents the structure of the nucleon and can be parameterized, at leading-order PQCD, in terms of four generalized structure functions, known as the OFPDs.

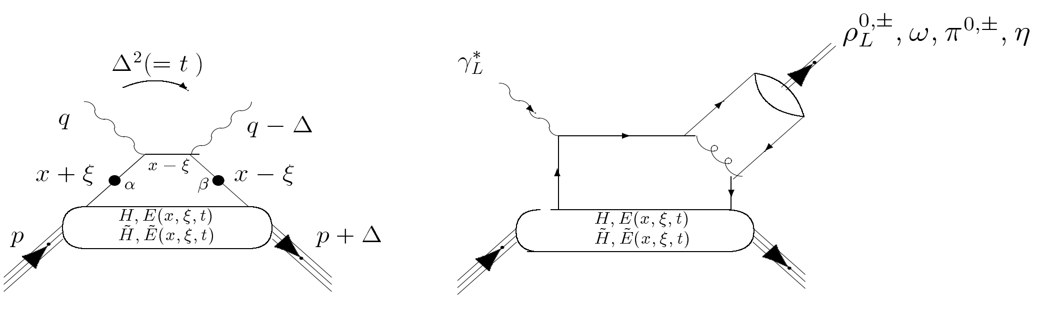

Figure 15: "Handbag" diagrams for (a) DVCS (left) and (b) meson production (right).

The OFPDs are defined as $H, \tilde{H}, E$, and $\tilde{E}$, and depend upon three kinematic variables: x, ξ, and t. x is the momentum fraction of the struck quark in the quark loop and, as such, is not accessible experimentally. ξ is the longitudinal-momentum fraction of the transfer Δ and reduces to $x_B/(2-x_B)$. $t=\Delta^2$ is the standard momentum transfer between the final-state meson and the virtual photon.

H and E are spin-independent and $\tilde{H}$ and $\tilde{E}$ are spin-dependent functions. More precisely, the light-cone matrix element of the bilocal quark operator that enters in these hard-electroproduction reactions (represented by the lower blobs in Fig. 15) is at leading twist in Q^2 given by:

$$\begin{aligned}
&\frac{P^+}{2\pi}\int dy^-\, e^{ixP^+y^-}\langle p'|\bar{\Psi}_\beta(-\frac{y}{2})\Psi_\alpha(\frac{y}{2})|p\rangle\Big|_{y^+=\vec{y}_\perp=0} \\
&=\frac{1}{4}\Big\{(\gamma^-)_{\alpha\beta}\Big[H^q(x,\xi,t)\;\bar{N}(p')\gamma^+N(p)\;+\;E^q(x,\xi,t)\;\bar{N}(p')i\sigma^{+\kappa}\frac{\Delta_\kappa}{2M_N}N(p)\Big] \\
&\qquad+(\gamma_5\gamma^-)_{\alpha\beta}\Big[\tilde{H}^q(x,\xi,t)\;\bar{N}(p')\gamma^+\gamma_5N(p)\;+\;\tilde{E}^q(x,\xi,t)\;\bar{N}(p')\gamma_5\frac{\Delta^+}{2M_N}N(p)\Big]\Big\}\;. \qquad (1)
\end{aligned}$$

This formula explicitly shows the vector (axial) nature of the H, E ($\tilde{H}$, $\tilde{E}$) OFPDs associated or not with the γ_5 matrix.

The OFPDs H and $\tilde{H}$ are actually a generalization of the parton distributions measured in deep inelastic scattering. Indeed, in the forward direction (defined by $q=q'$), H reduces to the quark distribution $q(x)$ and $\tilde{H}$ to the quark-helicity distribution $\Delta q(x)$ measured in deep inelastic scattering. Furthermore, at finite momentum transfer, there are model-independent sum rules that relate the first moments of these OFPDs to the standard elastic form factors. Also Ji [1] has shown that the second moment of these OFPDs gives access to the sum of the quark spin and the quark orbital angular momentum to the nucleon spin, which may shed light on the "spin-puzzle". The OFPDs reflect the structure of the nucleon independently of the reaction that probes the nucleon. They can also be accessed through the hard exclusive electroproduction of mesons -$\pi^{0,\pm}$, $\rho^{0,\pm}$, ω, ϕ,...- (see Fig. 15b) for which a QCD factorization proof was given recently [3]. In this proof it was shown that factorization applies when the virtual photon is longitudinally polarized because, in this case, the end-point contributions to the meson wave function are power suppressed. It was also shown that the cross section for a transversely polarized photon is suppressed by $1/Q^2$ compared to a longitudinally polarized photon, so that asymptotically, only σ_L survives. Ref. [3] showed as well that leading-order pQCD predicts that the vector meson channels ($\rho_L^{0,\pm}$, ω_L, ϕ_L) are sensitive only to the unpolarized OFPDs (H and E), whereas the pseudoscalar channels ($\pi^{0,\pm},\eta,...$) are sensitive only to the polarized OFPDs ($\tilde{H}$ and $\tilde{E}$). In comparison to meson electroproduction, we recall that DVCS depends on *both* the polarized and unpolarized OFPDs. Therefore, by selecting the nature of the outgoing meson, one selects the spin-dependent or spin-independent generalized parton distributions. Note that in this latter case, one can access polarized nucleon structure information without any polarization of external particles.

For a first exploratory approach, the meson channels hold the best promise due to the relatively high cross sections. First estimates for cross sections at forward angles were given in Refs. [4, 5] using an educated guess for the H and $\tilde{H}$ OFPDs. This consists of a product of elastic form factors and quark distributions measured in DIS. In this "toy" model, E and $\tilde{E}$ are set to 0, as they enter with a kinematic factor proportional to the momentum transfer, as shown in eq(1). This ansatz satisfies the model-independent sum rules linking the OFPDs to the nucleon form factors, and reduces to the quark distributions from DIS in the forward direction. In other words, the normalization is well determined. In Ref. [6], estimates using a more sophisticated ansatz for the OFPDs, including ξ dependence, are given.

The OFPD formalism is valid at small momentum transfers t and large Q^2. Fig. 16 shows the forward $\gamma_L^* + p \to M + p$ cross sections as a function of Q^2, and compares the leading-order predictions with the ξ-dependent ansatz for different mesons. The leading-order longitudinal cross section $d\sigma_L/dt$ for meson electroproduction shows a $1/Q^6$ behavior. This scaling behavior is analogous to the one observed in DIS, and is a prediction of pQCD at large Q^2.

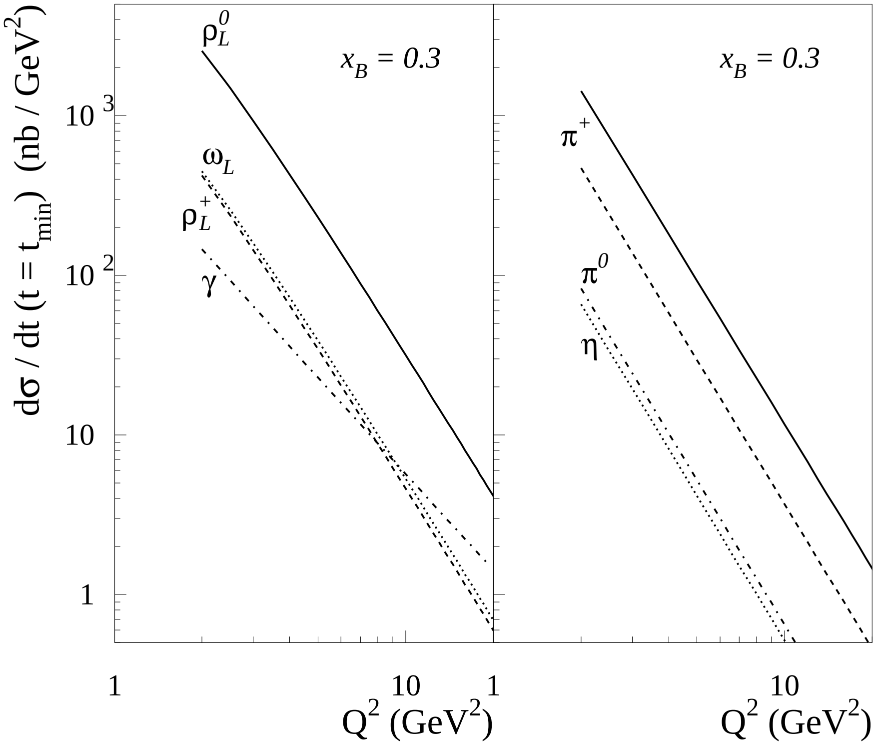

Figure 16: Scaling behavior of the leading-order predictions for the forward differential electroproduction cross section $d\sigma_L/dt$ on the proton for vector mesons (left panel) and pseudoscalar mesons (right panel). For the π^+, the pion-pole contribution is given by the full line, whereas the pseudovector contribution is given by the dashed line. Also shown is the scaling behavior of the forward transverse cross section $d\sigma_T/dt$ for the leading-order DVCS cross section (dashed-dotted line in left panel).

One sees that the ρ_L^0 and ω_L channels, which are sensitive to the *unpolarized* OFPDs, yield the largest cross sections. Then come the π^+ and π^0 channels, which are proportional to the *polarized* OFPDs. The π^0 channel is about a factor of 5 below the pseudovector part ($\tilde{H}$) of the π^+ channel due to the different isospin structure of the corresponding OFPDs. In the π^0 channel, the u- and d-quark polarized OFPDs enter with the same sign, whereas in the π^+ channel, they enter with opposite signs. As the polarized OFPDs are constructed here from the corresponding polarized-parton distributions, the fact that the polarized d-quark distribution is opposite in sign to the polarized u-quark distribution, explains the difference of the predictions for the π^0 and π^+ channels.

It is important to measure the Q^2 dependence of the forward differential cross section at fixed x_B. Although it is unlikely that we can reach the pQCD leading-order domain of applicability at currently available Q^2 values at 6 GeV, the way the asymptotic $1/Q^6$ behavior is approached is an important source of information on pre-asymptotic effects. "Soft" contributions are expected to drop as $1/Q^8$. An estimate of these pre-asymptotic effects in hard electroproduction reactions in the valence region is given in Ref. [6], where the effects of the intrinsic transverse momentum dependence of the quarks in the nucleon and in the meson are quantified.

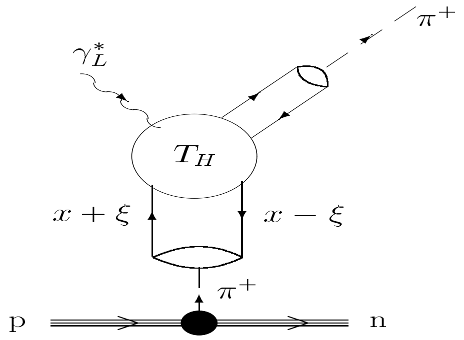

Figure 17: Pseudoscalar contribution to "hard" π^+ electroproduction. The virtual photon knocks out a pion from the meson cloud of the nucleon.

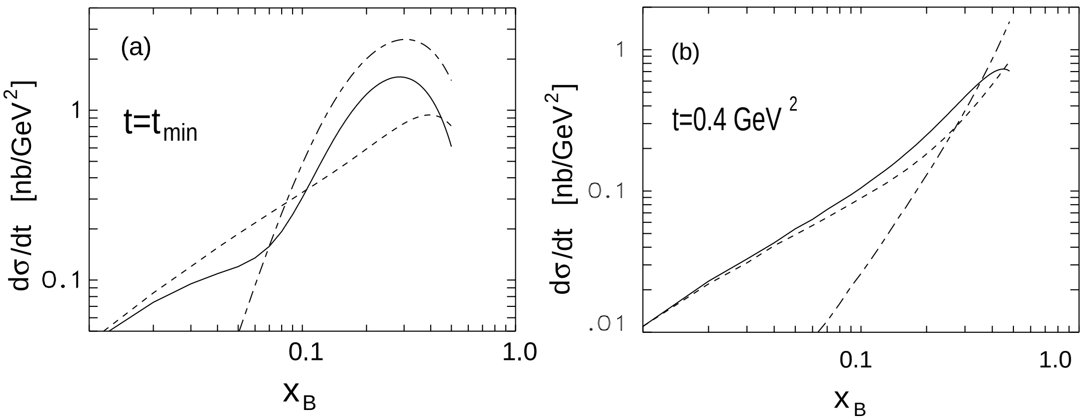

Figure 18: Differential production cross section for exclusive π^+ production through the scattering of longitudinally polarized photons from protons at $Q^2 = 10$ (GeV/c)^2 for (a) $t = t_{\min}$ and (b) $t = -0.4$ (GeV/c)^2. The dashed and dot-dashed curves show the pseudovector and pseudoscalar contributions, respectively.

For the case of charged-pion electroproduction, it was shown recently in Refs. [7, 8] that there should be a strong contribution from the pseudoscalar structure (connected to $\tilde{E}$, see eq(1)) as it is related to the one-pion exchange process, which, due to the small mass of the pion, should be quite important at forward angles. This feature is unique to the charged-pion process due to the proximity of the pion pole to the physical region, in contrast to the other (heavier) meson channels. As explained in Ref. [7], one can picture the process in a simple way, where one identifies the pseudovector contribution (proportional to $\tilde{H}$) as the virtual photon interacting with a quark of the nucleon, which after a hard-gluon exchange, combines with a second quark of the nucleon to form the final pion (see Fig. 15b). The pseudoscalar contribution (proportional to $\tilde{E}$) represents the process where the virtual photon knocks out a pion from the meson cloud of the nucleon (see Fig. 17). These two processes are predicted to have distinct behaviors in the x_B and t dependences of the cross sections. This deserves thorough experimental investigation.

It is seen in Fig. 16 that for π^+ electroproduction in the valence region ($x_B \approx 0.3$) and in the forward direction, the pseudoscalar contribution (pion pole) is about three times as large as the pseudovector contribution. This was also found in the calculation of Ref. [7] that is shown in Fig. 18a for $t = t_{min}$. The authors of Ref. [7] concluded that one obtains a dominance of the pseudovector at $t = t_{min}$ only at quite small values of x_B. At larger momentum transfers, as shown in Fig. 18b for $-t$=0.4 (GeV/c)^2, the pseudoscalar contribution decreases faster. The pseudoscalar and the pseudovector contributions become comparable around $x_B \approx 0.2$. Clearly, detailed x_B (W) and t dependent experimental scanning is needed in order to validate and quantify these pictures for the π^+ channel.

4.3 Deeply Virtual Electroproduction of Vector Mesons

Spokespersons: M. Guidal[a], C. Marchand[a], and E.S. Smith[b]

[a]Institut de Physique Nucléaire, Orsay, France, F-91406
[b]Jefferson Laboratory, Newport News, VA, 23606

The $ep \rightarrow e'(\rho, \omega)p$ channels are fully detailed in the individual proposal E98-107 [10] that was submitted to CEBAF PAC-14. It was approved with the condition of being run simultaneously with other experiments at 6 GeV. We will give below a brief summary of the proposal and refer the reader to Ref. [10] for full details regarding the measurement.

It is proposed to measure the exclusive electroproduction of the ρ^0 and ω vector mesons in the Bjorken regime ($Q^2, \nu \gg$ and $x_B = \frac{Q^2}{2M\nu}$ finite). Due to its predicted cross section in the asymptotic regime (see Fig. 16), the vector meson channel is one of the first channels to be explored. As mentioned above, leading-order pQCD gives predictions for the $\gamma^*_L p \rightarrow p(\rho_L, \omega_L, \phi_L)$ channels (where the subscript L denotes the longitudinal-polarization state of the particle) for which the factorization theorem, on which the OFPD formalism is based, holds. Experimentally, longitudinal vector mesons will be identified through their decay-pion angular distributions. Assuming s-channel helicity conservation (SCHC), Ref. [11] then permits extraction of the cross section for the reaction $\gamma^*_L p \rightarrow p(\rho^0_L, \omega_L, \phi_L)$. We will check the validity of the SCHC hypothesis by studying those vector-meson decay-density matrix elements that are zero when SCHC applies.

Our detailed simulations have shown that the combination of the 6 GeV CEBAF electron beam and the CLAS detector will allow study of these reactions up to $Q^2 \approx 4.5$ (GeV/c)^2 in the range $0.1 < x_B < 0.45$ (depending on Q^2) with reasonable count rates.

4.4 Deeply Virtual Electroproduction of Pseudoscalar Mesons

Spokespersons: A. Empl[a], M. Guidal[b], V.D. Burkert[c], and P. Stoler[a]

[a]Rensselaer Polytechnic Institute, Troy, NY, 12180
[b]Institut de Physique Nucléaire, Orsay, France, F-91406
[c]Jefferson Laboratory, Newport News, VA, 23606

JLab energies and moderate x_B are at kinematics involving quark currents, as opposed to gluonic currents, that can only be accessed at much higher energies. Specific to pseudoscalar mesons, there is currently considerable theoretical activity to calculate the possible experimental manifestations. Among the important questions that need to be addressed is how to handle the hard kernel. The simplest method would be to treat it in terms of valence pQCD. The issue, as previously mentioned, is at what Q^2 does pQCD for the meson form factor become valid. The lower the Q^2 the more higher-twist effects need to be considered, even for the separated longitudinal cross section. However, we can for the first time provide very high quality cross section data. Also, since we do obtain a complete ϕ distribution, one can obtain information about the σ_{LT} and σ_{TT} interference cross sections. We expect the rapid current theoretical progress in this field will make it possible to include higher-order effects to model these new data. There are many theorists currently working in this area of research, and new cross section data are eagerly waited to spur on the theoretical activity.

4.4.1 $ep \to e'\pi^+n$

The $ep \to e'\pi^+n$ reaction is the exclusive electroproduction reaction that is most easily accessible experimentally due to its relatively high cross section, and due to the simple identification of the long-lived pion. It is therefore an ideal process to be studied over a large kinematical range, from the "soft" to "hard" domain.

As emphasized in the previous sections, the separation of the longitudinal response function of the reaction is essential to make the connection with the OFPD formalism that relies on the factorization of the longitudinal part. Its study, as a function of Q^2 and x_B, is fundamental to test the validity of the pQCD predictions and their domain of applicability. In the previous section for vector mesons, this separation could be done through the study of their decay angular distributions and assuming SCHC. Clearly this cannot be done for spin-0 pions. The objective here is therefore to carry out the Rosenbluth L/T separation of the $ep \to e'\pi^+n$ reaction above the resonance region ($W > 2$ GeV). In the following we show that we can do so up to $Q^2 \approx 3.2$ (GeV/c)^2. This separation will allow, besides the exploration of the OFPD/pQCD domain, extraction of fundamental non-perturbative quantities of hadronic structure such as the π^+ form factor, and possibly the $\rho\pi\gamma$ transition form factor.

L/T separated data for the electroproduction of π^+ on the nucleon above the resonance region and $Q^2 > 1$ (GeV/c)^2 is extremely scarce. The only measurement has been done by Bebek *et al.* [12] at the Cornell accelerator. In that experiment, 5 points (2 points at $< x_B >= 0.24$, 1 point at $< x_B >= 0.35$, 1 point at $< x_B >= 0.5$ and 1 point at $< x_B >= 0.6$) were measured in total. Fig. 19 shows the three points measured about $< x_B >= 0.3$ as a function of Q^2. The 2 large Q^2 points are not incompatible with the leading-order pQCD calculation [6]. The leading-order PQCD calculation is done here with a running coupling constant extrapolated to lower Q^2. Power corrections to the leading-order amplitude (pre-asymptotic effects such as intrinsic transverse momentum dependence and overlap contribution to the pion form factor for instance) are also expected to contribute in this Q^2 domain. In any case, it is clear that a precise measurement and scan of this Q^2 region is needed in order to draw any conclusions about the domain of dominance and validity, and the nature of the various contributions.

We now show how the proposed measurement of exclusive π^+ electroproduction with CLAS can substantially improve the accuracy in the range covered previously by the Cornell data.

The procedure to separate the longitudinal from the transverse cross section in electro-

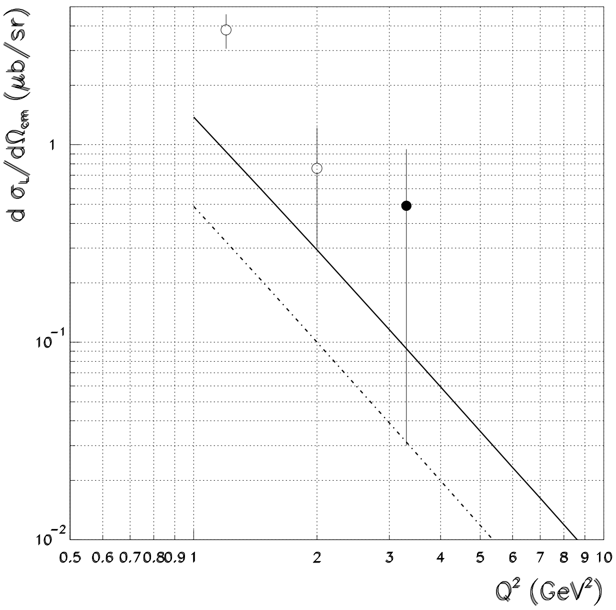

Figure 19: Longitudinal forward differential cross section for exclusive π^+ production as a function of Q^2 from the data of Bebek *et al.* [12]. Empty circles correspond to $< x_B >= 0.24$ and full circles to $< x_B >= 0.35$. The solid and dot-dashed curves are calculations of the total (pseudoscalar+pseudovector) and pseudoscalar contributions, respectively, for x_B=0.3 from Ref. [6]. The leading-order PQCD calculation was done here with a running coupling constant extrapolated to lower Q^2.

production is well known. The general form of the (unpolarized) differential cross section for the reaction $ep \to e'\pi^+n$ (integrated over the out-of-plane angle ϕ) is:

$$\sigma_{\gamma^* p} = \sigma_T + \epsilon\sigma_L, \tag{2}$$

where σ_T, σ_L (the transverse and longitudinal cross sections) depend on the variables Q^2 (virtuality of the photon), W (total energy of the virtual photon-proton system) (or x_B), and t (the squared momentum transfer between the virtual photon and the pion). ϵ represents the the virtual photon polarization parameter.

In order to separate σ_T and σ_L, it is necessary to vary ϵ, which can be done keeping x_B and Q^2 fixed, by varying only the beam energy (Rosenbluth separation). The choice of beam energies results from the compromise between two considerations: (1) higher beam energies allow measurements to higher Q^2, and (2) beam energies not too close to each other allow the benefit from a longer lever arm in ϵ to do a (linear) fit.

In the following studies, we have used the FASTMC program [13] to simulate the response (acceptance, resolution) of the CLAS detector. We restrict our study to $Q^2 > 1.5$ (GeV/c)^2 and $-t < 1.5$ (GeV/c)^2, as our domain of interest is the large Q^2 and small t region, as outlined in the previous section. To stay above the resonance region, we require $W >$2 GeV.

For the identification of the reaction, it is sufficient to detect the scattered electron and the charged pion, the neutron being reconstructed by the missing-mass technique (see section 3 for details). The electron has to be in the acceptance of the Čerenkov counter and the calorimeter, and the pion has to cross all layers of the drift chambers and hit the scintillator counters. This trigger being defined, Fig. 20 shows some aspects of the kinematics of the scattered electron.

Fig. 21 shows the phase space in the Q^2, x_B, W, and t accessible for the available beam energies. Most of these variables are correlated, and one sees that, for instance, for $Q^2 < 2$ (GeV/c)^2 the accessible range in x_B is 0.15 to 0.35, whereas at $Q^2 \approx 3.5$ (GeV/c)^2, it is $0.3 < x_B < 0.5$ at E_e=6 GeV. This range in x_B corresponds to the valence region that is particularly well suited for the study of the quark OFPDs as they are maximal in this region (see Fig. 18). For a fixed bin around $x_B \approx 0.3$, it is possible to scan the Q^2 range from $\approx$1.5 (GeV/c)^2 up to $\approx$3.1 (GeV/c)^2. Fig. 21 also shows the W range that can be accessed as a function of Q^2. Note also the well known kinematical effect that t_{min} increases as Q^2 increases. Fig. 22 shows that the (integrated) acceptances in the variables Q^2, x_B, W, and t are of the order of 40% at E_e=6 GeV, and are quite flat.

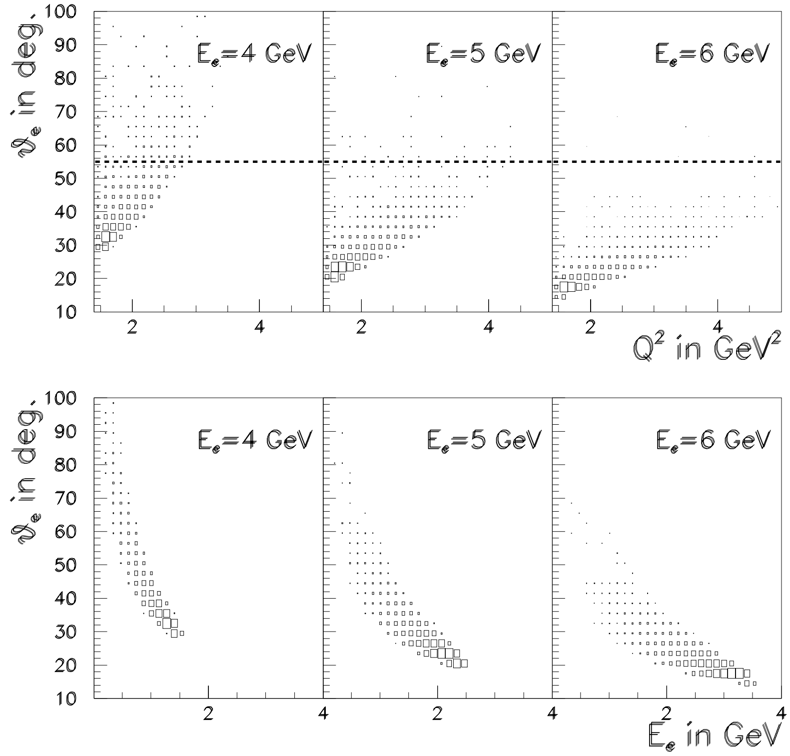

Figure 20: (Top) : Scattered electron angle versus Q^2 for E_e=4, 5, and 6 GeV (with the cut W >2 GeV). The 55° dashed line indicates roughly the maximum scattering angle for the electron to reach the CLAS electromagnetic calorimeter. (Bottom) : Scattered electron angle against scattered electron energy.

We present in Fig. 23 the results of the simulations for the Rosenbluth separation. We have used an event generator, adapted from Ref. [14], based on the model of Ref. [15]. This model gives a good description of all existing charged-pion electroproduction L/T-separated data. We generated events with a luminosity of 10^{34} cm^{-2}s^{-1} and 1000 hours of beam time for both the 4 and 6 GeV beam energies, and 500 hours of beam time at 5 GeV. As an example, Fig. 23 shows the reconstructed cross section as a function of ϵ from the Monte Carlo at $Q^2 = 2.5$ (GeV/c)^2 for $< x_B >$=0.35 and $t - t_{min}$=0.1 (GeV/c)^2. For the binning, we took Δx_B=0.1, Δt=0.1 (GeV/c)^2 and ΔQ^2=0.2 (GeV/c)^2. Up to Q^2=2.5 (GeV/c)^2, 3 points can be measured for the same values of Q^2, x_B, and t, corresponding to the 3 beam energies (4, 5, and 6 GeV). Above Q^2=2.5 (GeV/c)^2, only the 5 and 6 GeV beam energies (corresponding to $\epsilon \approx$0.4 and 0.6) can access these high Q^2 values as shown previously (see Fig. 20).

Acceptance has been taken into account bin by bin. The error bars are purely statistical. The procedure to extract σ_L and σ_T is then to simply fit by a straight line the cross sections thus obtained at the 3 (or 2) ϵ points. The intercept at ϵ=0 yields σ_T, and the slope gives σ_L. Fig. 23 compares the resulting linear fit (solid line) to the input model (dashed line). It is clear that at small Q^2 values, the agreement is very good, and as Q^2 increases, and thus the count rates diminish, the deviations of the fit from the input model become obvious.

The results of the fitted σ_T and σ_L cross sections are shown in Fig. 24 along with the existing point of Ref. [12]. This shows that, in terms of statistics, we can carry out an accurate measurement of the separated cross sections up to $Q^2 \approx 3.1$ (GeV/c)^2. Table 2 shows the corresponding number of events in each bin. Given the high statistics involved here, it is clear that the final error bars on the separated cross sections will be driven mainly by the systematic errors.

Rosenbluth separation of absolute cross sections has been one of the important tools in separating longitudinal and transverse cross sections. It has been used mostly in inclusive electron-scattering reactions. Usually, the accuracy of the separation is limited by the systematic errors of the two or more measurements performed at different beam energies, where the electron is detected at different angles. This requires excellent control of systematics in the various measurements. To this extent, such a separation using CLAS has the same stringent requirements. However, CLAS has a number of features that will allow excellent control of systematics between different experimental conditions.

First, CLAS measures the entire available phase space simultaneously. This means, for example, that processes are measured concurrently with the reaction of interest that may be used to control the normalization of any reaction by relating it to a well measured reaction. For example, elastic electron-proton scattering will be measured continuously over the entire available Q^2 range. Since this process has been well measured, and also the electric and magnetic form factors are now known with very high precision, we can use this to determine the relative luminosity for measurements done at different beam energies. We can also use a possible change in the position of the elastic peak to determine a relative shift in the beam energy. Another check comes from measuring the cross section for the $\Delta(1232)$ excitation in the $p\pi^0$ channel. This is known to be nearly purely transverse and should not be affected by changes in the beam energy at a fixed Q^2 and W, providing additional checks. We estimate, based on the experience with CLAS during past electron runs, that this part of the systematic uncertainty can be controlled at the level of $\approx$2%.

Another important contribution is the acceptance for the outgoing π^+. While an absolute uncertainty in the pion acceptance will not affect the extracted value for σ_L, an acceptance change for different energies will. This is particularly important since the pions of interest occupy the CLAS acceptance at relatively small angles where the acceptance is restricted by the torus coils. We estimate that the acceptance can be determined to $\approx$3%.

Since the two contributions to the systematics are largely independent, we add them quadratically and obtain a systematic uncertainty of less than $\approx$3.5%. For the fit to separate σ_L and σ_T, we assume a 4% error. As shown in Fig. 24, the effect of this error is largest at small Q^2 where the rate is higher, while at higher Q^2, the separation is dominated by the statistical uncertainties.

As a last point of this exclusive charged-pion electroproduction study, one of the advantages of CLAS is the possibility it allows to bin data in the kinematical variables relevant to the physics under study. For the present case, we have studied the L/T separation at fixed x_B, which is the appropriate variable for pQCD-related studies. However, similar L/T

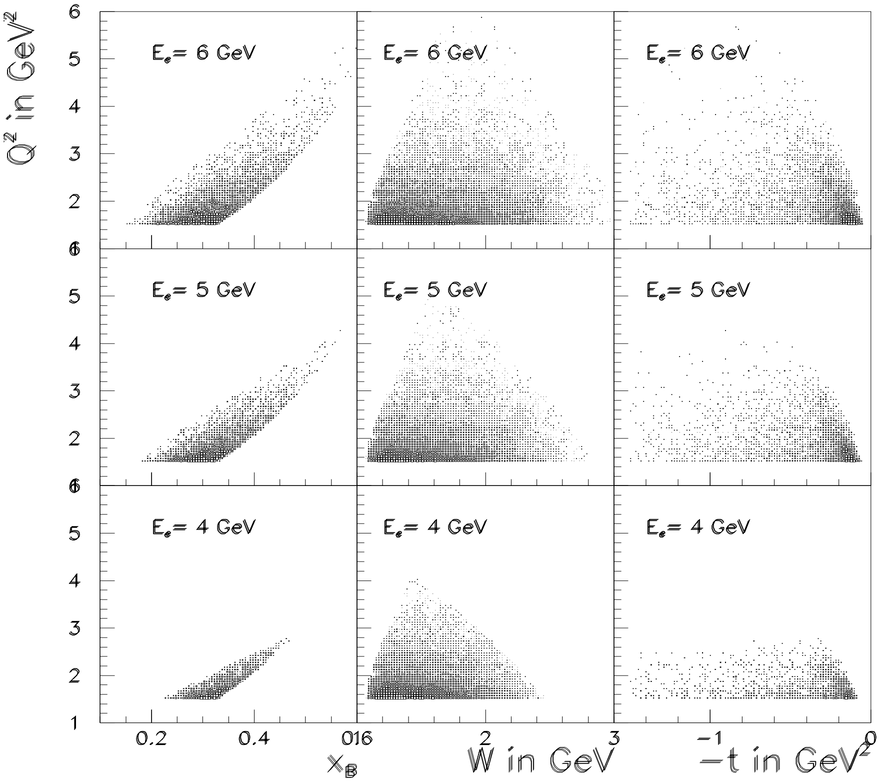

Figure 21: For the beam energies E_e=4, 5, and 6 GeV, correlations between Q^2, x_B, W, and t for accepted events (*i.e.* the scattered electron in the calorimeter and the π^+ detected). Left column: Q^2 vs. x_B (with $W > 2$ GeV cut); Middle column: Q^2 vs. W (no W cut); Right column: Q^2 vs. t (with $W > 2$ GeV cut).

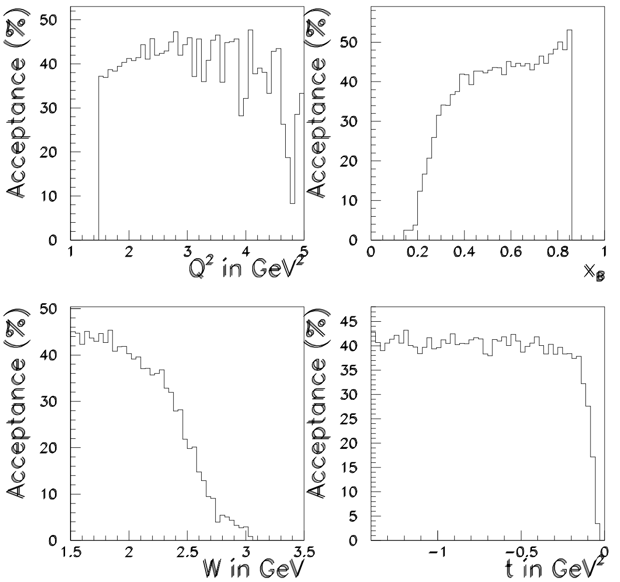

Figure 22: Integrated acceptance at E_e=6 GeV for the 4 kinematical variables Q^2, x_B, W, and t. The figure shows the percentage of accepted events in CLAS according to the criteria : one electron in the Čerenkov counter and in the electromagnetic calorimeter, and the charged pion crossing all layers of the drift chambers and hitting the scintillator counters.

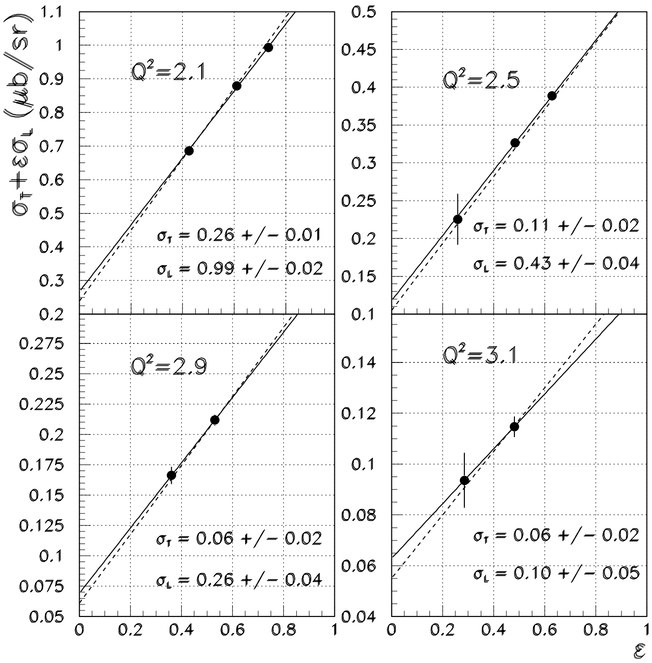

Figure 23: Simulated reconstruction of $d\sigma/dt$ as a function of ϵ for $< x_B >$=0.35 and $t - t_{min}$=0.1 (GeV/c)^2 for Q^2 = 2.5 (GeV/c)^2. The dashed line corresponds to the input model and the solid line is the result of the fit. The result of the linear fit yielding σ_T and σ_L is displayed.

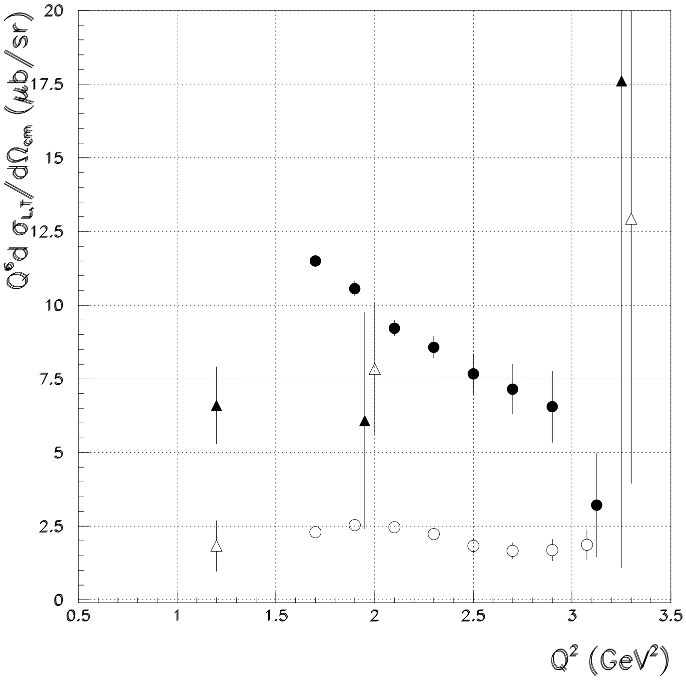

Figure 24: Separated differential cross section ($\times Q^6$) as a function of Q^2. The existing data [12] are displayed: open triangles correspond to σ_T and filled triangles to σ_L. The circles are the results of the simulations (see Fig. 23) - open circles correspond to σ_T and filled circles to σ_L.

Q^2	E_e=4 GeV		E_e=5 GeV		E_e=6 GeV	
(GeV^2)	*Gen.*	*Acc.*	*Gen.*	*Acc.*	*Gen.*	*Acc.*
1.6 - 1.8	148760	63880	98445	47742	229205	109762
1.8 - 2.0	77390	27560	55805	25202	134732	63685
2.0 - 2.2	38362	9065	30522	12205	76747	34322
2.2 - 2.4	18022	2142	18115	6302	48115	20255
2.4 - 2.6	5732	45	8102	1857	22695	7660
2.6 - 2.8	0	0	5007	800	15347	4542
2.8 - 3.0	0	0	2727	267	9775	2237
3.0 - 3.2	0	0	1047	37	4852	792

Table 2: Estimated number of events generated (Gen.) and accepted (Acc.) from Monte Carlo that are expected per (Q^2,x_B,t) bin for 1000 hours of beam time at E_e=4 and 6 GeV and 500 hours of beam time at E_e=5 GeV. x_B and $t - t_{min}$ are fixed at $< x_B >$=0.35 and $t - t_{min}$=0.1 (GeV/c)^2, and Δx_B=0.1 and Δt=0.1 (GeV/c)^2. The Q^2 bins are indicated on the right column of the table. Luminosity has been taken as 10^{34} cm^{-2}s^{-1}.

separations can be done at fixed W. One can then analyze differential cross section data in the framework of traditional t-channel meson exchanges (the only contributions "surviving" above the resonance region). It was shown, for instance, in Refs. [17, 16, 15] that a very successful and economical description of most of the (scarcely) available published charged-pion electroproduction data above the resonance region is provided by a (gauge-invariant) Regge model based on π and ρ Regge-trajectory exchanges. This allows us to also extract fundamental quantities of hadronic structure such as the π^+ form factor, and possibly the $\rho\pi\gamma$ transition form factor.

Fig. 25 shows the T and L cross sections for π^+ electroproduction for typical values of Q^2 that can be accessed around $W \approx 2$ GeV at CEBAF. It is seen that the L response function is independent of the ρ exchange at $t = t_{min}$, which makes it appropriate to extract the π electromagnetic form factor. Going to higher Q^2, the value of $-t_{min}$ increases (for a given W) as can be seen. Consequently, to extract the π electromagnetic form factor at higher Q^2, one has to extrapolate to the pion pole ($t = m_\pi^2$) which is further away at these higher Q^2 values. It is important to note that the t-dependence is very dependent on the model used. In Fig. 25, a traditional Born model (based on standard pole-like π and ρ Feynman propagators $(1/(t - m_{\pi,\rho})^2)$) is compared to a Regge-type model ($\propto s^{\alpha_{\pi,\rho}(t)}$, where $\alpha_{\pi,\rho}(t)$ is a Regge trajectory). This means that at higher Q^2, where the form factor fit has to be done using the data at higher t-values, the normalization will be quite different between a Born and a Regge model. Consequently, the extraction becomes more and more model dependent as one goes to larger Q^2 for a given W.

If one wants to correctly extract the pion form factor, it is important to provide thorough measurements of the t and W dependences of the differential cross section at various Q^2. This also motivates the push to higher energies, because in that case, the value of $-t_{min}$ decreases. For instance, Fig. 26 shows the π^+ electroproduction cross section for Q^2=1.2 (GeV/c)^2 at two energies for which data from a Cornell experiment [18] exist, and a Regge model is compared to a typical Born model again. As already noticed in Ref. [18], a Born-term model does not reproduce the t-dependence of the cross section. Usually, one "cures" this by adding another "hadronic" form factor at the πNN and ρNN vertices to

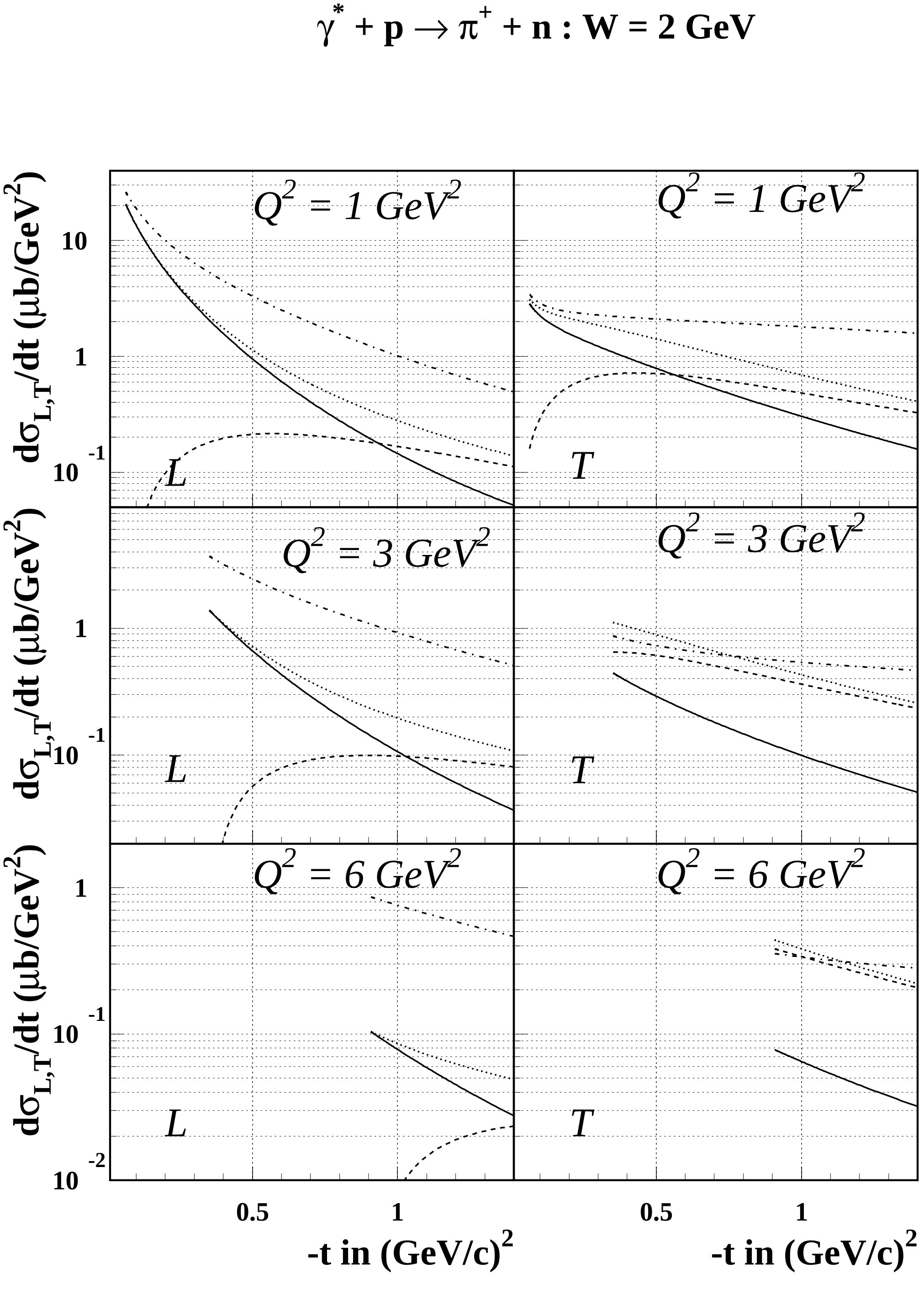

Figure 25: T and L response functions for π^+ electroproduction at $W = 2$ GeV for different values of Q^2. The first calculated point in $-t$ indicates the value $-t_{min}$. Full lines : $\pi + \rho$ Regge exchange model with $\Lambda_\pi^2 = \Lambda_\rho^2 = 0.462$ GeV^2, dashed-dotted lines : π Born exchange with $\Lambda_\pi^2 = 0.462$ GeV^2, dotted lines : $\pi + \rho$ Born exchanges with $\Lambda_\pi^2 = \Lambda_\rho^2 = 0.462$ GeV^2, dashed lines : $\pi + \rho$ Regge exchange model with $\Lambda_\pi^2 = \Lambda_\rho^2 = 0.462$ GeV^2.

steepen the t-dependence (this is done at the expense of an additional free parameter for the mass scale of this "extra" form factor). However, the t slope changes also with energy, and the data at the highest energy, $W = 3.1$ GeV, clearly favor a Regge model; it predicts a much steeper t-dependence at higher energy than a Born model. A Born model multiplied by a t-dependent off-shell form factor cannot reproduce this feature. This steeper t-dependence with increasing energy, proper to Regge theory and known as "shrinkage", was seen previously for photoproduction [15, 17], where data exist at higher energy compared with the electroproduction data. Furthermore, it is seen in Fig. 26 that including a t-channel ρ Born exchange leads to a rising t-behavior of the cross section at larger $-t$ values, which is clearly ruled out by the data. This different behavior in t between the Born and Regge models is of critical importance concerning the extraction of the pion electromagnetic form factor from the measured cross sections.

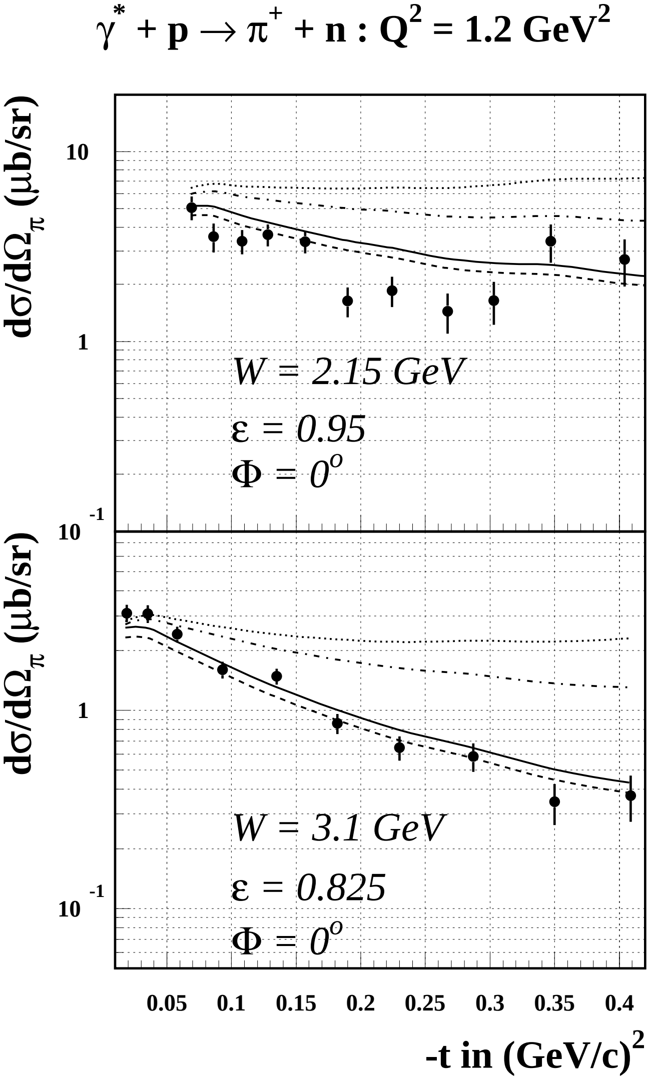

Figure 26: Comparison of the differential cross section for π^+ electroproduction at energies of W=2.15 GeV and 3.1 GeV at $Q^2 = 1.2$ (GeV/c)^2 and for ϕ= 0° (in plane). Dashed-dotted lines : π Born exchange with $\Lambda_\pi^2 = 0.462$ GeV^2, dotted lines : $\pi + \rho$ Born exchanges with $\Lambda_\pi^2 = \Lambda_\rho^2 = 0.462$ GeV^2, dashed lines : $\pi + \rho$ Regge exchange model with $\Lambda_\pi^2 = \Lambda_\rho^2 = 0.462$ GeV^2, full lines : $\pi + \rho$ Regge exchange model with $\Lambda_\pi^2 = \Lambda_\rho^2 = 0.50$ GeV^2 which gives a better fit to the data. The data are from Ref. [18].

The large acceptance in t provided by the CLAS detector (see Fig. 22) will allow us to measure this critical dependence and constrain the extrapolation procedure. This is a feature that experiment E93-021 [20], currently being run in Hall C, is not sensitive to as the spectrometers provide only a limited t acceptance around t_{min}.

We have done simulations and find that similar to the fixed x_B study, one can carry out the L/T separation with reasonable accuracy at fixed W up to $Q^2 \approx 3.1$ (GeV/c)^2. In addition to the σ_L/σ_T separation, which is the main physics focus, this experiment will produce high quality differential cross section data for the $n\pi^+$ channel covering the entire W range up to 3 GeV, Q^2 up to 5.5 (GeV/c)^2, and $-t$ up to 6 (GeV/c)^2. No such data have been measured in the past.

4.4.2 $ep \to e'(\pi^0, \eta)p$

Neutral pseudoscalar electroproduction is naturally complementary to the charged-pion study. It was already pointed out in the introduction that the x_B dependence of the π^+/π^0 ratio ought to be investigated as the presence of the π^+ pole mechanism in charged-pion electroproduction should yield a peculiar behavior, i.e. an enhancement, in the valence region.

Also, the comparison of both the π^0 and η (along with the η') cross-sections allows us to perform a flavor separation of the polarized OFPDs ($\tilde{H}^u$ and $\tilde{H}^d$) as these OFPDs enter with different combinations for these different channels. Recent articles point to the richness of the physics that can be accessed through the neutral pseudoscalar channels. Eides, Frankfurt, and Strikman [19] point out that "It seems likely that a *precocious factorization...* could be valid already at moderately high Q^2 [≥ 5 (GeV/c)^2], leading to *precocious scaling of the spin asymmetries and of the ratios of the cross sections* as a function of Q^2, and x_B". Thus, for example, in the naive quark model they find ratios $\pi^0 : \eta : \eta'$ of:

$$\frac{1}{2}(\frac{2}{3}\Delta u + \frac{1}{3}\Delta d)^2 : \frac{1}{6}(\frac{2}{3}\Delta u - \frac{1}{3}\Delta d + \frac{2}{3}\Delta s)^2 : \frac{1}{3}(\frac{2}{3}\Delta u - \frac{1}{3}\Delta d - \frac{2}{3}\Delta s)^2,$$

where Δu, Δd, and Δs correspond to the quark-spin helicity distributions. If $\Delta d \approx -\Delta u$ and $\Delta s = 0$, one obtains a ratio of $\pi^0 : \eta : \eta'$ = 1:3:6. This is modified if one includes SU(3) breaking and the axial anomaly, and one gets an x_B dependence when $q\bar{q}$ pairs are included.

Feasibility studies were carried out for the proposed experiment $ep \to e'p\pi_0(\eta)$ at an electron beam energy of 6 GeV for CLAS using Monte Carlo simulation results, as well as using the existing 4 GeV and 5.56 GeV data. Shown in Fig. 27a is the missing-mass squared spectrum below 0.6 GeV^2 obtained from a preliminary analysis of 4 GeV data. Only events with a mass of the recoiling hadron system $W>1.8$ GeV for virtual photons of $Q^2>2$ (GeV/c)^2 were selected. The spectrum shows clear peaks for both π_0 and η mesons. Cuts to suppress elastic, radiative, and multi-pion events were applied. For comparison, we display an equivalent missing-mass spectrum in Fig. 27b for data taken recently during a short test run at 5.56 GeV. This data set contains about 10 M triggers, which comprises a data taking period of 2 hours at a nominal instantaneous luminosity of 6.5×10^{33} cm^{-2}s^{-1}. Again, the π_0 and η peaks are clearly visible. This is the first time that deep exclusive π_0 and η production have been observed in this region.

In order to simulate the expected exclusive π_0 and η production equivalent to one month of beam time at an electron beam energy of 6 GeV and a luminosity of 1×10^{34} cm^{-2}s^{-1}, we modeled the differential cross section as:

$$d\sigma/dt = \sigma_0 f(t) g(Q^2). \tag{3}$$

σ_0 was obtained by extrapolation using comparable data that is only available at low Q^2 from a measurement at DESY [21]. The Q^2 dependence was assumed to follow $g(Q^2) \approx 1/Q^6$. From the 4 GeV CLAS data, we extracted the angular distribution of the produced π_0 mesons with respect to the direction of the virtual photon in the rest frame of the hadronic system $\cos(\theta^*_{\pi_0})$, as shown in Fig. 28a. In Fig. 28b we show the momentum transfer to the meson, $t = (q - p_{\pi_0})^2$. A function was fit to this spectrum to extract $f(t)$. This distribution is strongly forward peaked with a break at -t≈1 (GeV/c)^2 that agrees with observations at lower Q^2.

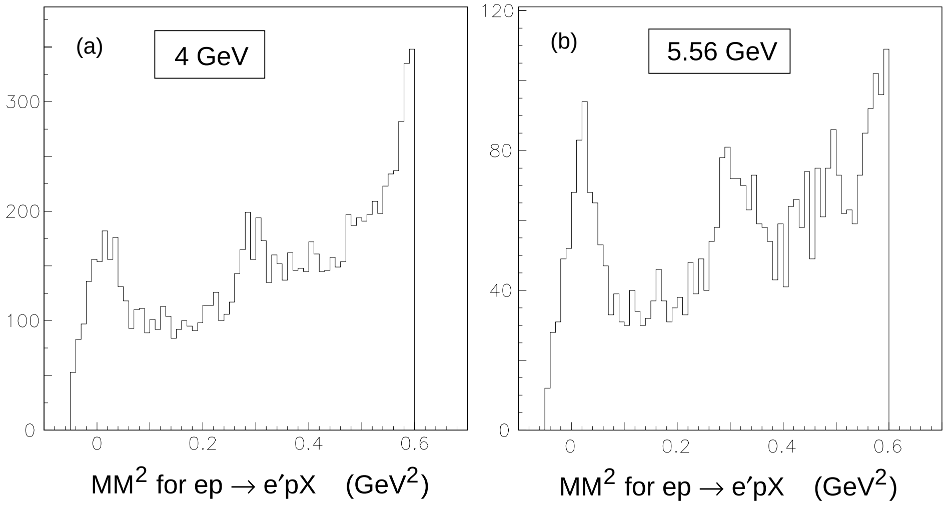

Figure 27: Missing-mass squared spectra for $ep \rightarrow e'pX$ for Q^2>2 (GeV/c)^2 for (a) 4 GeV data and (b) 5.56 GeV data. NOT ACCEPTANCE CORRECTED.

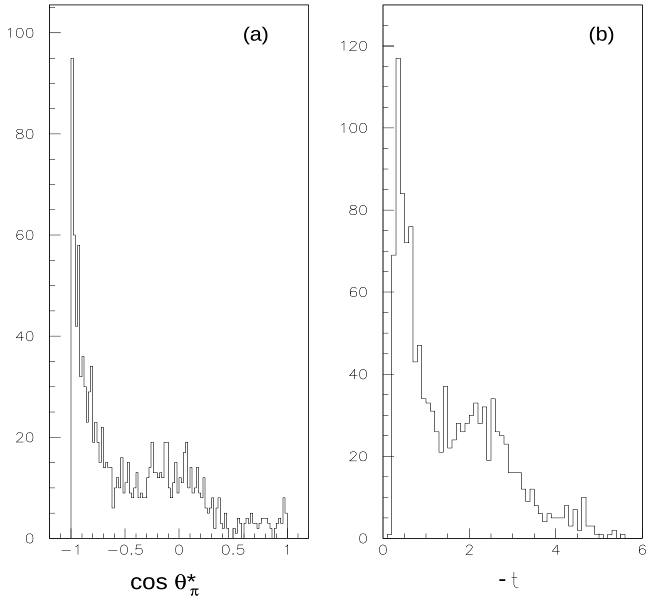

Figure 28: (a) Angular distribution $\cos\theta_{\pi^*_0}$ of the meson in the rest frame of the produced hadronic system, and b) momentum transfer $t = (q - p_{\pi_0})^2$ to the meson for 4 GeV data. NOT ACCEPTANCE CORRECTED.

As a final input to the simulation, we extracted a rough geometrical acceptance for the CLAS detector from the test data taken at 5.56 GeV. Fig. 29 shows the electron and proton correlated acceptance as a function of the angles θ and ϕ. An elliptical function was determined describing the envelope and used together with a θ_{max}=55° cut-off to accept events in the Monte Carlo.

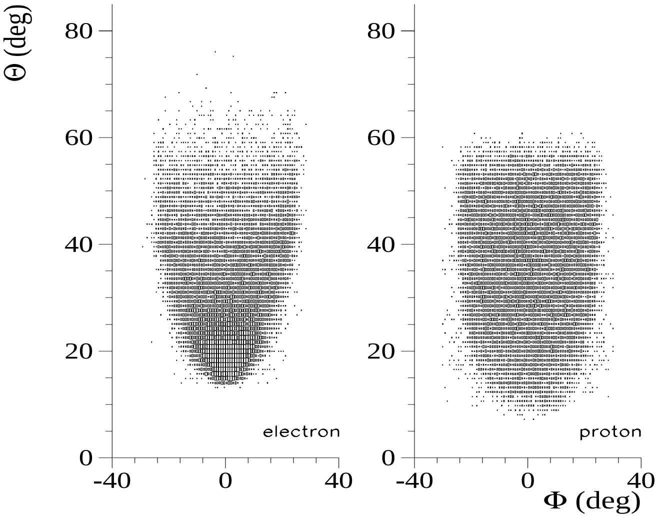

Figure 29: Correlated acceptances for electrons (left) and protons (right) for CLAS from 5.56 GeV data analysis.

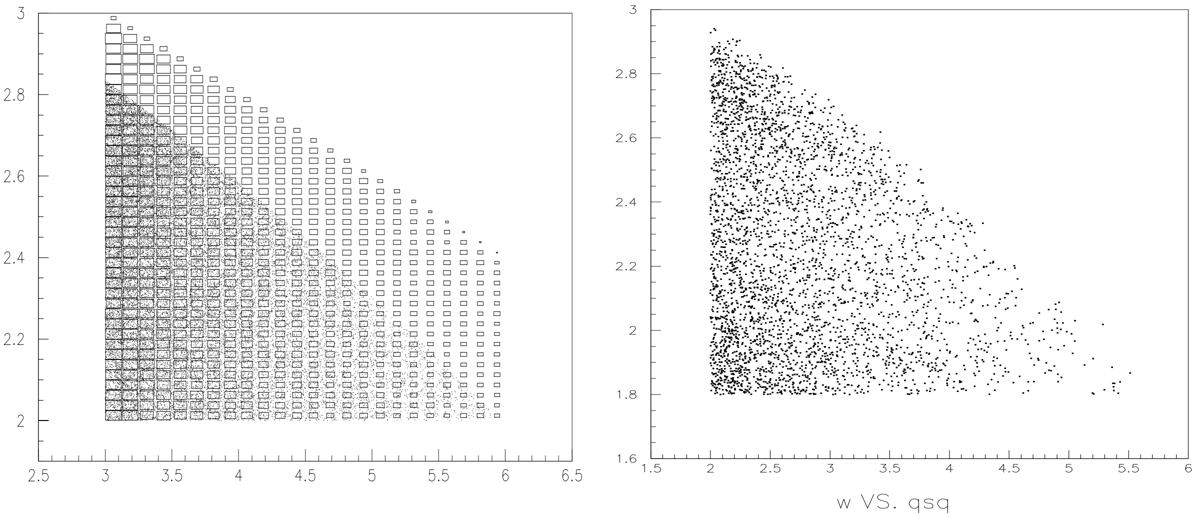

Figure 30: W vs. Q^2 distribution for *simulated* 6 GeV data (left) and *measured* data at 5.56 GeV (right).

The following graphs present findings and expected statistics from the simulation for a running period of one month. In Fig. 30a, W is plotted versus Q^2, for Q^2 between 3-6 (GeV/c)^2 and W between 2-3 GeV. The events that fall in the CLAS acceptance (dots) are compared to the generated events (boxes). 91k π_0 mesons are expected to be produced out of which 27k will be accepted. The W vs. Q^2 plot from 5.56 GeV data is shown in Fig. 30b. The W and t distributions and expected statistics for one month of running are shown for different Q^2 bins in Fig. 31. In each spectrum, both the Monte Carlo generated and accepted events are shown. The above findings apply similarly in the case of η production.

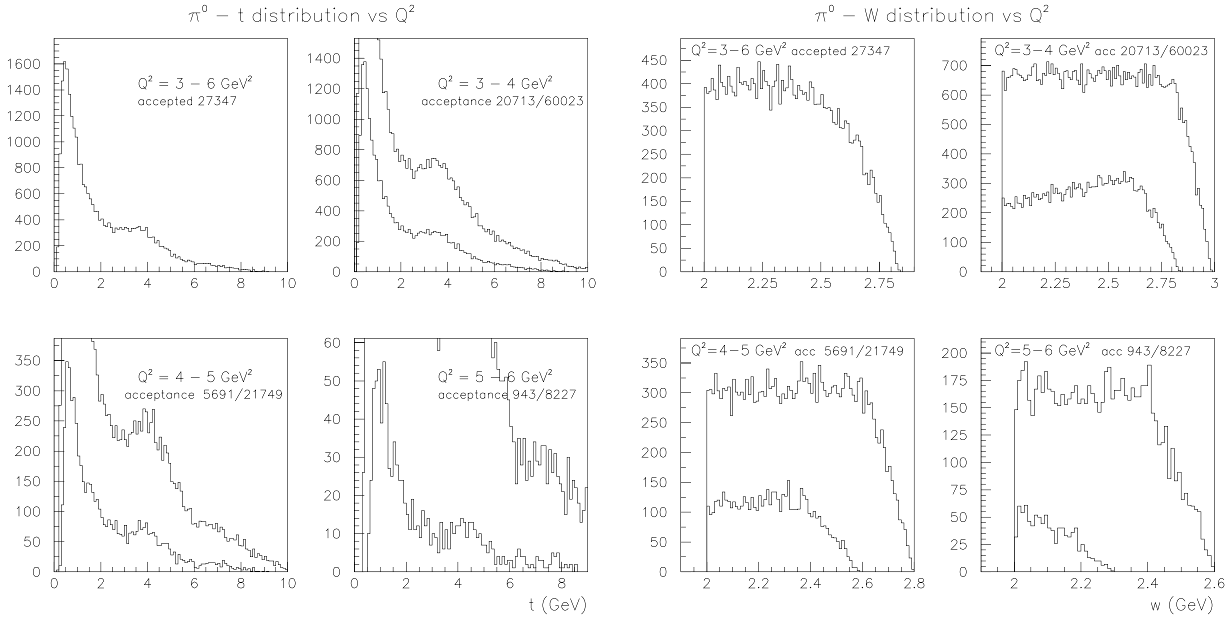

Figure 31: Simulation results for several Q^2 bins for (a) t distributions (left) and (b) W distributions. In each subplot the histrograms for both the Monte Carlo generated and accepted events are shown. The ratio yields the CLAS acceptance function. The data generated are what is expected in CLAS for one month of operation at a luminosity of 10^{34} cm^{-2}s^{-1}.

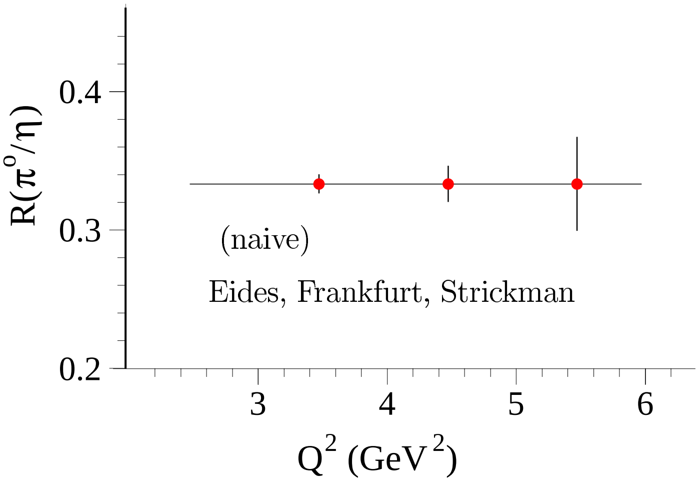

Figure 32: Simulation results for several Q^2 bins for the ratio $R(\pi^0/\eta)$, corresponding to the low t region of Fig. 28b. The error bars correspond to the statistical accuracy of accepted data, including the multi-pion continuum underlying the η missing-mass peak. The solid curve is the naive ratio as discussed in the text [19].

A very important advantage of the large kinematic acceptance of CLAS is that we can obtain the entire t distribution (Fig. 28b). This enables us to more effectively subtract out the s-channel processes, such as resonance production, and therefore obtain data at a lower W (where the cross sections are larger) than would otherwise be possible. Fig. 32 shows the statistical accuracy of the ratio $R(\pi^0/\eta)$ for increasing values of Q^2 for the forward-peaked portion of Fig. 28b for the accepted π^0 and η for one month of beam time.

We conclude that a measurement with reasonable statistics should be possible up to a Q^2 of about 5 $(\mathrm{GeV/c})^2$.

References

[1] X. Ji, Phys. Rev. Lett. **78**, 610 (1997); Phys. Rev. D **55**, 7114 (1997).

[2] A.V. Radyushkin, Phys. Lett. B **380**, 417 (1996); Phys. Rev. D **56**, 5524 (1997).

[3] J.C. Collins, L. Frankfurt, and M. Strikman, Phys. Rev. D **56**, 2982 (1997).

[4] M. Vanderhaeghen, P.A.M. Guichon, and M. Guidal, Phys. Rev. Lett. **80**, 5064 (1998).

[5] P.A.M. Guichon and M. Vanderhaeghen, Prog. Part. Nucl. Phys., Vol. 41 (1998).

[6] M. Vanderhaeghen, P.A.M. Guichon, and M. Guidal, Preprint hep-ph/9905372, (1999).

[7] L. Mankiewicz, G. Piller, and A. Radyushkin, Preprint hep-ph/9903531, (1999).

[8] L. Frankfurt, P. Pobylitsa, M. Poliakov, and M. Strikman, Preprint hep-ph/9901429, (1999).

[9] M. Tipton for the HERMES collaboration, J. Pochodzalla for the COMPASS collaboration, Talks presented at the JLAB Semi-Exclusive Workshop, May 1999.

[10] M. Guidal, C. Marchand, E. Smith *et al.*, JLab Experiment E98-107.

[11] T.H. Bauer, R.D. Spital, D.R. Yennie, and F.M. Pipkin, Rev. Mod. Phys. **50**, 261 (1978).

[12] C.J. Bebek *et al.*, Phys. Rev. D **13**, 1693 (1978).

[13] E.S. Smith, “Fast Monte Carlo Program for the CLAS Detector”, CLAS-Note 90-003, (1990).

[14] M. Morlet and J. Van de Wiele, private communication.

[15] M. Vanderhaeghen, M. Guidal, and J.M. Laget, Phys. Rev. **C57**, 1454 (1998).

[16] M. Guidal, J.M. Laget, and M. Vanderhaeghen, Phys. Lett. **B400**, 6 (1997).

[17] M. Guidal, J.M. Laget, and M. Vanderhaeghen, Nucl. Phys. **A627**, 645 (1997).

[18] C.J. Bebek *et al.*, Phys. Rev. D **13**, 25 (1976).

[19] M.I. Eides, L.L. Frankfurt, and M.I. Strikman, Phys. Rev. D **59**, 114025 (1999).

[20] D. Mack, H. Blok, G.M. Huber *et al.*, JLab Experiment E93-021.

[21] F.W. Brasse *et al.*, Phys. Lett. B **58**, 467 (1975).

5 The N^* 6 GeV Program

5.1 Introduction

The goal of the N^* program is to provide as complete a picture of the internal structure of baryons and their coherent excitations as possible. Distinct advantages of electrons over hadronic probes for the excitation of baryonic states have been pointed out in the proposals for that program [1]. Conventional experiments employ magnetic spectrometers and focus on specific excitations at specific kinematics. On the other hand, with CLAS it is possible to measure simultaneously angular distributions over a wide range of W and Q^2 for many channels, including not only single-meson production processes, such as π^+, π^0, and η, but multi-pion final states as well. Even reactions with $\eta' p$ in the final state that have not yet been investigated in electroproduction can be studied using CLAS. The broad range and overall unity of the CLAS program and its physics issues have been described in numerous proposals and in several summary documents (e.g. Ref. [2]). In this section we review the high Q^2 extension of the program that is possible with a 6 GeV electron beam, and request allocation of 40 days of beam time for experiment E91-002, in concert with the other accepted and proposed experiments in this package. We also discuss the extension of the N^* program to higher W and request allocation of 15 days of beam time with reversed torus field.

First, we briefly review the physics motivation, including recent developments. We then argue that the analysis of data already obtained at 4 GeV, along with data from a short 5.56 GeV test run, demonstrate that the proposed 6 GeV measurement will yield data of excellent quality for single-meson and two-pion production for Q^2 up to $\approx$5 (GeV/c)^2.

5.2 Physics of the N^* Program with the CLAS

One of the fundamental subjects in sub-atomic physics is the structure of baryons and their excitations in terms of quark and gluon constituents. A central issue concerns which models are valid for describing excitation processes in different domains of Q^2. At low Q^2 ($<$1 (GeV/c)^2), the structure of the interaction is very complex, and as yet unsolved, although the constituent quark model (CQM) has proven to be a very powerful and widely accepted basis. At low Q^2 the CQM has been combined with the single-quark transition assumption to describe with some success the electromagnetic transitions to resonant states. A good introduction to the systematics of these calculations and their Q^2 dependence is provided by Close [3]. Experimentally, the limits of the CQM have still not been adequately explored. With increasing Q^2, smaller hadronic substructures are probed, so that the spatially extended constituent quarks would become less useful as fundamental basis states. It is widely believed that at asymptotically high Q^2, coherent reactions such as elastic and transition scattering are dominated by states involving very small baryon size. In this regime the physical description is expected to be greatly simplified by describing the interactions in terms of hard perturbative QCD (pQCD), with contributions only from the leading-order Fock state (valence pQCD). The signatures of these hard processes are helicity conservation and the well known pQCD constituent scaling in Q^2. Many theorists believe that the few-GeV regime accessible at JLab is a transition region involving, as yet undetermined, combinations of the soft processes associated with the CQM and the hard processes associated with valence pQCD.

Currently, many theoretical groups are investigating the range in Q^2 for which the hadron and CQM bases are valid, and a number of these have been calculating the Q^2 variation of the resonance amplitudes. For example see the conference proceedings for Baryon-98 [4], Trento (1998) [5], and Seattle (1996) [6]. For the high Q^2 region there was a flurry of activity, summarized in several review articles [7, 8], to calculate elastic and resonance transition form factors to test the pQCD predictions.

Currently, important progress is being made in describing exclusive reactions in the transition region in terms of combinations of soft and hard processes, in which the soft processes are described in terms of quark-distribution functions that are generalizations of inclusive deep inelastic scattering structure functions and a pQCD kernel with higher-twist corrections. Thus, the different approaches for studying the baryon form factors define three distinct regimes: the low Q^2 CQM, the high Q^2 pQCD, and the transition region. These are schematically illustrated in Fig. 33. Experimental study of the transition region is well-matched to CEBAF's current and future capabilities. One purpose of this experiment is to look for signatures of the transition region by studying the Q^2 evolution of the form factors for transitions to excited resonant states. The use of CLAS to detect the mesons and measure their angular distributions both tags the produced baryon states, and provides their helicity (or multipole) amplitudes.

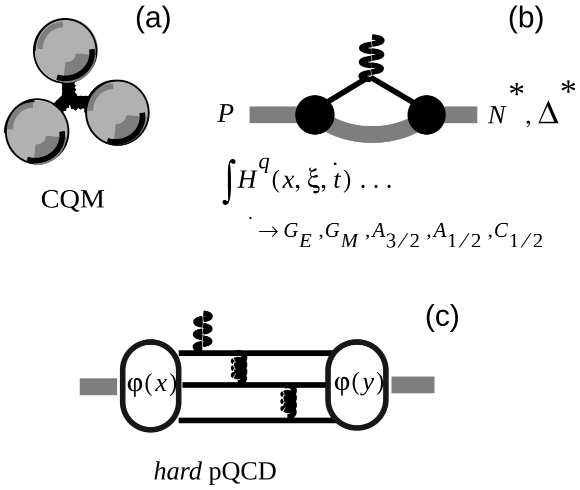

Figure 33: Schematic illustration of exclusive resonance production in the three regions of Q^2: a) constituent quarks, b) transition region with separation in terms of soft and hard sectors, and c) high Q^2 valence pQCD regime.

The importance of high Q^2 measurements is not limited to the possibility that they may reveal evidence of a transition to pQCD. One way of testing the CQM is to study ratios of transition amplitudes of states belonging to the same supermultiplet. In the amplitude ratio,

$$\frac{A_{\frac{1}{2}}(N^*(1520))}{A_{\frac{1}{2}}(N^*(1535)),} \tag{4}$$

effects of the radial wave function drop out, and since both states have the same mass, kinematical effects should be small. Fig. 34 shows the data in comparison with model predictions. This ratio is rather insensitive to relativistic effects and other model ingredients. At high Q^2, the predictions are close to the SU(6) limit for the pure spin transitions that are expected to dominate. While the data agree very well at low Q^2, the highest Q^2 point indicates a significant deviation. Whether this is a sign for a non-trivial breakdown of the CQM at small distances remains to be seen with improved data.

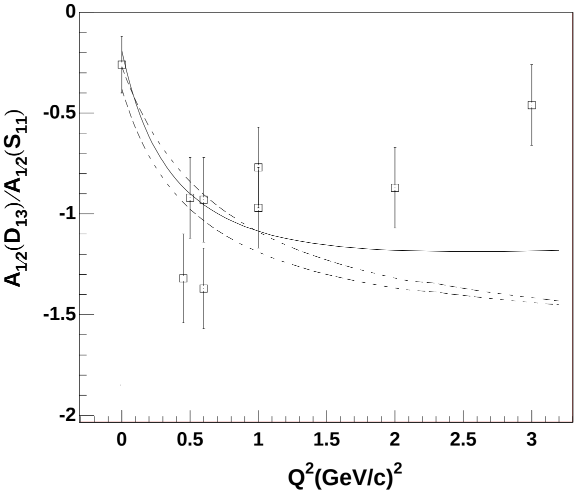

Figure 34: Test of the CQM symmetry structure; the curves are from Ref. [9].

Using experimental information on states belonging to the same supermultiplet, one can test symmetry properties of the electromagnetic transition between supermultiplets. In a single-quark transition model (SQTM), radiative transitions from the ground state to the $[70, 1^-]$ supermultiplet are described by a one-body current operator:

$$J^{em}_+ = A \cdot L_+ + B \cdot S_+ + C \cdot L_+ S_z, \tag{5}$$

corresponding to orbit, spin, and combined spin-orbit coupling, respectively. Deviations from the SQTM predictions may therefore yield information about multiple quark contributions. Using the data on the $N^*(1535)$ and $N^*(1520)$, we can determine A, B, and C as a function of Q^2, and predict transition amplitudes to all other states belonging to $[70, 1^-]$. The predictions agree quite well with the data at the photon point, showing that SU(6) symmetry is approximately correct. However, this symmetry might break down at high Q^2. This can presently not be tested as electroproduction data on most of the higher-mass states are lacking.

It is clear that a study to compare and contrast the Q^2 dependence of the form factors for transitions to a number of different resonances will be very useful in understanding fundamental properties of these structures, independent of any model used to explain them. For electron beams with a maximum energy of 4 GeV, the CLAS N^* program is limited to momentum transfers of <3 (GeV/c)^2 for the low-mass states, and to 2 (GeV/c)^2 for states with masses of ≈1.7 GeV. For higher momentum transfer, the N^* program has used the two Hall C spectrometers in coincidence to study production of the $\Delta(1232)$ via its decay to the $p\pi^0$ channel [10], and production of the $S_{11}(1535)$ via its decay to the $p\eta$ channel [11] at two specific values of Q^2 with a maximum of 4 (GeV/c)^2. At least for the $\Delta(1232)$, the onset of pQCD was not observed. However, the detailed characteristics of extracting the small contributing amplitudes are ambiguous for several reasons. For one thing, the limited solid angle prevented full out-of-plane coverage, and even more importantly, the study of the π^+ channel was not carried out.

The Hall C experiment was limited to the $\Delta(1232)$ and $S_{11}(1535)$ because the proton is emitted in a narrow cone around the $\vec{q}$ direction when the excited resonance is near the threshold of the produced mesons. For a complete study of these states, one should study both their charged- and neutral-pion channels. Furthermore, both the $\Delta(1232)$ and $S_{11}(1535)$ states have some unusual characteristics that make it important to study high-Q^2 behavior of other states as well. First, the $\Delta(1232)$ excitation strength falls off much more rapidly with Q^2 than other resonances such as the $D_{13}(1520)$ or $F_{15}(1680)$. It has been suggested that perhaps its leading-pQCD amplitude may be anomalously small so that experiments at even higher Q^2 may be required to study the transition to dominant pQCD behavior [12]. Secondly, the $S_{11}(1535)$ is the only strongly excited state with a large η decay, and there have even been suggestions that the $S_{11}(1535)$ is not dominantly a regular $|qqq\rangle$ state, but is instead dynamically generated, as suggested by some recent studies [13].

To obtain a more complete picture of resonance production and avoid these difficulties of interpretation, measurements of transitions to other states are needed. However, with the exception of the $\Delta(1232)$, states with large photo-coupling strength are mostly isospin-1/2 states that couple more strongly to the $n\pi^+$ channel than to the $p\pi^0$ channel. Their study requires measurement of the π^+ in the final state. Pion production through these resonances is far above the pion threshold. Measurement of the angular distribution of the resonance decay angles, ϕ and θ, with conventional spectrometers is difficult, especially since particle detection out of the electron scattering plane is required. Large acceptance spectrometers such as CLAS are most appropriate for such measurements. Moreover, to obtain a broader picture of the high Q^2 behavior, it is necessary to measure the Q^2 evolution for several states in the baryon spectrum. Many of these states have larger branching ratios into multi-pion channels, and therefore it is required to extend the measurements beyond single-meson electroproduction.

The large kinematical coverage of CLAS allows the measurement of resonances such as $D_{13}(1520)$, $F_{15}(1680)$, $\Delta^*(1620)$, and $\Delta^*(1700)$ at high Q^2 in decay channels that are significantly above the meson-production threshold. The CLAS program has already shown that some resonances in the mass region of 1.5 to 1.8 GeV/c^2 are strongly excited in the $p\pi^+\pi^-$ channel, especially the $\Delta^{++}\pi^-$ channel [14]. For baryon resonances with masses above 1.9 GeV/c^2, η' mesons may provide an excellent probe as they couple only to isospin-1/2 states. The quark model predicts that only a few resonances may have considerably large couplings to $\eta' N$ as well as γN.

5.3 N^* Excitations at High Q^2 in the $p\pi^0$, $p\eta$, and $n\pi^+$ Channels

Spokespersons: V.D. Burkert[a], R. Minehart[b], P. Stoler[c], and M. Taiuti[d]

[a]Jefferson Laboratory, Newport News, VA 23606
[b]University of Virginia, Charlottesville, VA 22901
[c]Rensselaer Polytechnic Institute, Troy, NY, 12180
[d]INFN-Sezione di Genova, Genova, Italy, I-16146

5.3.1 Preliminary CLAS Results at Lower Q^2

We have obtained large quantities of unpolarized and polarized electroproduction data at beam energies of 1.6, 2.4, and 4.0 GeV that, once the full complement of data has been accumulated, will provide information on resonance amplitudes at lower Q^2. The data at the lowest beam energy have been carefully analyzed in the $p\pi^0$, $n\pi^+$, and $p\eta$ channels, and preliminary cross sections and angular distributions have been extracted and presented at conferences.

Where comparisons with other data are possible, and very limited data are available from previous experiments, our results are in agreement. Currently, acceptance calculations are being refined to allow extraction of cross sections in areas of phase space where the accepted solid angles are small. Multipole analyses are used to extract resonance transition multipoles from the data. First results in the $\Delta(1232)$ region are very encouraging.

The π^0 production is strongly dominated by the $\Delta(1232)$, and the η production by the $S_{11}(1535)$. The π^+ data show clear resonance structure in the region of the $D_{13}(1520)$. Resonance structure in the region of the $N^*(1700)$ is also clearly seen in the higher-energy $n\pi^+$ data, but has not been fully analyzed. Figs. 35 and 36 show some of the CLAS data taken at 4 GeV in the $p\pi^0$, $n\pi^+$, and $p\eta$ channels. The rates for the two different pion channels reflect the isospin structure of the various resonance contributions. The $\Delta(1232)$, with I=3/2, couples twice as strongly to the $p\pi^0$ channel as the higher-mass I=1/2 N^* resonances, which couple more strongly to the $n\pi^+$ channel, as is evident in Fig. 35. Fig. 36 shows the unique selectivity of the $p\eta$ channel for the $S_{11}(1535)$.

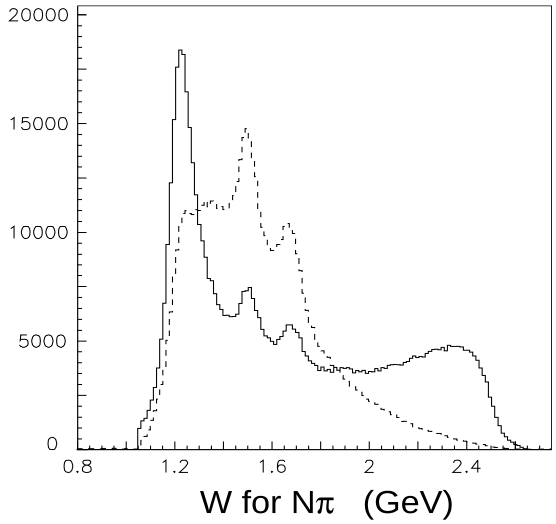

Figure 35: W dependence of the $p\pi^0$ (solid line) and $n\pi^+$ (dashed line) production yields at 4.05 GeV beam energy.

The isospin 1/2 of the dominant higher-mass states makes the $n\pi^+$ channel very attractive for the study of resonance transition amplitudes. A disadvantage is the large contribution due to the pion t-channel exchange term that dominates $n\pi^+$ production at forward angles. However, this contribution is quite well known, and is usually included in the analysis. Two states that we expect to be able to measure well in this channel are (1) the $D_{13}(1520)$ with a 50-60% branching ratio into $N\pi$, and (2) the $F_{15}(1680)$ with a 60-70% branching ratio to this channel [15]. We note that 2/3 of the $N\pi$ decays proceed through the $n\pi^+$ channel for these states. For the $D_{13}(1520)$ there is a strong competitor, the $S_{11}(1535)$, with a 30-40% branching ratio into the $N\pi$ channel. Fortunately, the strength of this state can be measured well in the $p\eta$ channel. Moreover, analysis of the angular distributions allows one to separate the d-wave behavior of the $D_{13}(1520)$ from the s-wave behavior of the $S_{11}(1535)$. Similarly, the $F_{15}(1680)$, which has an f-wave behavior, can be isolated from the competing $S_{11}(1650)$,

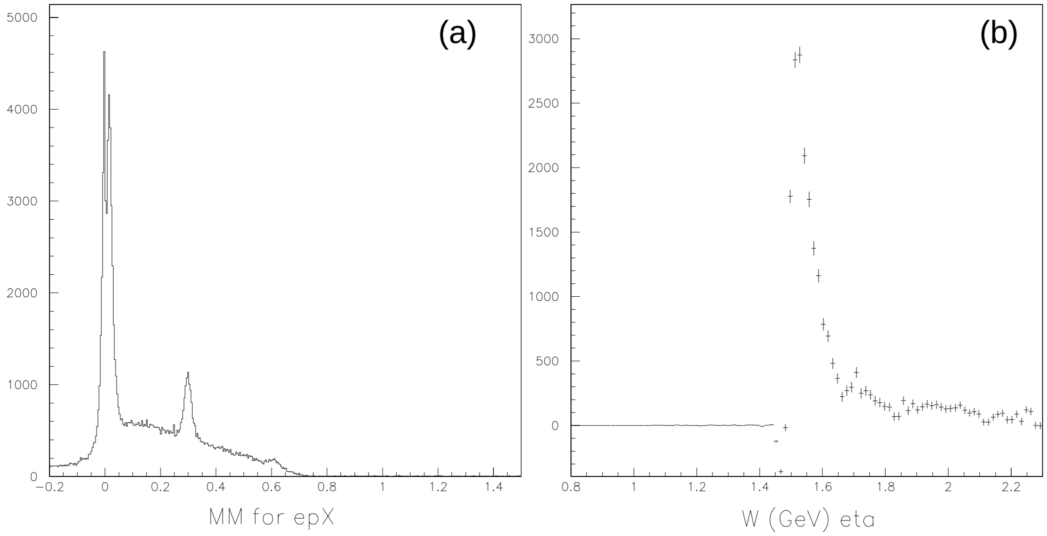

Figure 36: (a) Missing-mass squared spectrum of $ep \to e'pX$, (b) W dependence at 4 GeV beam energy corresponding to a cut in the missing-mass spectrum around the η mass with cuts on Q^2>2 (GeV/c)^2 and W<1.8 GeV. This spectrum clearly shows the $S_{11}(1535)$ peak.

which has an s-wave behavior. In addition to the partial wave analysis, another experimental handle is that the strength of the $S_{11}(1650)$ is constrained by its strong mixing with another s-state, the $S_{11}(1535)$.

In summary, the isospin selectivity of the $n\pi^+$ versus the $p\pi^0$ channel, and the $S_{11}(1535)$ selectivity of the $p\eta$ channel, will allow a very accurate determination of the transition multipole strength for the strongly excited nucleon and delta states.

5.3.2 Preliminary Results at High Energy

Isolating the single-meson channels at 6 GeV in CLAS will be more difficult than at lower energies, as discussed in section 3. The neutral-meson channels have been identified primarily by the missing mass of the final-state electron and proton. For the π^0 channel the major contaminant is the elastic radiative tail, which becomes worse at higher energies due to worsening missing-mass resolution. Fortunately, there are various cuts that can be selectively applied to essentially eliminate this contamination. For the η channel the most important contamination is multi-pion emission, and the radiative tails from lower missing-mass channels. However, these contaminations are relatively smooth functions of missing mass, and can be reliably subtracted. Fig. 37 shows the missing-mass distribution for $ep \to e'pX$ for various intervals of Q^2. The π^0 and η are clearly evident at even the highest Q^2 interval.

Although the statistical precision is low, the W distributions in Fig. 38 for the $n\pi^+$ channel show resonance behavior around 1.5 GeV, likely due to the excitation of $N^*(1520)$. The data also indicate an increase in the relative strength of the peak around 1.5 GeV in comparison with the $\Delta(1232)$ peak. Qualitatively, this is expected from the lower Q^2 data, where in comparison to higher-mass resonances, a faster fall-off of the $\Delta(1232)$ excitation with increasing Q^2 was observed.

Similar W plots for various values of Q^2 for the $p\pi^0$ and $p\eta$ channels are shown in Fig. 39. Note that for the $p\pi^0$ channel the dominant role of the $\Delta(1232)$ peak is reduced with increasing Q^2, and that the $S_{11}(1535)$ state dominates the $p\eta$ channel for all Q^2. These

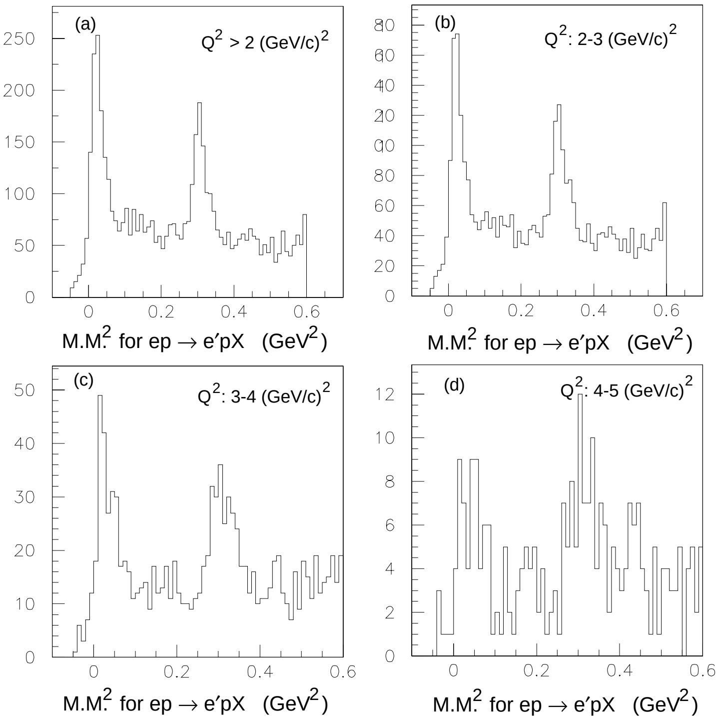

Figure 37: Missing-mass squared spectra for $ep \rightarrow e'pX$ data taken at 5.56 GeV for various bin of Q^2. NOT ACCEPTANCE CORRECTED.

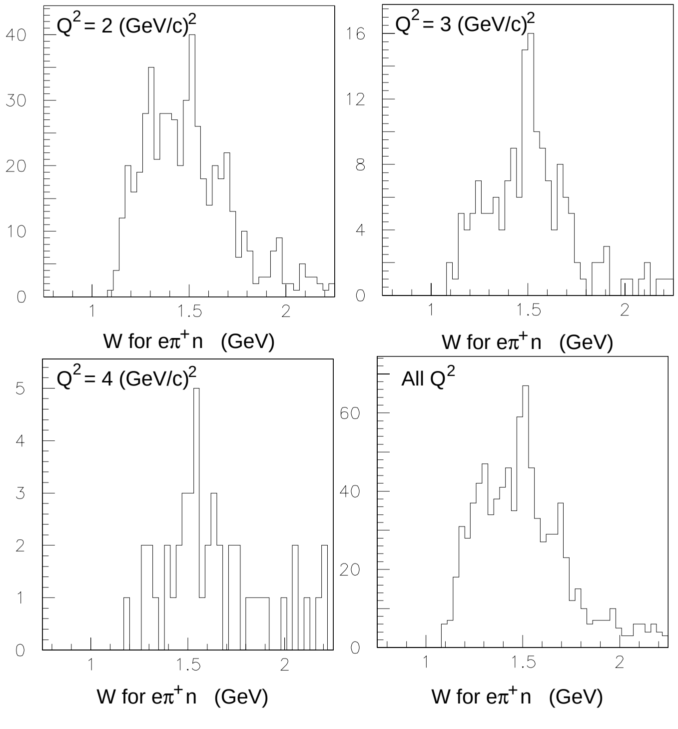

Figure 38: W dependence of the $n\pi^+$ yield at 5.56 GeV beam energy for various Q^2 bins. The $\Delta(1232)$ and a state with mass near 1.5 GeV are clearly visible, especially at high Q^2.

W spectra have included crude side-band subtractions.

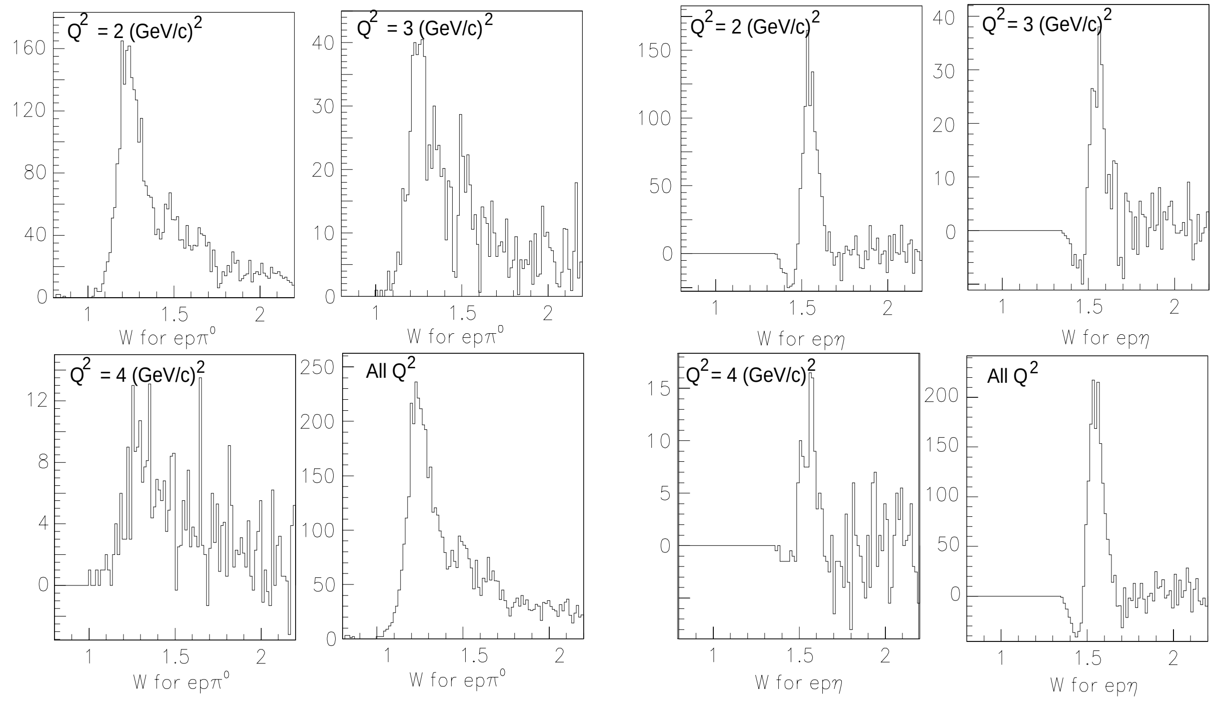

Figure 39: W dependence of the $p\pi^0$ (left) and $p\eta$ (right) yields at 5.56 GeV beam energy for various Q^2 bins. The $\Delta(1232)$ and $S_{11}(1535)$ states are clearly visible. Note that crude side-band subtractions have been performed on these spectra.

5.3.3 Proposed Measurements

We propose to extend the measurements of experiment E91-002 to 6 GeV. The kinematic range covered will be slightly larger in Q^2 than observed in the 5.56 GeV test run data. The differential cross section will be measured with a polarized electron beam as a function of the invariant mass W, the azimuthal hadronic angle ϕ_π, and the π^+ center-of-mass (CM) angle θ_π of the final-state pion. The differential cross section for this process can be written as:

$$\frac{d\sigma}{d\Omega_\pi} = \sigma_T + \epsilon\sigma_L + \epsilon\sigma_{TT}\cos 2\phi_\pi + \sqrt{\epsilon(\epsilon+1)/2}\ \sigma_{TL}\cos\phi_\pi + P_e\sqrt{\epsilon(1-\epsilon)/2}\ \sigma_{TL'}\sin\theta_\pi\sin\phi_\pi. \tag{6}$$

Out-of-plane measurements that allow a determination of the ϕ_π-dependence of the cross section enable a separation of the four response functions, $\sigma_T + \epsilon\sigma_L$, σ_{TT}, σ_{TL}, and $\sigma_{TL'}$. A separation of σ_T and σ_L is not required for this proposal as the resonance couplings are known to be mostly transverse. Moreover, information on longitudinal amplitudes can be extracted with greater sensitivity from the interference terms σ_{TL} and $\sigma_{TL'}$ than from the total cross section. However, we will have sufficient statistics in the lowest Q^2 bin to carry out such a separation with sufficient accuracy to add independent information and allow cross checks. As shown in Fig. 40 from analysis of 5.56 GeV CLAS data, full angular coverage in the polar and azimuthal pion angle is provided by the large acceptance of CLAS.

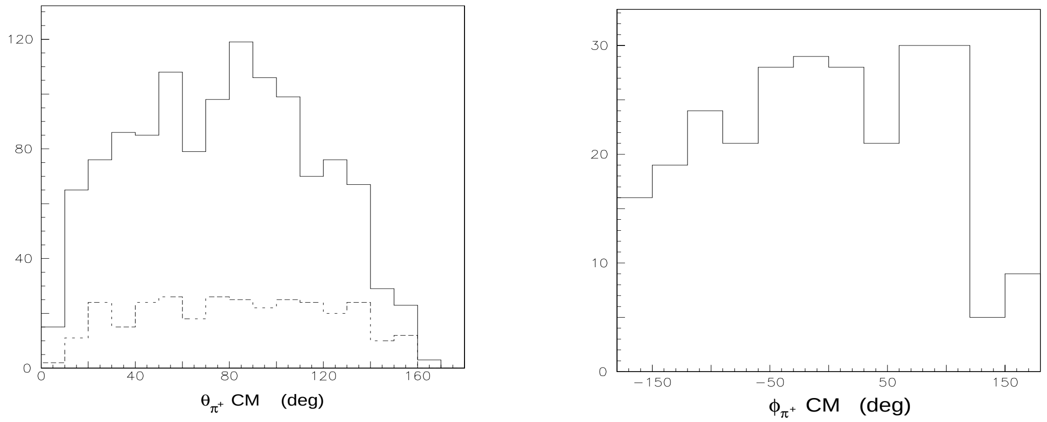

Figure 40: Pion polar and azimuthal angle distributions from 5.56 GeV $n\pi^+$ CLAS data in the hadronic center-of-mass system. The range in W is from 1.07 to 1.7 GeV. Solid line - all Q^2; dashed line - Q^2>2.5 (GeV/c)^2.

5.3.4 Expected Statistical Accuracy

The expected statistical accuracy for the $p\pi^0$ and $p\eta$ channels was presented in our previous high-Q^2 proposals and found to be favorable. Here we present the results from the test run at 5.56 GeV to obtain a reliable estimate of the expected $n\pi^+$ rates. We consider $n\pi^+$ production as a function of Q^2 in the resonance region. Table 3 shows our expected rates for a 1000 hour run at a luminosity of 1×10^{34} cm^{-2}s^{-1} with a detector and data collection efficiency of 100%. We expect to bin the data into 12 W bins of 50 MeV, 6 ϕ_π bins, and 10 θ_π bins, for a total of 720 bins. This will result in sufficient statistics per bin for the physics analysis, even at the highest Q^2. The lowest Q^2 bin will overlap with the data taken at 4 GeV. For this Q^2 value, we may also attempt a σ_L/σ_T separation.

W = 1.1 - 1.8 GeV				
Q^2 (GeV/c)^2	1.5 - 2.5	2.5 - 3.5	3.5 - 4.5	4.5 - 5.5
no acceptance cuts	950k	300k	70k	26k
w/electron cuts	180k	220k	66k	24k
w/e$^-$, π^+ cuts	135k	185k	52k	20k

Table 3: Estimated rates in the $n\pi^+$ channel for a 1000 hour run.

5.3.5 Data Analysis

The techniques developed for analyzing the data at lower energies will be fully applicable at 6 GeV. The raw data are converted to cross sections using acceptances obtained from the GEANT-based CLAS GSIM simulation package. A Fortran program was written to perform radiative corrections to the exclusive data. This program has already been used to correct the $p\pi^0$ and $n\pi^+$ data at lower energies.

The cross section data will be analyzed first with a partial wave analysis and a multipole analysis in the $n\pi^+$ channel alone. This will allow checks of the integrity of the data. Next we will perform a partial wave analysis of combined data in the $p\pi^0$ and $p\eta$ channels. By utilizing the selectivity for each of the decay channels, more accurate information will be obtained about weaker states by including information from all channels, with different flavor compositions. This will allow us not only to identify the partial wave content, but also the isospin of the resonant state. The single-channel analyses allow consistency checks, since all channels must give the same results within the accuracy of the analysis. The multi-channel analysis provides many more constraints and much reduced fit uncertainties.

In contrast to general belief, partial wave analyses of higher-mass states at high Q^2 should become easier. This is due to the reduced strength of the $\Delta(1232)$ at high Q^2, as well as the dominance of the D_{13} and F_{15} resonances that can be used as constraints to the fit.

There are currently a number of groups that have developed analysis codes that are applicable for the expected data, including an "isobar" approach [16], a fixed-t dispersion relation integration procedure [17], and effective Lagrangian-based procedures [18, 19, 20]. The isobar model that was developed includes resonant and non-resonant amplitudes. The resonances are parameterized in terms of relativistic Breit-Wigner forms with momentum-dependent widths. The background is due to single-pion Born terms at the tree level with absorption terms to conform to unitarity constraints. Additional background is modeled with correct threshold behavior for the multipoles, and with high momentum fall-off as required by pQCD. The dispersion-relation approach uses an integration over the entire W range including the resonance region and the deep inelastic region. A K-matrix unitarization method is used in this analysis. The two methods have been used on the same data for the $p\pi^0$ channel in the $\Delta(1232)$ region and give consistent results for the E_{1+}/M_{1+} ratio of the $N\Delta$ transition. We will continue to refine the analysis methods, e.g. by using more flexible parameterizations for the background amplitudes.

Several theoretical groups have developed dynamical effective Lagrangian models. Although they are consistent among themselves, a theoretical controversy has developed regarding the role of channel coupling between resonant and non-resonant amplitudes in the interpretation of the resonances.

5.3.6 Summary

A test run at 5.56 GeV has demonstrated the feasibility of experiment E91-002 to use 6 GeV incident electrons on a proton target in the CLAS detector to study electro-excitation of nucleon resonances at high Q^2 through a measurement of the $n\pi^+$, $p\pi^0$, and $p\eta$ decay channels. The analysis procedures developed for lower energy measurements in CLAS can be applied for this work. With a 40 day run using a 6 GeV beam, good statistical accuracy can be achieved for both all the single-meson channels considered.

5.4 N^* Excitations at High Q^2 in the Two-Pion Channel

Spokespersons: M. Ripani[a] and V.D. Burkert[b]

[a]INFN-Sezione di Genova, Genova, Italy, I-16146
[b]Jefferson Laboratory, Newport News, VA 23606

Any constituent quark model incorporating the basic features of approximate SU(6) symmetry with explicit flavor-breaking terms, a spin-spin interaction, and a confining potential, can give a satisfactory account of a number of general properties of baryon states, such as the main static properties of the ground state and the first excited states. However, besides the well-known problems involving electromagnetic properties, such as differences between calculated and measured transition form factors, there are problems regarding the number of states. The symmetric quark model predicts more states in the second orbital band than are seen in experiments. This problem of "missing states" has stimulated the development of other models.

Quark models with hyperfine mixing and explicit meson couplings predict a very weak pion coupling to some states, which decay predominantly through multi-pion channels [21], a decay channel experimentally observed in many high-lying states. Since the evidence for the existence of resonant states is primarily derived either from pion-nucleon reactions or from photo-production of one-pion final states, the lack of evidence for baryon states with a very small pion coupling is not surprising. Models based on various meson creation assumptions found similar results [22, 23, 24]. Other models offer alternative explanations for the missing states. For instance the Quark Cluster Model [25], which has fewer spatial degrees of freedom, predicts fewer states. A table of established resonant states with sizeable branching ratios in the two-pion channel, as well as a table reporting predicted missing states with large two-pion branches, can be found in the proposal for E93-006.

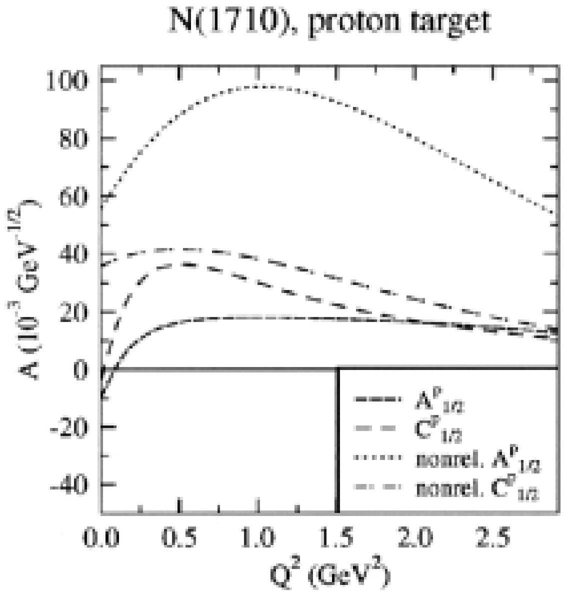
N(1710), proton target

Figure 41: Prediction from Ref. [26] for the photocoupling of the $N(1710)$. The dotted line is the non-relativistic calculation for the transverse photocoupling, while the dashed line is the result of the relativistic calculation.

It is well known that the non-relativistic quark model is not successful in describing the Q^2 evolution of the elastic form factors or the transition to the $\Delta(1232)$ [26]. Although experimental information about the transition form factors for higher-mass resonances is more limited, serious discrepancies between the predictions of the non-relativistic quark model and the extracted amplitudes for these states have been observed. Some models, such as that of Ref. [26], show sizeable changes in the Q^2 evolution of the photocouplings by using some specific prescriptions for incorporating relativity into the quark model. One example for a particular high mass resonance is shown in Fig. 41. On the other hand, from the analysis of Ref. [27], there is the claim that non-perturbative ingredients, in conjunction with a constituent quark form factor derived from the elastic proton and $N-\Delta$ experimental data, can describe resonance photocouplings up to Q^2=10-20 (GeV/c)^2.

If a satisfactory description of the excitation of higher-mass resonances at high Q^2 can not be provided by a relativistic constituent quark model or by the introduction of new ingredients such as constituent quark form factors, an explanation in terms of the onset of different physics (pQCD) may be in order. The predictions of the asymptotic behavior of resonance photocouplings made by the pQCD calculations are very specific. Measuring the Q^2 evolution of the photocouplings to the higher-mass states, which are difficult to access by studying single-pion production, will provide a broader picture of the approach to the asymptotic regime. Moreover, both isospin 1/2 and 3/2 resonances can contribute to two-pion electroproduction. The CLAS detector [28, 29], with its high luminosity, large acceptance, and good momentum resolution, along with a beam energy of 6 GeV, provides an ideal opportunity to study multi-particle final states over a Q^2 range that may show phenomena related to the breakdown of constituent quark models, and the onset of pQCD [30].

5.4.1 CLAS Data from the 1998 4 GeV Electron Run

A total of about 20 M inclusive electrons were collected in the 4 GeV e1 run in February 1998. The data were analyzed using standard particle identification procedures developed for CLAS. To get the overall yield for two-pion final states, we selected four reaction topologies:

- $ep \to e'p\pi^+$ (missing π^-)
- $ep \to e'p\pi^-$ (missing π^+)
- $ep \to e'\pi^+\pi^-$ (missing p)
- $ep \to e'p\pi^+\pi^-$ (complete detection)

A preliminary approximate procedure was developed to estimate the detector acceptance and reconstruction efficiency as a function of W in each Q^2 bin. The procedure was based on throwing Monte Carlo events in the Q^2/W space subtended by CLAS, passing them through the GEANT detector simulation, and then applying the same reconstruction and identification chain as used for the analysis of the experimental data. In this way both the acceptance and the reconstruction efficiency were derived in a somewhat model-dependent way, as there was no specific binning in the hadronic variables. The resulting corrections for the acceptance and reconstruction efficiency were then applied to the data. Radiative corrections were not applied in this analysis. These analysis indicated good agreement with existing data from an old DESY experiment [31], indicating that our normalization was reasonably understood. Fig. 42 shows W spectra from analysis of high-field 4 GeV CLAS data for the reaction $ep \to e'\Delta^{++}\pi^-$ for two different Q^2 bins. The overall acceptance for the two-pion events in CLAS is $\approx$5%. At higher Q^2 values, structures corresponding to excited resonances are apparent.

5.4.2 CLAS Data from the 1999 5.56 GeV Electron Run

The data from the short 5.56 GeV test run in March 1999, which used a 90% torus field, were analyzed with the detector calibrations derived for 4 GeV. We analyzed a total of 1.3 M events, of which about 140,000 contain an electron track. In Fig. 43a the inclusive electron spectrum as a function of W for all Q^2 is shown, while in Fig. 43b the data are restricted

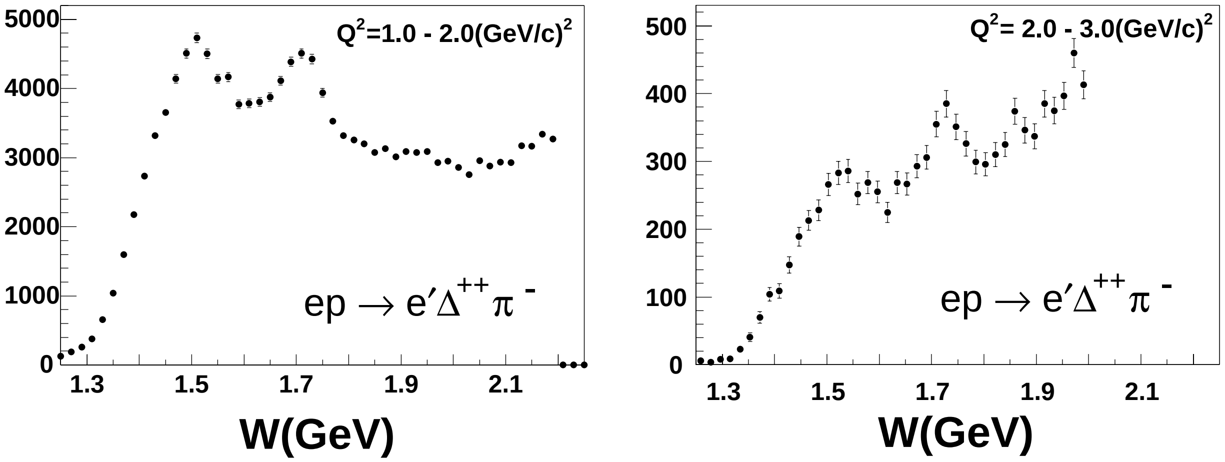

Figure 42: W distribution from 4 GeV high-field CLAS raw data for the $ep \to e'p\pi^+\pi^-$ reaction with a cut on the Δ^{++} mass in the $p\pi^+$ invariant-mass spectrum for two different Q^2 bins. No detector corrections are applied.

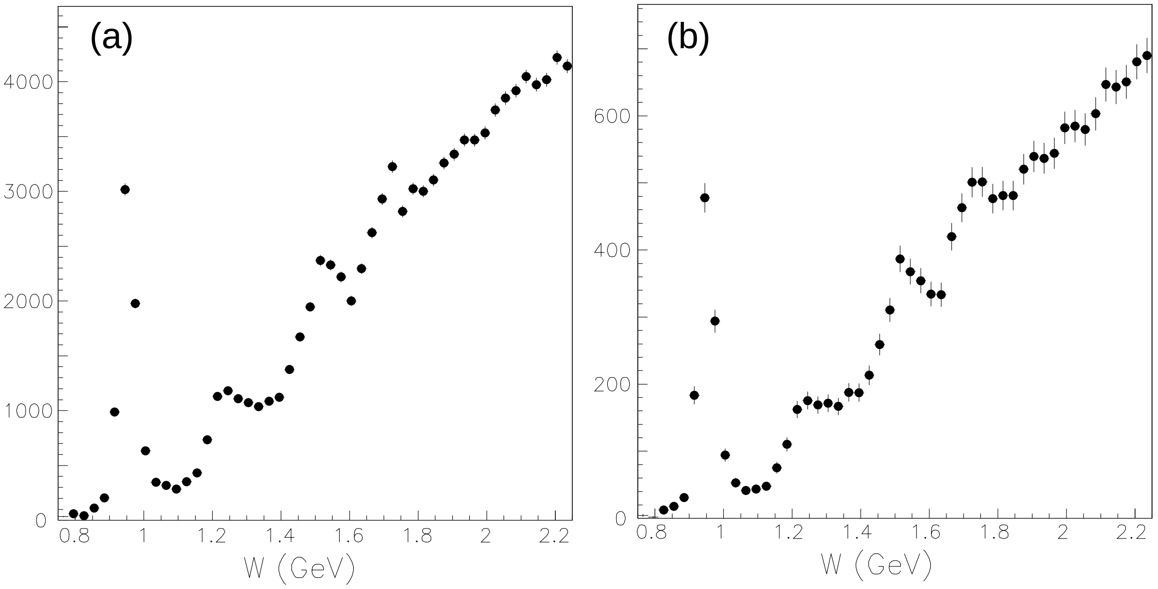

Figure 43: W distribution from 5.56 GeV CLAS raw data for the inclusive electron scattering for (a) all allowed Q^2 values and (b) Q^2 values between 2.5 and 3 (GeV/c)^2. Errors are statistical only and no detector corrections are applied.

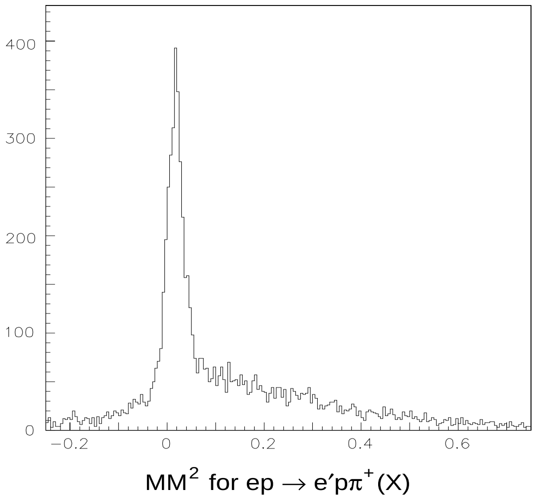

Figure 44: Missing-mass squared distribution from 5.56 GeV CLAS data for the $ep \to e'p\pi^+$ events. Errors are statistical only and no detector corrections are applied.

to Q^2 from 2.5 to 3 (GeV/c)^2. In both spectra, resonance structures are clearly visible, and the known fast fall-off of the $\Delta(1232)$ production relative to elastic scattering is evident.

To get an idea about the two-pion yield, we selected the $ep \to e'p\pi^+$ (missing π^-) event topology for the two-pion final-state identification. In Fig. 44 we show the missing-mass distribution for events belonging to that topology. The missing π^- peak is clearly visible, although not perfectly calibrated due to the use of previous calibration constants, showing that reaction discrimination should still be possible at these energies.

Using data in the missing-pion peak, we estimated the two-pion yield. For all Q^2 values we got about 800 events, while for Q^2 values between 2.5 and 3 (GeV/c)^2 we got about 100 events. Overall, two-pion production with all four topologies will be about 30% more. Assuming a DAQ rate of about 1500 Hz and a 50% overall data collection efficiency, it will be possible to collect about 60 M triggers per day, corresponding to about 50,000 overall two-pion events per day, of which about 6,000 will be in the Q^2 range from 2.5 to 3 (GeV/c)^2. In 40 days of operation we should collect about 240,000 two-pion events in that Q^2 bin. Using 30 bins in W, this would result in about 8,000 high Q^2 two-pion events per W bin, enough for a reasonable analysis in the W and Q^2 two dimensional space, and probably enough to even make an analysis in other hadronic kinematical variables like the invariant masses of hadronic pairs.

5.4.3 Data Analysis

To analyze the data from two-pion production, efforts have been made by a collaboration between INFN, the University of Genova, and the Nuclear Physics Institute of Moscow State University [32] to incorporate a phenomenological analysis of the data. This has been based on a diagrammatic description of the basic non-resonant reaction mechanisms in two-pion electroproduction, along with a standard parameterization of the resonance contributions in terms of photocouplings and decay amplitudes. With this set of codes it will be possible to make a first analysis of quantities such as the total cross section and invariant-mass distributions in order to extract information on resonant states with sizeable branches in the two-pion channel.

5.4.4 Summary

In the first data from CLAS it is already possible to recognize the N^* formation in two-pion final states with good statistics even at relatively high Q^2, around 2 (GeV/c)^2. Measurements at higher momentum transfer will be important in understanding the nature of the excitation in terms of relativistic quark models and perturbative QCD. They will also provide comparisons of the behavior with increasing Q^2 of specific resonance transitions and the related background. With a 40 day run using a 6 GeV beam, good statistical accuracy can be achieved for both the single meson and two-pion channels.

5.5 Measurement of η' Electroproduction

Spokespersons: F.J. Klein[a] and J.A. Mueller[b]

[a]Jefferson Laboratory, Newport News, VA 23606
[b]University of Pittsburgh, Pittsburgh, PA, 15260

5.5.1 Physics Motivation

The electroproduction of the pseudoscalar meson η' has not yet been investigated. The scarce photoproduction data show a strong excitation near threshold (W=1.896 GeV) that is interpreted as s-channel resonance production (cf. section 5.5.3). As the threshold energy of the reaction $\gamma^{(*)}p \to \eta' p$ is above the second resonance region, data from this reaction may provide an excellent probe to the structure of resonances around 1.9 to 2.3 GeV. Because of its vanishing isospin, η' only couples to $N^*(I = \frac{1}{2})$ states, and hence simplifies the extraction of the resonant state. The background t-channel exchanges involve the vector mesons ρ^0 and ω, where the coupling to the ρ is about 10 times larger than the coupling to the ω, corresponding to the radiative decay widths into ρ^0 and ω. Near threshold, however, contributions of t-channel exchange mechanisms are expected to be small.

Investigation of the properties of the η' meson itself is of great theoretical interest in its own right as these are related to fundamental questions of QCD. One of the most challenging questions concerning the classification of light mesons is the relation of the comparatively heavy η' meson ($m'_\eta = 957.8$ MeV) to the flavor singlet state of the SU(3) 0^- nonet. Contrary to the 1^- nonet, for instance, linear and quadratic mass formulae do not hold for the 0^- nonet due to the large mass difference between the η and the η' [3, 33, 34]. The masses of both physical particles can only be fitted when adding a large gluonic contribution of the flavor-singlet state [35, 36].

Information about the quark content of η and η' is crucial to settle the question of the flavor singlet in the 0^- nonet [34, 37]. This is conveniently expressed in terms of a mixing angle θ between the flavor-singlet combination η_0 and the flavor octet η_8 as:

$$\eta = \eta_8 \cos\theta - \eta_0 \sin\theta, \qquad \eta' = \eta_8 \sin\theta + \eta_0 \cos\theta. \tag{7}$$

The fit to the quadratic mass formula that includes a gluonic term corresponds to a mixing angle $\theta \simeq -18.2^\circ$. Measurements of η and η' decays that have been performed at e^+e^- colliders yield $\theta \simeq -18.4 \pm 2^\circ$ [38].

Connection to this experiment comes through the extended Goldberger-Treiman relation for the flavor singlet. It relates these questions of the so-called $U_A(1)$ anomaly to the isosinglet charge $g_A^{(0)} = \Delta u + \Delta d + \Delta s$, and hence to the spin structure function $g_1(x, Q^2)$ of the nucleon [39]. The relationship can be written as the sum of two terms involving the coupling of the η' and a pseudoscalar glueball object G to the nucleon [40]:

$$2mg_A^{(0)} = Fg_{\eta' NN} + \frac{1}{2f}F^2 m_{\eta'}^2 g_{GNN}, \tag{8}$$

where F is a scale-invariant decay constant and f=3 is the number of light flavors.

η' production above the resonance region ($W > 2.3$ GeV) with electromagnetic probes can contribute to the measurement of the $\eta' NN$ coupling. However, the existing photoproduction data show little strength above the resonance region (cf. Fig. 45). In this experiment we will focus on the resonance production of η'.

5.5.2 Baryon Resonances Coupling to η'

The quark-model calculations by Capstick and Roberts [9] predict coupling to η' for the resonances below 2.5 GeV/c^2 listed in Table 4. Tentative matching to observed resonances is also shown. No resonance in this table has been observed to decay into η'.

The strength of the coupling to $N\eta'$ in electromagnetic excitation can be estimated by the product [41]:

$$\chi_\lambda = |A_{N\eta'}||A_\lambda|/\Gamma_{tot}, \qquad \lambda = 1/2, 3/2. \tag{9}$$

Based on this quark-model calculation, we find that only two N^* resonances may contribute to the reaction $\gamma^{(*)}p \rightarrow \eta' p$ with reasonable strength: $N\frac{3}{2}^-(1960)$, $N\frac{1}{2}^-(2030)$. The first of these resonances is not firmly established, and the second has not been experimentally observed.

The RPI group has studied the $\eta' NN^*$ coupling using an effective Lagrangian approach [41]. They took into account the S_{11} and D_{13} resonances around 2 GeV/c^2 predicted by the Capstick-Roberts quark model (see Table 4). They found that the main contribution to the η' photoproduction amplitude comes from the $D_{13}(2080)$ alone, with contributions from higher-spin states (J=5/2, 7/2) being negligible. Their analysis implies that the η' meson is an important probe to study the properties of this resonance. A surprising aspect from their results is that the E_{0+} multipole, to which $D_{13}(2080)$ contributes as a background, provides most of the strength of the photoproduction cross section from threshold to W=2.2 GeV, whereas the resonant multipoles E_{2-} and M_{2-} are less important.

However, the RPI analysis truncates the model space because it discards off-shell contributions from resonances in the second resonance region. This was pointed out by Li [42] whose investigation of η' photoproduction is based on the framework he developed for meson photoproduction from the nucleon in the quark model [43]. His result is also surprising; the threshold behavior of the η' photoproduction is dominated by off-shell contributions from s-wave resonances in the second resonance region, especially the $S_{11}(1535)$. Additionally – and contrary to the results of Mukhopadhyay *et al.* –, the higher-spin states, especially the $G_{17}(2190)$ for the N=3 band and $H_{19}(2220)$ for the N=4 band, give major contributions to the η' cross section.

5.5.3 Previous Experiments

The pseudoscalar meson η' has not yet been studied in electroproduction. Even for photoproduction there are only few data available. The data set of the early experiments [44,

Model State	$N\pi$ State,Rating	$A^p_{\frac{1}{2}}$	$A^p_{\frac{3}{2}}$	$A_{N\eta'}$	Γ^{tot}	$\chi^2_{1/2}$	$\chi^2_{3/2}$
$[N\frac{3}{2}^+]_3(1910)$		-21	-27	-0.2	368	0.12	0.23
$[N\frac{3}{2}^+]_5(2030)$		-9	+15	+0.2	74	0.58	1.68
$[N\frac{5}{2}^+]_3(1995)$	$F_{15}(2000)$ **	-18	+1	+0.2	174	0.44	0.
$[N\frac{7}{2}^+]_1(1980)$	$F_{17}(1990)$ **	-1	-2	-0.2	46	0.02	0.06
$[N\frac{1}{2}^+]_6(2065)$	$P_{11}(2100)$ *	-12		-0.6	245	0.84	
$[N\frac{7}{2}^+]_2(2390)$		-14	-11	+1.3	134	18.49	11.45
$[N\frac{7}{2}^+]_3(2410)$		+1	-1	-1.1	51	0.44	0.44
$[N\frac{9}{2}^+]_1(2350)$	$H_{19}(2220)$ ****	-29	13	+0.2	58	0.96	2.02
$[N\frac{1}{2}^-]_3(1945)$	$S_{11}(2090)$ **	+12		-3.6	454	9.03	
$[N\frac{1}{2}^-]_4(2030)$		+20		+1.3	85	93.63	
$[N\frac{3}{2}^-]_3(1960)$	$D_{13}(2080)$ **	+36	-43	+2.3	429	37.25	52.91
$[N\frac{3}{2}^-]_4(2055)$		+16	0	+0.1	268	0.04	0
$[N\frac{5}{2}^-]_2(2080)$		-3	-14	+3.1	343	0.026	0.126
$[N\frac{5}{2}^-]_3(2095)$	$D_{15}(2200)$ **	-2	-6	-0.2	171	0.68	0.05
$[N\frac{7}{2}^-]_1(2090)$	$G_{17}(2190)$ ****	-34	+28	+0.6	162	15.88	10.82

Table 4: $N\eta'$ decay amplitudes for N^* resonances below 2.5 GeV/c^2 in the Capstick-Roberts quark model. The $N\pi$ state and rating are taken from Ref. [15]. Helicity amplitudes are in units 10^{-3} GeV$^{-\frac{1}{2}}$ and decay amplitudes in units of MeV$^{\frac{1}{2}}$. A factor of $+i$ is suppressed for the negative-parity states. The coupling strength χ^2_λ is given by expression (9) in units of 10^{-3} MeV^{-2}.

45] consists of only eight cross section points with poor statistics between $E_\gamma = 1.7-6.2$ GeV. The recently published SAPHIR data [46] for η' photoproduction near threshold contain the total and differential cross section in seven energy bins between threshold and E_γ=2.64 GeV.

The shape of the total cross section, shown in Fig. 45, suggests dominant resonance production near threshold. For η photoproduction, a similar peak in the cross section near threshold signals a single strong resonance. Here the interpretation is likely to be more complicated. As the angular distribution is forward peaked in each energy bin, resonant production requires at least two interfering amplitudes of opposite signs. As shown in Fig. 46, the differential cross section can be fit reasonably well by assuming two multipole contributions, E_{0+} and M_{1-} as:

$$\frac{d\sigma}{d\Omega} = \frac{q^*_{\eta'}}{k^*_\gamma}(A + B\cos\theta^* + C\cos^2\theta^*), \tag{10}$$

where parameter C was consistent with zero for all energy bins. In this expression the parameters A and B can be expressed as:

$$A = |E_{0+}|^2 + |M_{1-}|^2, \quad B = -2Re(E^*_{0+}M_{1-}). \tag{11}$$

Best fit values for the induced S_{11} and P_{11} resonances, assuming that the competing channel is $N^* \to \pi N$, were obtained for the following masses, widths, and branching ratios:

S_{11} ($M = 1.897 \pm 0.010$ GeV, $\Gamma = 0.396 \pm 0.155$ GeV, b'_η=5%)
P_{11} ($M = 1.986 \pm 0.026$ GeV, $\Gamma = 0.296 \pm 0.100$ GeV, b'_η=25%).

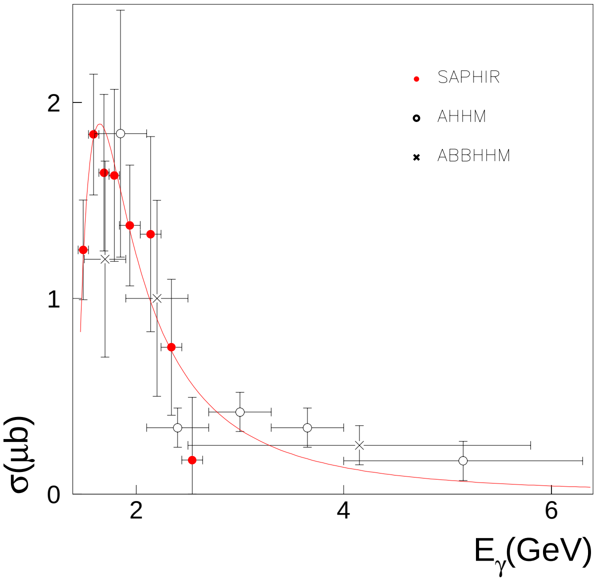

Figure 45: Measured η' total cross section for $\gamma p \to \eta' p$ from SAPHIR data (•) [46], from ABBHHM (×) [44], and from AHHM (○) [45]. The solid curve represents the two-resonance fit to the SAPHIR data.

Except for the mass of the P_{11}, the extracted values are compatible, within errors, with PWA results of Manley [48].

The photoproduction of η' will also be studied with CLAS in an experiment that has already taken first data [47]. This experiment promises much greater statistics than any of the currently published photoproduction experiments of η'.

5.5.4 Experimental Method

The η' cannot be simply identified by missing-mass cuts in the electroproduction data if only the scattered electron and recoil proton are reconstructed. The probability that additionally all the η' decay products are measured in CLAS is too low. Candidates for the reaction $ep \to e'p\eta'$ will be identified via selected cuts on the reconstructed quantities. The most promising procedure at present involves looking for a peak in the $ep \to e'pX$ missing-mass distribution for certain semi-exclusive modes. Table 5 shows all decay modes for the η' and η mesons with branching ratios greater than 1%. The η' signal can then be enhanced by careful cuts that selectively delete events from competing processes.

Decay Mode	Fraction (%)	Decay Mode	Fraction (%)
$\eta' \to \pi^+\pi^-\eta$	43.7 ± 1.5	$\eta' \to \rho^0\gamma$	30.2 ± 1.3
$\eta' \to \pi^0\pi^0\eta$	20.8 ± 1.3	$\eta' \to \omega\gamma$	3.02 ± 0.30
$\eta' \to \gamma\gamma$	2.12 ± 0.13	$\eta' \to \pi^+\pi^-\pi^0$	< 5
$\eta \to \pi^0\pi^0\pi^0$	32.1 ± 0.4	$\eta \to \pi^+\pi^-\pi^0$	23.2 ± 0.5
$\eta \to \gamma\gamma$	39.25 ± 0.31	$\eta \to \pi^+\pi^-\gamma$	4.78 ± 0.12

Table 5: Decay modes for η' and η with branching fractions greater than 1% (cf. Ref. [15]).

Large coverage in W, Q^2, $\theta^*_{\eta'}$, and ϕ^* will give us the opportunity to span the whole W regime where resonance production may contribute, and to extract the N^* candidates by

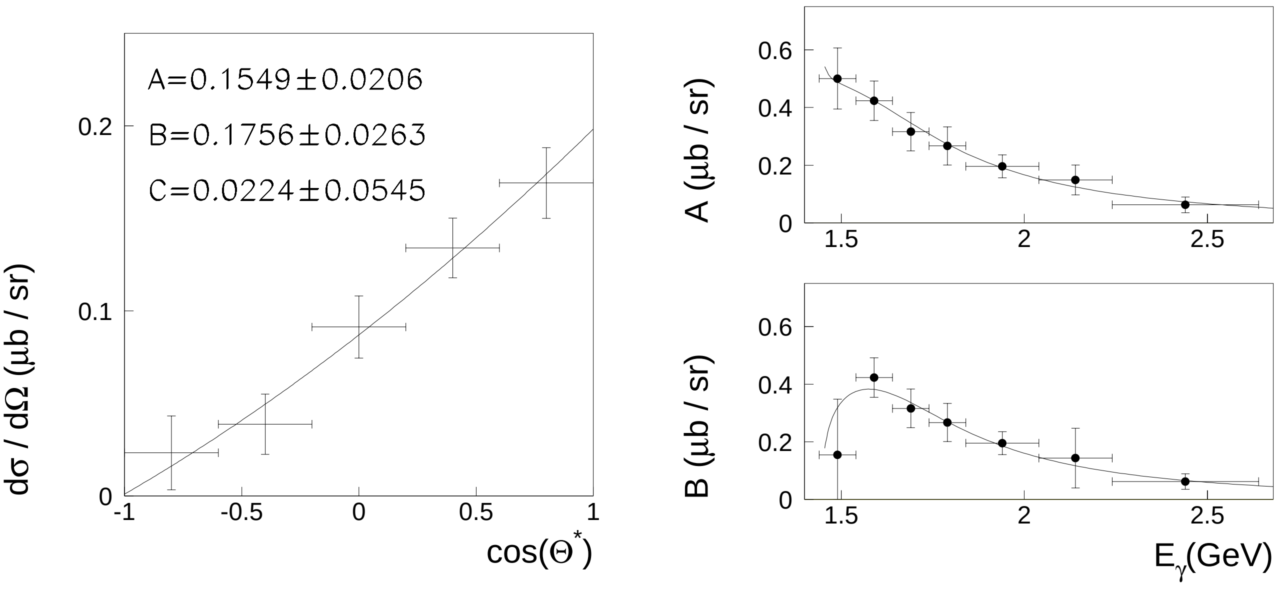

Figure 46: Differential cross section for $\gamma p \to \eta' p$ between threshold and E_γ=2.62 GeV (left) and fit parameters for each energy bin as defined in the text (right).

fitting to the total and differential cross section. For a limited range in W and Q^2, we expect sufficiently high statistics to separate the structure functions $\sigma_T + \epsilon\sigma_L$, σ_{TT}, and σ_{LT}, which gives access to the photon-excitation amplitudes.

5.5.5 Identifying η' in the e1 data at 4.0 GeV

In March 1998, CLAS took data with a proton target and 4 GeV electrons as part of the e1 run group. The total beam time was approximately one beam day that was split 2:1 between "high-field"(B/B_0=88%) and "low-field" (B/B_0=60%) torus settings. Many more data were taken in 1999, but as of yet, only a small fraction have been processed to the point where analysis can be done. A fairly complete analysis of the 1998 e1 data has been performed; the 5.56 GeV data taken in March 1999 has also been examined in a preliminary way. With the limited statistics of these data, only a small sample of η' candidates can be extracted. The results do indicate that we can extract η' signals, and the rates are consistent with expectations from Monte Carlo studies. Although the 4 GeV data taken in 1998 amount to only a few percent of the total 4 GeV data when e1 running is complete, it does allow identification of the modes in which the reaction $ep \to e'p\eta'$ can be measured. For a final analysis, all modes with reasonable statistical accuracy will be combined in order to obtain the best overall result.

Since the η' decays to π^0s in many ways, cuts on the number of photons are useful. For events reconstructed in the low-field data with an electron, proton, and two photons, the missing mass ($MM_{e'p}$) can be plotted. The data in Fig. 47 has no additional cuts, and an enhancement around the η' is already evident. By comparing the data near the η' mass with Monte Carlo simulation of η' production in CLAS, additional means to separate the signal can be determined. For the Monte Carlo, the η' was allowed to decay into one of the dominant decay modes $\eta' \to \rho\gamma$ or $\eta' \to \eta\pi\pi$. In Fig. 48, one can see that the data is dominated by π^0 production, while the true η' events divide into two regions resulting from the acceptance of the CLAS calorimeter, and the combinatorics in multi-photon decay modes of the η' (η' can decay into as many as ten photons). The low $M_{\gamma\gamma}$ events in the Monte Carlo occur when the two photons come from the same, or more often, different π^0s. The events at higher $M_{\gamma\gamma}$ occur when at least one of the photons comes from $\eta \to \gamma\gamma$ decays.

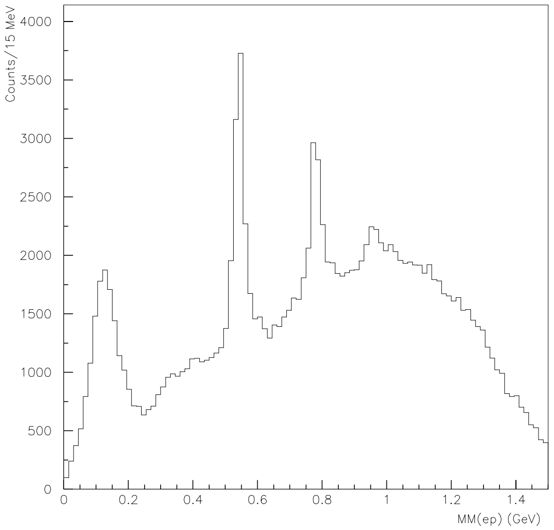

Figure 47: $e'p$ missing-mass distribution for events with at least 2 photons. This plot is from the low-field 4 GeV data taken in 1998. Easily seen are the π^0, η, and ω peaks, as well as a bump at the $\eta'/f_0/a_0^0$ mass.

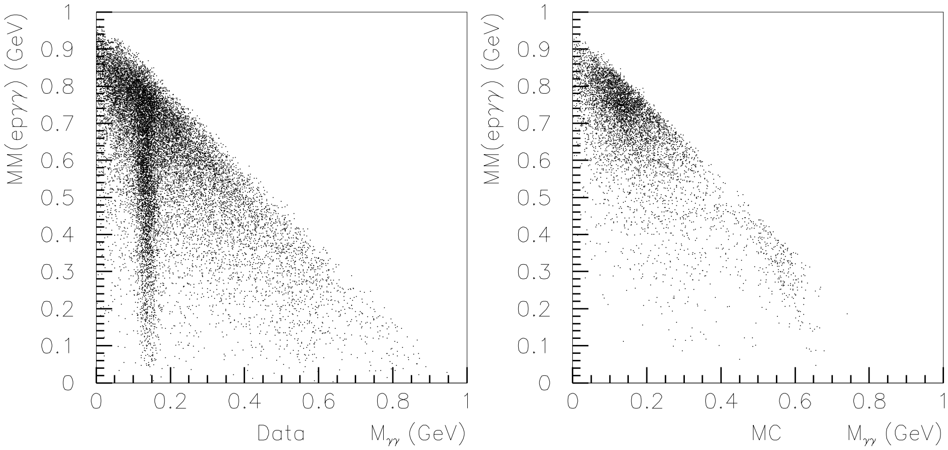

Figure 48: Scatter plots of the missing mass in events with an electron, proton and at least two photons ($MM_{ep\gamma\gamma}$) verses the two photon mass. The left plot is from 4 GeV low-field data from 1998, while the right plot is the η' Monte Carlo.

The charged η' decay modes can also be identified by using CLAS. For the case when four charged particles (e, p, π^+, π^-) are reconstructed, the η' channel can be identified via its radiative decay to ρ^0 (missing γ) or via the decay mode $\eta' \to \pi^+\pi^-\eta$ as shown in Fig. 49 for the 4 GeV data set where the plots on the right side show the distribution after a mass cut on the missing η. The low-field data has higher acceptance for the soft pions, but the high-field data corresponds to twice as much beam time. A striking feature of this channel is the large rate for $e'p\pi^+\pi^-\eta$ for W >2.3 GeV (cf. difference between solid and dotted lines in top left figure). None of this rate appears to come from η' production. The data are too few to allow us to definitely determine the source of these events at this time. The larger data sets being acquired, plus the additional reach into this higher W region afforded by the 6 GeV data, will allow us to investigate this channel more thoroughly.

For the case that three charged particles (e', p, π^+) and one photon are measured, the missing-mass distributions MM_{ep} in various W bins show a small signal around the η' mass that may be contaminated by a_0 production (cf. Fig 50). The low signal to noise ratio does not favor the extraction of the signal, whereas with an additional cut on a π^- in the missing mass, the radiative decay $\eta' \rightarrow \rho\gamma$ can be identified. In Fig. 51 one sees a clear η' peak for events with $0.00 < MM^2_{ep\pi^+\gamma} < 0.05$ as indicated by the Monte Carlo with the additional cut that $|M_{\pi^+(\pi^-)} - M_\rho| < \Gamma_\rho$. This mode shows a reasonably low background and a reasonably high CLAS acceptance.

5.5.6 Backgrounds

The backgrounds to this reaction come from two sources, multi-pion production, and production of meson resonances near the η'. The former produces a large but smooth background underneath the peak, while the latter can yield structure that could be hard to disentangle from the signal.

The two resonances closest to the η' are the $a_0(980)$ and $f_0(980)$. Very little is known about the electroproduction of these resonances. An experiment at CLAS is planning to measure the f_0 through the decays $\pi^+\pi^-$ and K^+K^- using the same data sets we are working with. The Omega experiment measured the photoproduction of $a_0^+ \rightarrow \eta\pi^+$ at higher energies in the reaction $\gamma p \rightarrow a_0^+ n$ [49]. There is no evidence for a_0^0 production, consistent with what one would expect from the Born terms. Thus we expect a small contribution from a_0^0 at our energies, unless there is a threshold enhancement due to $N^*/\Delta^* \rightarrow a_0^0 p$.

The sensitivity to the a_0^0 and f_0 depends on our mode of reconstructing the η'. In the reaction $ep \rightarrow e'p\gamma\gamma X$, both the $a_0^0 \rightarrow \pi^0\eta$ and $f_0 \rightarrow \pi^0\pi^0$ modes can contribute if they are produced at appreciable rates. Our Monte Carlo studies indicate that the acceptance for the neutral a_0 production is comparable to that for η'. By using the more fully reconstructed modes, $\pi^+\pi^-(\eta)$ and $\rho\gamma$, we can eliminate the a_0 and f_0, since they don't decay to these modes. Unfortunately the $\pi^+\pi^-(\eta)$ mode seems to have too low an acceptance to use for the η' search, except as a check on the more inclusive reconstruction methods. The mode $\eta' \rightarrow \rho\gamma \rightarrow \pi^\pm\gamma(\pi^\mp)$, does provide a way to isolate the η' with adequate acceptance and reasonable background. Thus by comparing the rates in each of these modes, we can separate the contributions from the individual mesons. Although the limited statistics of the 1998 e1 run precludes making any statements as to a_0^0 or f_0 backgrounds at this time, the increased statistics of the 1999 run should allow us to experimentally verify that this background is small.

5.5.7 Angular Distributions

We have examined the expected acceptance as a function of the decay angles in the hadronic center-of-mass system. For this section we restrict our analysis to the Q^2 region covered by the two main running conditions, $0.85 < Q^2 < 1.55$ (GeV/c)^2 for the 4 GeV electron beam data, and $0.75 < Q^2 < 1.75$ (GeV/c)^2 for the 6 GeV electron beam data with reversed torus field. For $Q^2 > 1.75$ (GeV/c)^2, the 6 GeV data with normal torus field will also be used, but the expected statistics, even with that additional data, would be inadequate to examine angular distributions. The plots from the Monte Carlo are shown in Fig. 52.

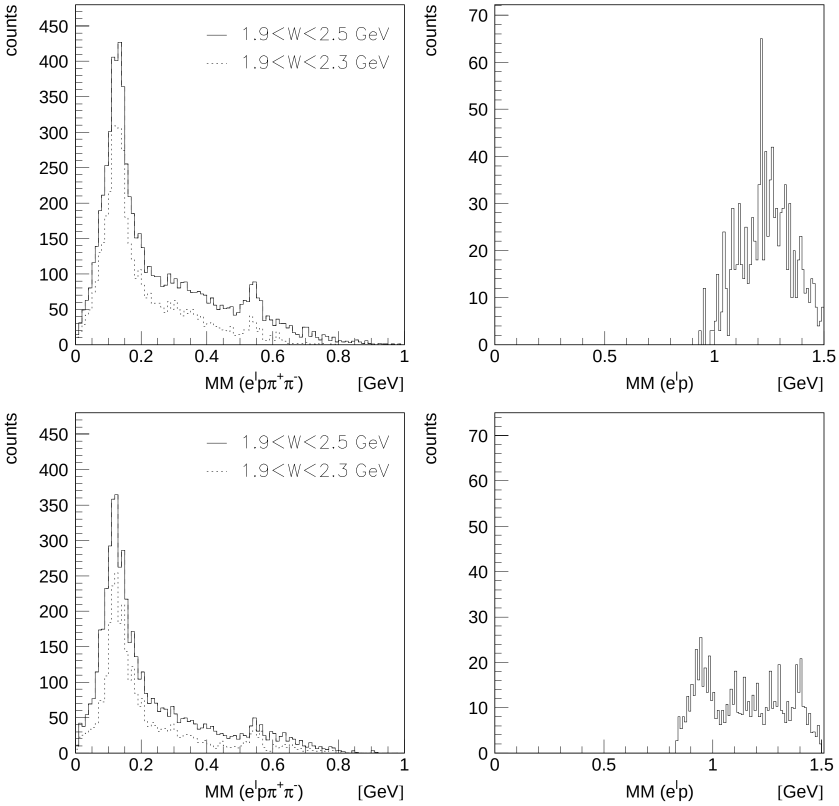

Figure 49: Missing-mass distributions for $ep \to e'p\pi^+\pi^-$ (left) and corresponding $MM_{e'p}$ distributions (right). The dotted lines in the left plots indicate the spectrum for 1.9< W <2.3 GeV. The right plots show the distribution after a mass cut on the missing η ($0.52 < MM_{e'p\pi^+\pi^-} <$ 0.58 GeV/c^2). The top plots are from the low-field 4 GeV data, while the bottom plots are from the high-field 4 GeV data.

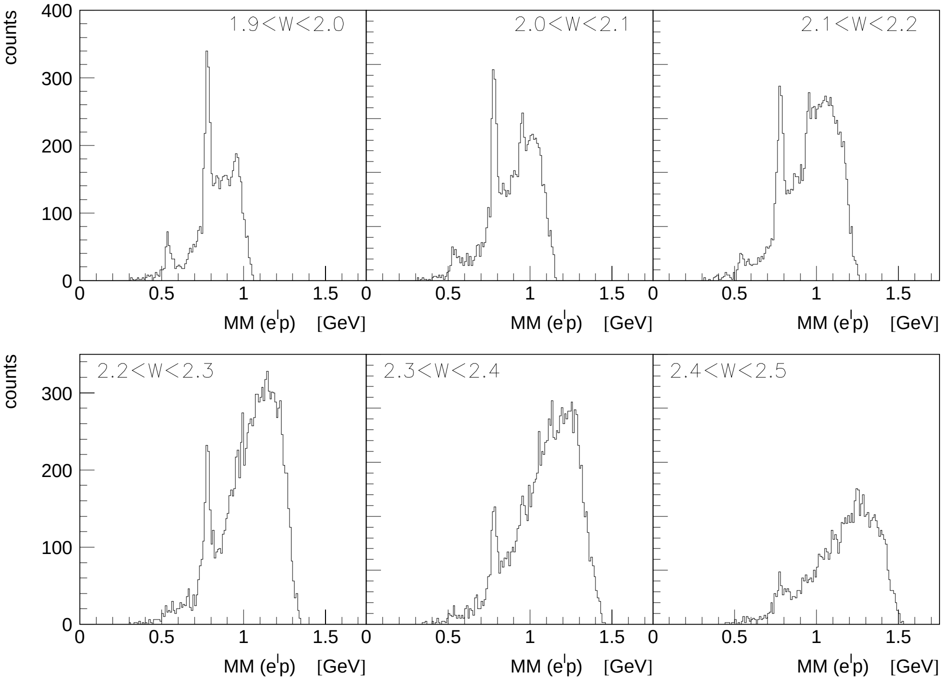

Figure 50: Missing-mass distribution $MM_{e'p}$ for reconstructed $ep \to e'p\pi^+\gamma X$ in various W bins.

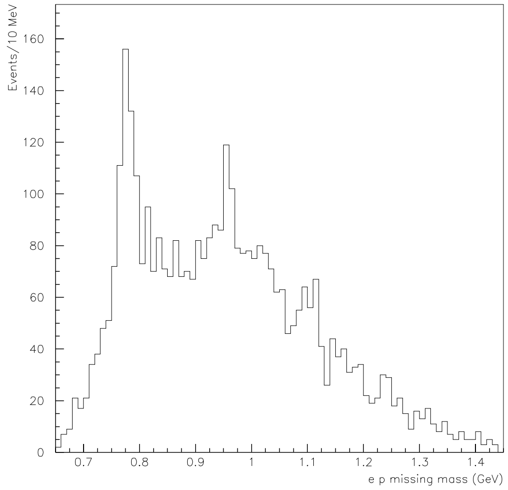

Figure 51: Missing-mass distribution $MM_{e'p}$ for reconstructed $ep \to e'p\pi^+\gamma(\pi^-)$ with $M_{\pi^+(\pi^-)}$ within one full-width of the ρ mass.

This figure shows sample plots for the acceptance for the electron and proton to be in the fiducial regions of CLAS. In this figure the relative acceptance is signified by the size of the box drawn. We have examined the same plots with the requirement of finding various decay products of the η'. Although the absolute acceptance changes, the relative acceptance as a function of angle remained unchanged within statistics. This is due to the fact that our relative acceptance is determined dominantly by whether or not the proton falls within the fiducial volume of CLAS.

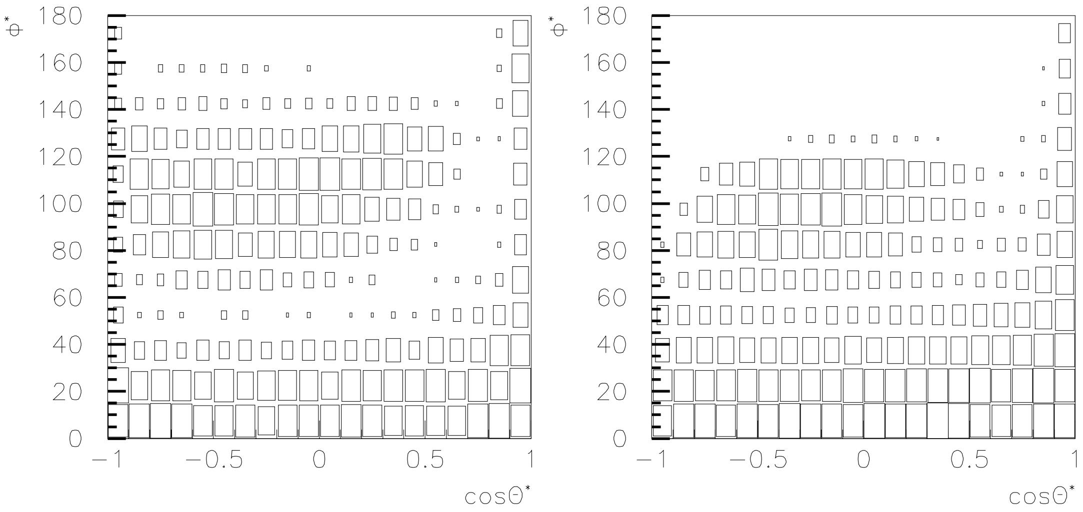

Figure 52: Monte Carlo acceptance verses center-of-mass angles, $\cos\theta^*$ and ϕ^*. The left plot is for 4 GeV data with a normal 60% torus field, and the right plot is for 6 GeV data with a reversed 60% torus field. The plots are for the electron and proton to be in the fiducial volume. Due to the symmetry of CLAS, these plots are folded about $\phi^* = 0$.

For the 4 GeV data, one can see the reduced acceptance at $|\phi^*| \approx 50°$ and $\approx 160°$. This is due to cases where the proton falls into the regions in ϕ_{lab} between the individual sectors of CLAS. For $|\phi^*| \approx 0°$, $|\phi^*| \approx 180°$, or $\cos\theta^* \approx 1$, the proton is within the sector opposite the electron. For $|\phi^*| \approx 90°$ and $\cos\theta^* \approx 0$, the proton goes through a sector next to the one opposite the electron. For the 6 GeV data, we see in Fig. 52 that the events are restricted to $|\phi^*| < 120°$. This is due to losing in-bending protons to the forward hole. For larger ϕ^*, the coverage is actually better for the 6 GeV beam energy than for 4 GeV. In the differential cross section, the σ_{TT} term is proportional to $\cos 2\phi^*$. This leads to the greatest effect being the difference between $\phi^* = 0°$ and $\phi^* = 90°$, where we have the largest acceptance.

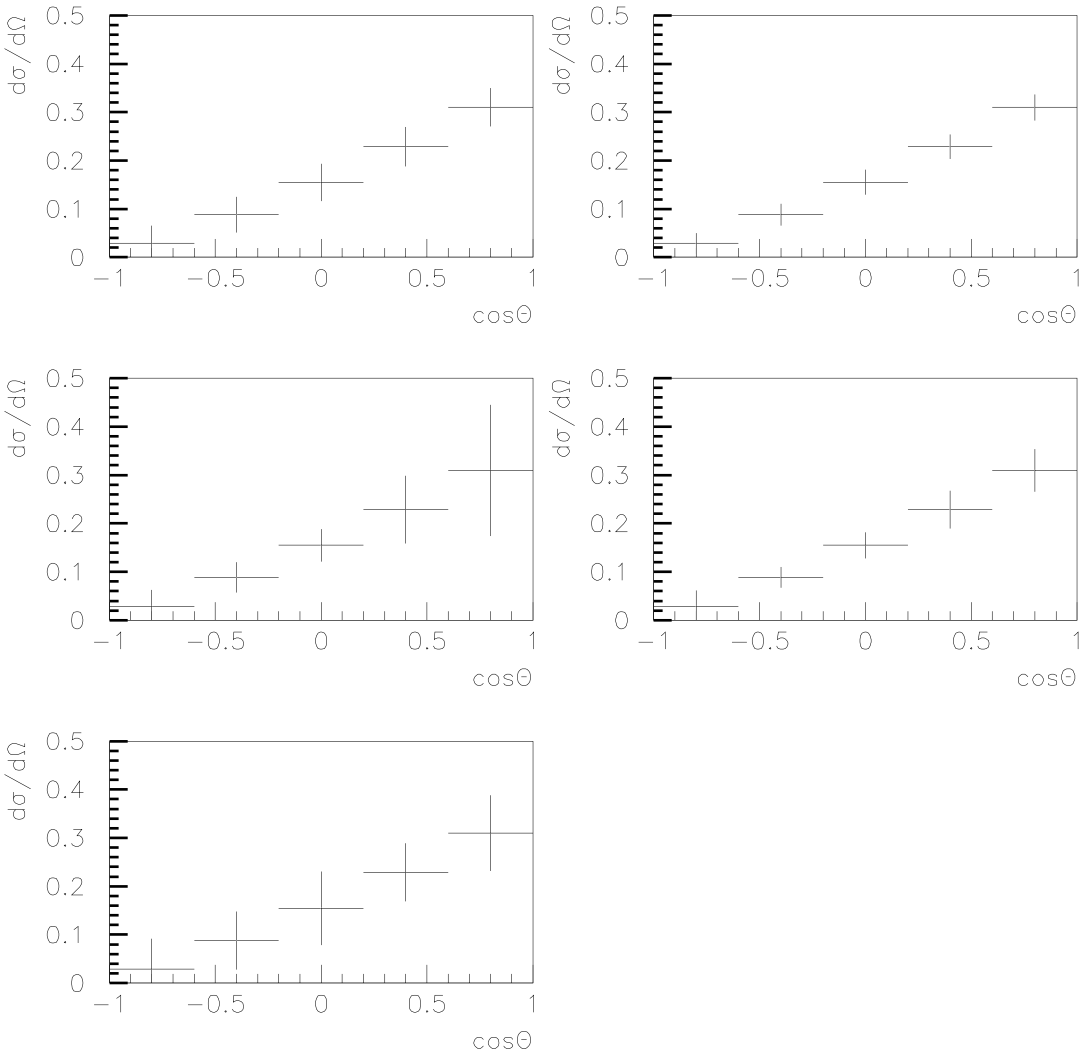

Figure 53: The expected statistical accuracy with course angular binning for $2.0 < W < 2.1$ GeV and the Q^2 ranges described in the text. For each plot the cross section is taken from the fit to the global SAPHIR data (see Fig. 46), while the expected error bar is derived from the Monte Carlo estimate of expected rates, and the observed signal/noise ratio in the data for the $\pi^{+(-)}\gamma(\pi^{-(+)})$ reconstruction modes. The top plots are for $|\phi^*| < 60°$, the middle plots are for $60° < |\phi^*| < 120°$, and the bottom plot is for $|\phi^*| > 120°$. The plots on the left show the expectations for using the data from the currently approved e1 experiments. The plots on the left show the expectations for the requested 6 GeV beam time with reversed torus field.

Obviously, the statistics available with the beam time requested will not allow for such fine binning. In Fig. 53 we show the expected statistical errors as a function of $\cos\theta^*$ for three bins in ϕ^* for a single 100 MeV bin in W with the Q^2 ranges given above. This figure is for the $\eta' \to \pi^+\gamma(\pi^-)$ reconstruction mode (with charges reversed for reversed torus polarity).

The $\gamma\gamma(X)$ mode is statistically independent and yields comparable results.

5.5.8 Expected Rates

The rate estimates were calculated for η' electroproduction on a hydrogen target of 5 cm length at a luminosity of 1×10^{34} cm^{-2}s^{-1} for the following beam times:

- 30 days at 4 GeV with normal torus field: B/B_0=+60% (shown in Table 6)
- 15 days at 6 GeV with reversed torus field: B/B_0=-60% (shown in Table 7)
- 40 days at 6 GeV with normal torus field: B/B_0=+60% (shown in Table 8)

The detector acceptance is based on Monte Carlo studies assuming the $\eta' p$ channel to be identified in the missing-mass distribution $MM_{e'p}$, with the additional requirements that either two additional photons were detected, or the $\eta' \rightarrow \pi^{\pm}\gamma(\pi^{\mp})$ reaction was observed (cf. section 5.5.7). The magnitude of simulated $\eta' p$ events was estimated with regard to the photoproduction results of the SAPHIR collaboration. The Q^2 dependence was parameterized by applying a pole term $\propto (1 + Q^2/0.7)^{-2}$.

W range (GeV)	Q^2 Range ((GeV/c)^2)					
	0.75 – 1.25	1.25 – 1.75	1.75 – 2.25	2.25 – 2.75	2.75 – 3.25	3.25 – 3.75
η' produced at 4 GeV (normal field)						
1.9-2.0	111291	18504	4278	1282	372	0
2.0-2.1	120799	20606	4768	1467	483	0
2.1-2.2	86387	14967	3552	1044	321	0
2.2-2.3	54399	9686	2272	465	118	0
2.3-2.4	33221	5834	1422	254	0	0
η' accepted at 4 GeV in $\gamma\gamma X$ mode						
1.9-2.0	789	792	260	111	1	0
2.0-2.1	1328	1017	339	93	0	0
2.1-2.2	1567	933	269	18	0	0
2.2-2.3	1477	728	145	0	0	0
2.3-2.4	1351	510	17	0	0	0
η' accepted at 4 GeV in $\pi^+\gamma(\pi^-)$ mode						
1.9-2.0	271	262	71	32	2	0
2.0-2.1	439	294	99	19	0	0
2.1-2.2	494	269	94	8	0	0
2.2-2.3	520	224	44	0	0	0
2.3-2.4	435	160	4	0	0	0

Table 6: Expected rates for beam energies of 4 GeV (30 days beam time) with normal torus field settings $B/B_0 = 60\%$.

5.5.9 Summary of η' Proposal

We propose new beam time at 6 GeV using CLAS in a standard configuration that will be in conjunction with a number of other proposals. Although we will use the beam time

W range (GeV)	Q^2 Range ((GeV/c)^2) 1.00 – 1.25	1.25 – 1.75	1.75 – 2.25	2.25 – 2.75	2.75 – 3.25	3.25 – 3.75
η' produced at 6 GeV (normal field)						
1.9-2.0	43311	27551	6981	2134	767	332
2.0-2.1	49014	31972	8170	2604	927	385
2.1-2.2	37036	24621	6459	1980	765	305
2.2-2.3	24469	16539	4323	1397	507	200
2.3-2.4	15971	11181	2888	938	355	187
2.4-2.6	19816	13488	3878	1194	452	195
2.6-2.9	14199	10056	2729	919	333	125
η' accepted at 6 GeV in $\gamma\gamma X$ mode						
1.9-2.0	0	198	508	189	89	37
2.0-2.1	1	327	512	182	63	31
2.1-2.2	1	371	425	158	78	28
2.2-2.3	0	385	364	110	47	17
2.3-2.4	0	386	248	83	33	10
2.4-2.6	6	835	326	79	30	15
2.6-2.9	60	335	166	83	20	4
η' accepted at 6 GeV in $\pi^+\gamma(\pi^-)$ mode						
1.9-2.0	0	52	168	60	23	12
2.0-2.1	0	62	164	54	29	9
2.1-2.2	0	125	150	45	35	5
2.2-2.3	0	108	96	37	11	1
2.3-2.4	0	109	78	28	8	4
2.4-2.6	0	235	96	20	8	3
2.6-2.9	15	83	39	16	5	3

Table 7: Expected rates for beam energies of 6 GeV (40 days beam time) with torus field settings $B/B_0 = 60\%$.

W range (GeV)	Q^2 Range ((GeV/c)^2)					
	$0.75-1.25$	$1.25-1.75$	$1.75-2.25$	$2.25-2.75$	$2.75-3.25$	$3.25-3.75$
η' produced at 6 GeV (reversed field)						
1.9-2.0	62134	10812	2794	853	280	142
2.0-2.1	69415	12717	3231	1048	359	145
2.1-2.2	51206	9740	2558	805	305	115
2.2-2.3	34137	6614	1722	553	207	78
2.3-2.4	21805	4289	1211	384	152	64
2.4-2.6	26663	5381	1486	503	212	69
2.6-2.9	19329	3971	1064	353	126	48
η' accepted at 6 GeV in $\gamma\gamma X$ mode						
1.9-2.0	2872	706	225	69	36	16
2.0-2.1	3259	741	206	75	20	15
2.1-2.2	2725	615	173	60	30	13
2.2-2.3	1949	435	133	45	18	6
2.3-2.4	1467	305	110	30	16	7
2.4-2.6	2020	452	138	38	25	8
2.6-2.9	1521	376	116	40	4	0
η' accepted at 6 GeV in $\pi^+\gamma(\pi^-)$ mode						
1.9-2.0	887	217	82	25	5	4
2.0-2.1	1008	215	57	17	8	5
2.1-2.2	882	179	49	16	3	2
2.2-2.3	612	125	33	6	2	0
2.3-2.4	431	96	25	5	4	0
2.4-2.6	601	128	30	18	6	1
2.6-2.9	430	114	33	12	3	0

Table 8: Expected rates for 6 GeV beam energy (15 days beam time) with reversed torus field setting B/B_0 = -60%.

at both normal and reversed field, the reversed field data will give us the most interesting coverage. We also propose to analyze already approved beam time in coordination with the e1 run group. We do not request any additional 4 GeV beam time for this experiment.

The most straightforward consequence of the new data will be a new window to N^* resonances in the W range of 1.9-2.4 GeV. A few states have been found in this range, but only those that couple strongly to πN. Many of the so-called missing states are at $W > 2$ GeV, and the η' reaction should be an interesting way to focus on a few of them. Many final states have threshold enhancements, and in some cases the threshold is resonance dominated, most notably by $P_{33}(1232)$ for π^0 production, and $S_{11}(1535)$ for η production. Based on the recent low statistics Bonn results, η' might be another case.

We have searched for a few modes of η' identification in the existing CLAS data. There is a well-calibrated but poor statistics set of data taken at 4 GeV in the first e1 run in 1998. There is also a smaller data sample from the exploratory few hour run at 5.56 GeV in 1999. There are many decay channels of the η' that could be useful and we have explored a few of them, however, we will always detect the scattered electron and the recoil proton in the final state. The most promising decay channels presently are $\eta' \to \rho^0\gamma$ (B.R. about 30%) and $\eta' \to \eta\pi\pi$ (B.R. about 65%). We see a good signal (see Fig. 51) for the first mode when we cut on 1 and only 1 photon and one of the charged pions from the ρ decay. We can also see a strong η' signal when cutting on 2 fairly high-energy photons in the final state. At present, we see signal to noise ratios of roughly 1:1. For the size of the data sample used, the signal is quite large and may be partly a_0 instead of η'. This study is still in progress, and more improvement is expected.

We presented detailed Monte Carlo results for the two most likely decay modes. The CLAS acceptance is reasonable for such a complicated final state. Coverage in the decay angles is fairly large and a multipole decomposition is possible in the W range of 1.9-2.3 GeV. Good statistics are possible in 15 θ^*, ϕ^* bins.

References

[1] The N^* Proposal package, (1989).

[2] V.D. Burkert, Nucl. Phys. A **623**, 59c (1997).

[3] F.E. Close, An Introduction to Quarks and Partons (New York, 1979).

[4] Baryons '98, 8^{th} International Conference on the Structure of Baryons, Bonn, Sept. 22-26, 1998, to be published by World Scientific, (1998).

[5] N. Kaiser, Proc. of the Workshop on N^* Physics and Non-perturbative QCD, Trento, Italy, 18-29 May 1998, Few Body Systems Suppl. **11**, 246 (1999).

[6] Proc. of the Workshop on N^* Physics, Seattle, (1996).

[7] P. Stoler, Phys. Reports **226**, 103 (1993).

[8] G. Sterman and P. Stoler, Ann. Rev. Nucl. Part. Sci., (1997).

[9] S. Capstick and W. Roberts, Phys. Rev. D **49**, 4570 (1994); S. Capstick, Phys. Rev. D **46**, 2864 (1992);

[10] V. Frolov, J. Price, P. Stoler, C. Armstrong *et al.*, JLab Experiment E97-101.

[11] C. Armstrong *et al.*, submitted to Phys. Rev. D, (1999).

[12] C.E. Carlson and J.L. Poor, Phys. Rev. D **38**, 2758 (1988).

[13] N. Kaiser, Proc. of the Workshop on N^* Physics and Non-perturbative QCD, Trento, Italy, 18-29 May 1998, Few Body Systems Suppl. **11**, 246 (1999).

[14] E. Anciant *et al.*, CLAS Internal Analysis Report 99-002, (1999).

[15] Review of Particle Physics, Eur. Phys. J **C3**, 1-794 (1998).

[16] V. Burkert and L. Elouadrhiri, Phys. Rev. Lett. **75**, 3613 (1995).

[17] I.G. Aznauryan and S.G. Stepanyan, Phys. Rev. D **59**, 1 (1999).

[18] S.S. Kamalov, D.Drechsel, O. Hanstein, and L. Tiator, Proc. of the Workshop on N^* Physics and Non-perturbative QCD, Trento, Italy, 18-29 May 1998, Few Body Systems Suppl. **11**, 246 (1999); D.Drechsel, O. Hanstein, S.S. Kamalov, L. Tiator, Preprint nucl-th/9807001, (1998).

[19] R. Davidson, N.C. Mukhopadhyay, and R. Whittman, Phys. Rev. Lett. **56**, 804 (1986); R. Davidson and N.C. Mukhopadhyay, private communication (1998).

[20] T. Sato and T.S.H. Lee, Phys. Rev. C **54**, 2606 (1996).

[21] R. Koniuk and N. Isgur, Phys. Rev. Lett. **44**, 845 (1980); Phys. Rev. D **21**, 1868 (1980).

[22] R. Koniuk, Nucl. Phys. B **195**, 452 (1982).

[23] F. Stancu and P. Stassart, Phys. Rev. D **47**, 2140 (1993).

[24] S. Capstick and W. Roberts, Phys. Rev. D **49**, 4570 (1994).

[25] K.F. Liu and C.W. Wong, Phys. Rev. D **28**, 170 (1983).

[26] S. Capstick and B. Keister, Phys. Rev. D **51**, 3598 (1995).

[27] F. Cardarelli *et al.*, Proc. of the Workshop on N^* Physics and Non-perturbative QCD, Trento, Italy, 18-29 May 1998, Few Body Systems Supplement **11**, (1999).

[28] J.J. Domingo, Proc. 5th Workshop on Perspectives in Nuclear Physics at Intermediate Energies, Trieste, Italy, May 6-10, 1991, eds. S. Boffi, C. Ciofi degli Atti and M. Giannini, (World Scientific, 1992) p. 260.

[29] V.D. Burkert, Nucl. Phys. A **59C**, 623 (1997).

[30] M. Ripani, V. Burkert *et al.*, JLab Experiment E93-006.

[31] V. Eckart *et al.*, Nucl. Phys. B **55**, 45 (1973); P. Joos *et al.*, Phys. Lett. B **52**, 481 (1974); K. Wacker *et al.*, Nucl. Phys. B **144**, 269 (1978).

[32] M. Ripani and V. Mokeev *et al.*, Proc. of the Workshop on N^* Physics and Non-perturbative QCD, Trento, Italy, 18-29 May 1998, Few Body Systems Supplement **11**, (1999).

[33] F. Lenz, Nucl. Phys. B **279**, 119 (1987).

[34] S. Weinberg, The Quantum Theory of Fields, Vol. 2 (New York, 1996), ch. 19.

[35] E. Witten, Nucl. Phys. B **156**, 269 (1979); G. Veneziano, Nucl. Phys. B **159**, 213 (1979); G. Christos, Phys. Rept. **116**, 251 (1984).

[36] H.P. Pavel, D. Blaschke, V.N. Pervushin, G. Röpke, M.K. Volkov, Squeezed condensate of gluons and the mass of the η', Preprint hep-ph/9706528, (1997).

[37] J.L. Rosner, Phys. Rev. D **27**, 1101 (1983).

[38] T.N. Pham, Phys. Lett. B **246**, 175 (1990); P. Ball, J.-M. Frère, and M. Tytgat, *ibid.* **365**, 367 (1996); E.P. Venugopal and B.R. Holstein, Phys. Rev. D **57**, 4397 (1998); J. Cao *et al.*, *ibid.* **58**, 1130 (1998).

[39] S.D. Bass, Constituent quarks and g_1, Preprint hep/ph-9902280 (and references therein), (1999).

[40] G.M. Shore and G. Veneziano, Nucl. Phys. B **381**, 23 (1992).

[41] J.F. Zhang, N.C. Mukhopadhyay, and M. Benmerrouche, Phys. Rev. C **52**, 1134 (1995)

[42] Z.P. Li, J. Phys. G **23**, 1127 (1997).

[43] Z.P. Li, H.X. Ye, and M.H. Lu, Phys. Rev. C **56**, 1099 (1997); Z.P. Li and F.E. Close, Phys. Rev. D **42**, 2194 (1990); Z.P. Li, Phys. Rev. D **48**, 3070 (1993), ibid. **50**, 5639 (1994), ibid. **52**, 4961 (1995), Phys. Rev. C **52**, 1648 (1995).

[44] R. Erbe *et al.* (ABBHHM coll.), Phys. Rev. **175**, 1669 (1968).

[45] W. Struczinski *et al.* (AHHM coll.), Nucl. Phys. B **108**, 45 (1976).

[46] R. Ploetzke *et al.* (SAPHIR coll.), Phys. Lett. B **444**, 555 (1998).

[47] B. Ritchie *et al.*, JLab Experiment E91-008.

[48] D.M. Manley and E.M. Saleski, Phys. Rev. D **45**, 4002 (1992).

[49] Atkinson *et al.* (OMEGA coll.), Phys. Lett. B **138**, 459 (1984).

6 Exclusive Kaon Electroproduction

Spokespersons: D.S. Carman[a], K. Joo[b], L.H. Kramer[c], and B.A. Raue[c]

[a]Carnegie Mellon University, Pittsburgh, PA 15213
[b]University of Virginia, Charlottesville, VA 22901
[c]Florida International University, Miami, FL 33199

6.1 Introduction

We propose to use CLAS to study kaon electroproduction from a hydrogen target at a beam energy of 6 GeV. This proposal is an extension of the existing Hall B kaon electroproduction program that currently encompasses experiments to measure cross sections and to separate response functions [1, 2], and to measure single-polarization [3] and double-polarization observables [4]. By extending the measurements to 6 GeV, this new proposal will not only complement the lower-energy program, but will also enter a realm of new physics beyond the resonance region that will help to elucidate the transition from conventional hadronic dynamics to quark-gluon degrees of freedom.

Strange quark production in electro-induced reactions at intermediate energies allows study of this transition regime since a strange quark and antiquark must be created during the reaction. Measurements of the hyperon cross sections and polarizations should provide for a deeper insight into the leading contributions to the process. The data should allow us to better understand whether quark degrees of freedom control the open-strangeness production process, and whether chiral symmetry governs the hyperon production threshold region [5, 6]. The data can also address whether Feynman-graph techniques through isobaric models are sufficient for an accurate description of the process, or if different concepts such as quark models or Regge exchanges are more appropriate. Obviously data of sufficient accuracy are needed before these questions can be answered.

The large two-body and three-body acceptances of CLAS will allow us to detect efficiently the $e'K^+$ and $e'K^+p$ final states. Furthermore, the large acceptance of CLAS allows for study of the reaction over varying kinematical regions where the relative importance of the s, t, and u channels will vary. By emphasizing specific channel processes we can limit the intermediate baryonic or mesonic resonances involved in the reaction, which in turn, simplifies the analysis.

The present understanding of electromagnetic kaon production is limited by a sparsity of data. Existing cross section measurements cover a limited range of kinematics and suffer from relatively large experimental uncertainties. This has limited our understanding of the underlying reaction mechanism. In addition, the lack of knowledge of the coupling constants $g_{K\Lambda N}$ and $g_{K\Sigma N}$ adds to the complexity of the phenomenological investigations. This leads to large uncertainties in constraining existing models.

The $ep \rightarrow e'K^+Y$ reaction provides the opportunity to study physics not accessible in other reactions. The simple fact that there are no valence s quarks in the proton means that strangeness-production mechanisms are at play that are absent in, for example, pion production. We can study $s-$channel processes that specifically include or exclude the Δ since we have an automatic isospin filter through selection of either the $K\Lambda$ or $K\Sigma$ final state. Additionally, using a polarized-electron beam, and utilizing the self-analyzing nature of the hyperon weak decays, allows us to study various spin characteristics of the reaction through polarization measurements. In particular, Λ polarization data may shed light on the quantum numbers of the $s\bar{s}$ pair created in the intermediate state.

6.2 Physics Analyses

There are several distinct measurements that make up the program for this proposal. Each measurement provides sensitivity to a slightly different aspect of the strangeness production process. As each is essentially an extension of a measurement already approved for lower-energy running in Hall B, the analysis techniques are the same as those discussed in the original proposals, and so are not discussed in any more detail here. This section is devoted to providing details as to how the individual measurements will benefit from the increased electron-beam energy.

6.2.1 Structure Function Extraction

The most general form for the $p(e,e'K)$ differential cross section with an unpolarized-electron beam is given by:

$$\sigma_0 \equiv \frac{d\sigma_v}{d\Omega_K} = \sigma_T + \epsilon\sigma_L + \epsilon\sigma_{TT}\cos 2\phi_K^* + \sqrt{\epsilon(\epsilon+1)/2}\,\sigma_{TL}\cos\phi_K^*. \tag{12}$$

The four structure functions, σ_T, σ_L, σ_{TT}, and σ_{TL}, can be determined as a function of bins in the kinematic variables Q^2, W, and t. σ_T and σ_L are extracted by comparing measurements at different values of beam energy, and thus different values of the photon polarization parameter ϵ. This "Rosenbluth"-type separation is done most precisely for large ϵ coverage in a given bin of Q^2 and W. σ_{TT} and σ_{TL} are extracted from a fit to the ϕ_K^*-dependence of the cross section, resulting in a complete separation of the four structure functions. The range in ϵ spanned as a function Q^2 for one representative bin in W at 1.8 GeV and various beam energies is shown in Fig. 54.

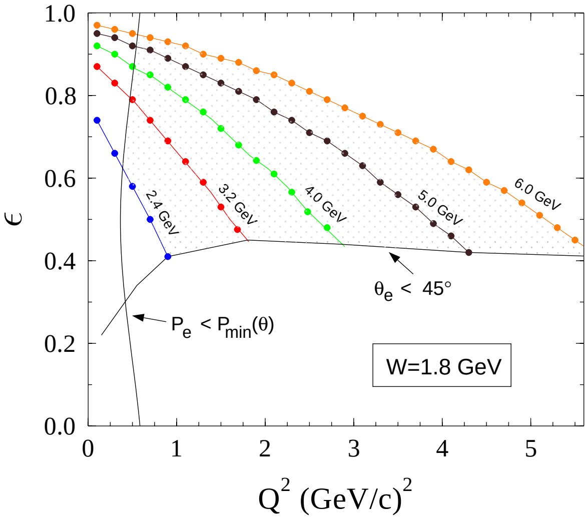

Figure 54: CLAS acceptance (shaded region) of the scattered electron in terms of ϵ and Q^2 in a representative W bin of 1.8 GeV for planned Hall B e1 beam energies in the range from 2.4 to 6.0 GeV.

Combining the 6 GeV data set with the lower-energy measurements should enable important reductions in the uncertainties on the extracted structure functions. With a maximum beam energy of 4 GeV, this extraction can be performed up to $Q^2 \approx 2$ (GeV/c)^2, while increasing the beam energy to 6 GeV allows this extraction to be pushed out to Q^2 values closer to 4 (GeV/c)^2. As well, increasing the energy range of these measurements will allow for extensions in the kinematic range of the σ_{TT} interference term, which is a measure of the dependence of the amplitudes upon the transverse polarization of the virtual photon. The goal is to study how σ_{TT} changes with Q^2 and t, since the kaon form factor causes the dominant t-channel term to diminish. Of other interest is a more broad-range t-dependent measurement of the ratio of σ_L/σ_T. This ratio is sensitive to the spin and transverse momentum of the object which absorbs the virtual photon. At 6 GeV, this ratio can be measured up to $|t| \approx 5$ (GeV/c)^2, compared to the 4 GeV upper limit in $|t|$ of only 3 (GeV/c)^2 .

6.2.2 Σ^0/Λ Production Ratios

A long-standing question in kaon electroproduction centers on the ratio of the cross section for Σ^0 to Λ production. Experimentally, the $K^+\Sigma^0$ cross section decreases faster with increasing Q^2 than the $K^+\Lambda$ cross section. There are two explanations proposed to account for this behavior. The first assumes that $\sigma_L >> \sigma_T$ at high Q^2. In this case the t-channel processes would be enhanced since the main contribution to σ_L is from K^+ exchange. Therefore as $\mathrm{g}^2_{K\Lambda N} >> \mathrm{g}^2_{K\Sigma N}$, Λ production would be favored over Σ production. However, there is no evidence for the longitudinal response dominating the $K^+\Lambda$ channel [7, 8].

The second explanation regarding the Σ^0 to Λ ratio is given in terms of the quark-parton model [9]. Inclusive electron scattering data has shown that the ratio of the neutron to proton structure functions in deep inelastic scattering (DIS), F_2^n/F_2^p, goes to 1/4 as Q^2 increases. This is interpreted to mean that when the virtual photon hits a valence u quark, the remaining ud quark pair is in an I=0 state and acts as a spectator to the reaction. This should tend to favor Λ (I=0) production over Σ^0 (I=1) production. However, the argument depends on being in the DIS region. With a 6 GeV electron beam, electroproduction experiments in Hall B could probe a much larger Q^2 range than at 4 GeV where the quark-parton model is expected to have more validity.

6.2.3 Λ Polarization Measurements

Polarization data will provide an important key for our understanding of the reaction mechanism by improving the constraints on the coupling constants that describe the intermediate reaction vertices, and the form factors that reflect the charge distributions of the quarks and gluons within the hadrons. Due to the large phase space coverage of CLAS, this experiment provides a unique opportunity to probe the response functions for this process, and hence the reaction mechanism, beyond the usual choices of parallel or in-plane kinematics. Furthermore, polarization observables are crucial to improve the partial wave analyses used to study the different intermediate resonances involved in the reaction. The polarization data remove external spin sums and impose additional constraints on the structure of the density matrix elements. Simply put, the polarization observables provide much more sensitivity to the reaction mechanism than the cross section data alone.

An attractive feature of the $K^+\Lambda$ reaction comes from its self-analyzing character. This allows straightforward measurements of the Λ polarization in the $\Lambda \to p\pi^-$ decay branch from the decay-proton angular distribution [4]. The important measurements to consider are determinations of the induced, or electron beam helicity independent, and transferred, or electron beam helicity dependent, hyperon polarizations as a function of Q^2 and t over the full W-range spanned. Note that as the cross section falls roughly as $1/Q^4$, the Λ polarization measurements cannot span as high in Q^2 as the cross section and asymmetry measurements. As discussed in section 6.5, due to statistical limitations, meaningful Λ polarization measurements will be limited to Q^2 <3.5 (GeV/c)^2.

Single-Polarization Data

The single-polarization experiments considered here include polarization of either the incident electron beam or the outgoing recoil hyperon. These measurements provide potential access to the response functions $R_T^{y'0}$, $R_L^{y'0}$, $R_{TL'}^{00}$, $R_{TL}^{i'0}$, and $R_{TT}^{i'0}$, $i' = x, y, z$, and are accessible only through this type of experiment [10].

The experiments made with a polarized-electron beam require detection of only two final-state particles, namely, the scattered electron and electro-produced kaon. For this final state, CLAS has a typical acceptance at 6 GeV of ≈20%. To measure the induced hyperon polarization, detection of an additional final-state particle, the decay proton, is also required. With this final state, CLAS has a typical acceptance at 6 GeV of ≈5%. See section 6.4 for more details on the CLAS acceptance for this process.

Including a polarized incident electron beam of helicity h, the kaon differential cross section from eq(12) now includes an additional term known as the fifth response term $\sigma_{TL'}$.

$$\frac{d\sigma_v}{d\Omega_K} = \sigma_0 + h\sigma_{TL'}, \qquad \sigma_{TL'} = \sqrt{2\epsilon_L(1-\epsilon)}\ {}^sR_{TL'}^{00} \sin\phi_K^*. \tag{13}$$

This measurement allows for sensitivity to the response function ${}^sR_{TL'}^{00}$ through the cross section difference between the two electron-beam helicity states. As $\sigma_{TL'}$ is zero in plane wave calculations, it provides a means of studying final-state interactions. This response function provides sensitivity to the interference between the transverse and longitudinal amplitudes. In fact, the TL and TL' responses differ in that they select different combinations of the real or imaginary parts of the interference multipoles.

For the case of a polarized outgoing Λ, the kaon differential cross section can be written in terms of the induced hyperon polarization components P_i^0 as:

$$\frac{d\sigma_v}{d\Omega_K} = \sigma_0 \left(1 + P_x^0 \hat{S}_x + P_y^0 \hat{S}_y + P_z^0 \hat{S}_z\right). \tag{14}$$

To provide for meaningful limits on the polarization measurement, the data analysis will integrate over all kaon azimuthal angles in CLAS just as was the case for E99-006. In this integration, the x and z-components of the induced polarization are zero, and only the y-component survives. The resulting polarization component P_y^0 in the electron-plane coordinate system is given by:

$$P_y^0 = \pi\sqrt{2\epsilon_L(1+\epsilon)}\frac{K}{\int\sigma_0}(R_{TL}^{x'0}\cos\theta_K^* + R_{TL}^{y'0} + R_{TL}^{z'0}\sin\theta_K^*). \tag{15}$$

With other choices of integration in the kaon center-of-mass (CM) angles θ_K^* and ϕ_K^*, sensitivity to other response functions may be achieved. Note that in this expression K represents a kinematic factor given by the ratio of the CM kaon momentum to the CM virtual photon momentum, and $\int\sigma_0$ represents the integral of σ_0 over ϕ_K^* from 0 to 2π.

Double-Polarization Data

The double-polarization experiment considered here includes polarization of both the beam and outgoing recoil hyperon. This measurement provides potential access to the TL' and TT' interference response functions $R^{i'0}_{TL'}$, $R^{y'0}_{TL'}$, and $R^{i'0}_{TT'}$, $i' = x, z$, that are not accessible through experiments with either polarized beams or polarized recoils alone. For this situation, the cross section can be written in terms of both the induced P^0_i and transferred P'_i hyperon polarization components as:

$$\frac{d\sigma_v}{d\Omega_K} = \sigma_0 + h\sigma_{TL'} + \sigma_0 \left(P^0_x \hat{S}_x + P^0_y \hat{S}_y + P^0_z \hat{S}_z + P'_x \hat{S}_x + P'_y \hat{S}_y + P'_z \hat{S}_z \right). \tag{16}$$

Again, to provide for meaningful limits on the polarization measurements, the data analysis will integrate over all kaon azimuthal angles in CLAS. In this integration, the y-component of the transferred polarization is zero, and only the x and z-components survive. The resulting non-zero transferred polarization components in the electron-plane coordinate system are given by:

$$\begin{aligned} P'_x &= \pi\sqrt{2\epsilon_L(1-\epsilon)}\frac{K}{\int\sigma_0}(R^{x'0}_{TL'}\cos\theta^*_K - R^{y'0}_{TL'} + R^{z'0}_{TL'}\sin\theta^*_K) \\ P'_z &= 2\pi\sqrt{1-\epsilon^2}\frac{K}{\int\sigma_0}(-R^{x'0}_{TT'}\sin\theta^*_K + R^{z'0}_{TT'}\cos\theta^*_K). \end{aligned} \tag{17}$$

As well, with suitable choices of integration in θ^*_K different sensitivities to the response functions may be achieved.

6.2.4 Missing N^* Resonances

The constituent quark model provides a reasonable description of the static properties of the known hadrons. This is quite surprising since it is not clear how QCD reduces to the quark model in the static limit. Any serious discrepancies between the quark-model predictions and experiment may give us insight into aspects of QCD, and how it may eventually be solved in the non-perturbative regime. However, despite the successes of the quark models, serious disagreements between their predictions and the known baryon spectrum have existed for some time. For example, a large number of negative-parity non-strange baryons, whose wavefunctions lie predominantly in the N=3 harmonic oscillator band, appear to be missing. One early explanation to this dilemma involved the notion that pairs of quarks bind tightly into "diquarks" [11]. Baryons are then considered as quark-diquark systems, and the resulting symmetry qualitatively accounts for the missing states.

A less dramatic solution has also been suggested that appears to have some agreement with experiment. Nearly all data on the non-strange baryon spectrum consists of experiments with $N\pi$ in the initial and/or final state. If the missing baryons do not couple strongly to $N\pi$, their signature may be extremely difficult to pull out from the data. However, if there is a significant strength for decays of these N^* resonances to the $K\Lambda$ or $K\Sigma$ channels, they may become accessible. This hypothesis is strongly supported by dynamical quark calculations. Fig. 55 highlights the mass predictions of one recent quark model for baryon states excited in the $\gamma N \to \Lambda K$ reaction [12].

Fig. 55 shows that the amplitudes for decays into strange final states are generally smaller than those into the non-strange final states. However, it should still be possible to extract

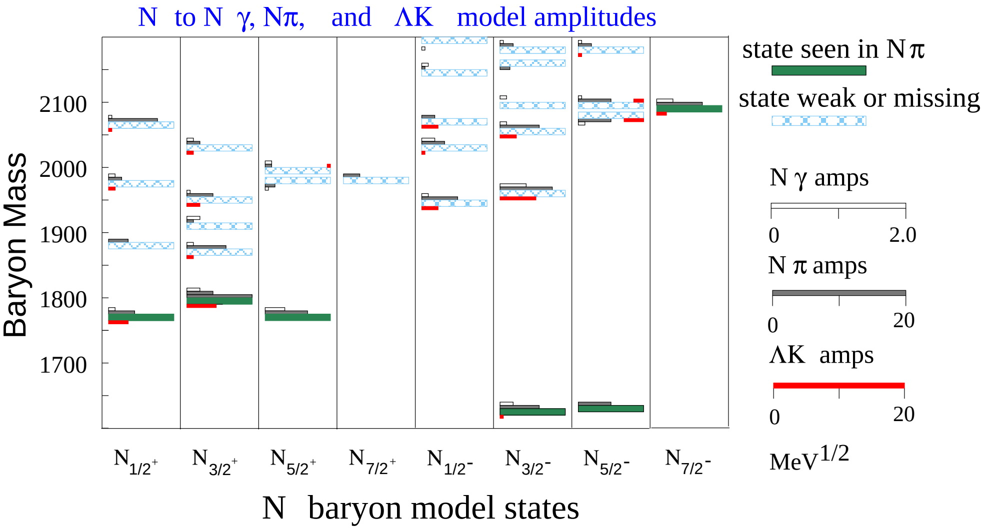

Figure 55: Mass predictions for N^* decays into $N\gamma$, $N\pi$, and ΛK for m$_{N^*}$ $\leq$ 2.2 GeV/c^2 and above the $K\Lambda$ production threshold [12]. States with significant amplitudes for $N\gamma$ and ΛK decays should contribute strongly to the process $\gamma N \rightarrow \Lambda K$.

useful information about intermediate non-strange baryon resonances from analyzing specific strange final states. In many strange channels, only a few higher-mass states contribute with appreciable amplitudes, and in several partial waves, one or two states should dominate. This is due in part to the higher thresholds in effect that allow these channels to turn on in the mass region where new states are predicted to be present. This is to be contrasted with the situation with non-strange final states where low-lying states with large amplitudes make extraction of information about higher-mass states with small amplitudes problematic.

The notion that decays of non-strange baryon resonances into strange final states should be present with a sizeable experimental signature have been backed up by recently published photoproduction data from SAPHIR [13]. This data has shown strong evidence through an angular decomposition of the differential cross section into polynomials that suggests the presence of N^* resonance production with decays to both the $K\Lambda$ and $K\Sigma$ final states.

This experiment will allow us to probe baryon masses from the K-Λ reaction threshold up to 3.0 GeV/c^2. Analysis of this data will yield information about the coupling of these resonances to the $K\Lambda$ and $K\Sigma$ final states, as well as allow for study of the Q^2 and t dependences of any resonance candidates. Ultimately, this experiment will most likely have its greatest impact focussing attention on the Λ production final states as, in general, channels involving Σ production will be more difficult to analyze as both N and Δ resonances contribute to the cross section.

6.2.5 Excited-State Hyperon Production

Any model for the electromagnetic production of strangeness through Λ or Σ production must also be able to properly account for the production of the related spin partners Λ^* and Σ^*. Thus in order to better understand the different s, t, and u-channel contributions involved in open-strangeness production reactions, matching the kinematic extents of the data analysis for both Y and Y^* hyperon states is important.

One clear example of the importance of studying higher-mass hyperon production involves the t-channel process for Λ production. While both K and K^* exchange can contribute to

Λ(gnd) production, no spin-zero kaon exchange can contribute to $\Lambda(1520)$ production due to angular momentum conservation. Detailed inter-comparisons of the angular distributions for the two different reactions can help to isolate the role of t-channel K^+ exchange. Some previously published data do exist, but the situation is still not clear, in fact, over a broad range of kinematics, fits to Λ(gnd) photo- and electroproduction data indeed seem to indicate substantial $K^*(892)$ exchange, but the fits must additionally include $\mathrm{K}_1(1280)$ and/or Regge t-channel exchanges along with additional s and u-channel diagrams. Data of photo-produced $\Lambda(1520)$ [14], indicate predominantly $K^*(892)$ t-channel exchange, with very little contribution from higher-mass kaons. An inclusive electroproduction experiment [15] indicates a substantially different Q^2-dependence of the cross section for Λ and $\Lambda(1520)$ production, with the $\Lambda(1520)$ having the more rapid fall off in cross section with Q^2. It is these direct comparisons of Y and Y^* production that are expected to be the most illuminating regarding the contributions in the different reaction channels, especially given the much increased Q^2 coverage of CLAS at 6 GeV compared to 4 GeV.

Another important reason to study excited-state hyperon production is to test the quark-model predictions for the relative strengths of s-channel N^* resonances that should decay to final states consisting of $\Lambda(1405)K$ and $\Lambda(1520)K$. Additionally, study of the $\Lambda(1520)$, along with its isospin partner $\Lambda(1405)$, are of fundamental importance to the understanding of the inter-quark potential [12].

Beyond allowing for an increased kinematic range for the higher-mass hyperon cross section measurements, this data at 6 GeV will allow study of the Q^2-dependence of the spin density matrices of the $\Lambda(1520)$ as determined by the K^-p decay branch, and of the Λ as determined by the π^-p decay branch. The spin-density matrices for these decays can then help determine the contributions of the competing production diagrams, as well as the spin of the exchanged kaon.

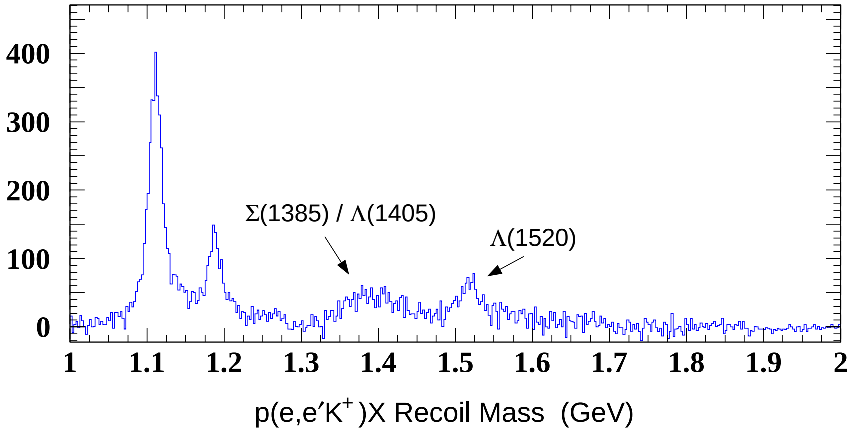

Figure 56: Recoil-mass spectrum for 4 GeV $p(e,e'K^+)X$ CLAS data with the pion background from misidentified kaons subtracted.

Fig. 56 highlights the $p(e,e'K^+)X$ recoil-mass spectrum showing the higher-mass hyperons $\Sigma(1385)/\Lambda(1405)$ and the $\Lambda(1520)$ for 4 GeV CLAS data. This spectrum has had the predominant pion background subtracted. The $\Lambda(1520)$ peak stands out quite distinctly in the spectrum, which makes event selection of the final state straightforward. The analysis of the 4 GeV data is currently ongoing and the extension to 6 GeV will allow for the analysis to be extended over a broader range of Q^2 and t.

6.2.6 Neutral Kaon Production

Since $K^0\Sigma^+$ electroproduction is related to $K^+\Sigma^0$ production through simple isospin relations, both processes should be described by the same models. Therefore, studies of K^0 electroproduction will provide complementary information to that given by charged-kaon electroproduction and by charged and neutral-kaon photoproduction. At present, no data have been collected for electroproduction of neutral kaons at moderate energies, and only one low statistics photoproduction measurement from SAPHIR has been published [16]. Just as in the case of charged-kaon production, studies of K^0 production can allow for insight into the reaction mechanism of strangeness production, better understanding of the contributing diagrams to each reaction channel, determination of the basic electromagnetic couplings of the nucleon, and clues into the internal structure of the nucleon. Extension of these measurements to 6 GeV will extend these studies over a much broader range of Q^2, W, t, and ϵ.

Comparison of the cross section data to hadrodynamical model predictions will allow for an indirect study of the neutral-kaon form factors. Part of the interest in this neutral-kaon channel is that the absence of Λs in the final state changes the character of the intermediate resonances that can contribute, which is to say that the resonance structure will be quite different. Additionally, the results of fits to the decay cross sections are a set of coupling constants that may be compared to SU(3) predictions. The uncertainty in estimation of model parameters is greatly reduced if one is in a position to include data for both charged and neutral-kaon electroproduction. This is an important justification to match the kinematic extent of the charged and neutral-kaon electroproduction data.

6.3 Theoretical Approaches

There are a number of distinct theoretical approaches used to describe electromagnetic interactions. The three major descriptions include hadrodynamic models, quark models, and models based on Regge theory. These data are expected to provide a unique opportunity for further development along each of these avenues. Furthermore, it is expected that detailed comparisons of these models to the observables of electroproduction, beyond allowing for an improved understanding of the reaction mechanism of open-strangeness production, will help to quantify the transition from non-perturbative to perturbative QCD. In the remainder of this section, further details regarding each of the three theories are described in specific relation to the data that will be acquired at 6 GeV.

6.3.1 Hadrodynamical Models

The main phenomenological method used in the investigation of the electromagnetic production of kaons is based on diagrammatic techniques through isobaric models [18, 19]. In this approach, an effective Lagrangian is constructed by summing the Feynman diagrams from the excitation of intermediate resonant states. The corresponding diagrams include the exchange of the N and N^* resonances in the s-channel, the K and K^* resonances in the t-channel, and the Y and Y^* resonances in the u-channel. The fact that both the incident photon and the outgoing kaon interact rather weakly with hadrons justifies the attempts to describe the process through models limited to first-order terms.

These models were developed mostly from fits to experimental data by allowing for a limited number of intermediate resonances and leaving their coupling constants as free parameters. However, the limited database permits only qualitative conclusions. For further development of these models, more cross section and polarization data is crucial to better understand which are the appropriate resonances to include in the intermediate state. Each reaction channel contributes to the process in varying degrees depending on the reaction kinematics, and each may go through a sizeable number of intermediate hadronic resonances. The presence of all these possible production mechanisms means that reliable hadrodynamic models require data over a broad kinematic range to constrain the parameters.

The forthcoming cross section and polarization measurements from JLab with energies up to 4 GeV should provide a wealth of data to strengthen and extend these models. However, higher-spin resonances are expected to contribute to a much greater extent as the energy available in the intermediate state increases. This fact represents one of the key aspects of extending the $K\Lambda$ and $K\Sigma$ reactions to 6 GeV. As well, the failures of the models to explain the data can be addressed given the coverage of the full resonance region. Only by learning where the models fail can we hope to learn the root causes of their deficiencies.

6.3.2 Quark Models

Hadrodynamic calculations are expected to become increasingly deficient as the energy in the intermediate state moves beyond the limits of the resonance region. This occurs as quark and gluon degrees of freedom begin to dominate the reaction mechanism and hadronic degrees of freedom become less important. Understanding the boundary between these two pictures is one of the key reasons for extending the measurement program to higher energies.

The extension of the electroproduction measurements to 6 GeV may shed further light on strange-quark production mechanisms, as well as the strange-quark content of the nucleon. In one naive kaon electroproduction scenario, highlighted in Fig. 57, a polarized virtual photon interacts with one of the two u quarks of the target proton. As the now polarized u quark recoils against the correlated ud pair, a color string is believed to stretch between the recoiling quark-diquark system of the decaying N^* resonance until it breaks, creating an $s\bar{s}$ pair. Since the K^+ has spin 0, and hence cannot carry polarization, this forces the spin of the $\bar{s}$ quark to be aligned opposite to that of the u quark. As the spin of the Λ is believed to be carried almost entirely by the s quark [20], the measurement of the Λ polarization can be used to study the spin alignment of the created $s\bar{s}$ pair.

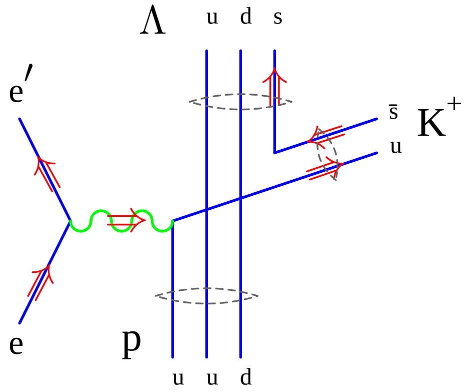

Figure 57: Quark level diagram for kaon electroproduction that is expected to become more valid as the energy of the virtual photon increases above the resonance region.

Quark models can provide the masses of intermediate resonances. This then needs to be coupled with quark-pair creation models (e.g. $^3\mathrm{P}_0$ or $^3\mathrm{S}_1$) that provide the strong-decay coupling constants of the baryonic resonances. One then uses a model for the photo-coupling vertices to produce the observables. Understanding the process of kaon electroproduction through quark-pair creation should improve at 6 GeV as W increases beyond the resonance region. We then no longer have to worry about attempting to isolate single resonances in the intermediate state or combining data sets to accomplish partial wave analyses. With appropriate kinematic cuts we can essentially concentrate directly on a pure s-channel quark picture of the reaction as highlighted in Fig. 57. Detailed tests of the decay models are therefore important and it is believed that polarization observables, and to some extent cross sections, will allow for sensitive tests. Also the large phase space coverage of CLAS can be used to study the different quark-level diagrams that contribute to $K\Lambda$ electroproduction through studies of the data as a function of Q^2, W, and t.

6.3.3 Regge-Exchange Models

Kaon photo- and electroproduction data for the reaction $\gamma^{(*)}p \to KY$ have been compared with a new gauge-invariant model based on a Regge description [23]. At intermediate energies ($E_\gamma \geq 4$ GeV) and intermediate momentum transfers ($-t \leq 3$ (GeV/c)^2), this model has proven to be superior to Born-diagram models when compared to the available cross section and asymmetry data.

It is expected that detailed comparisons of this model to the observables of electroproduction will also help to quantify the transition from the non-perturbative to perturbative QCD (pQCD) regimes. An extrapolation of the Regge model to momentum transfers where pQCD is valid has been performed for the pion photoproduction reaction with good results [23]. Similar extrapolations are planned for the kaon photo- and electroproduction reactions. As data at these kinematics are particularly sparse, measurements of kaon electroproduction observables above the resonance region are necessary for the development of theoretical models that bridge the transition region.

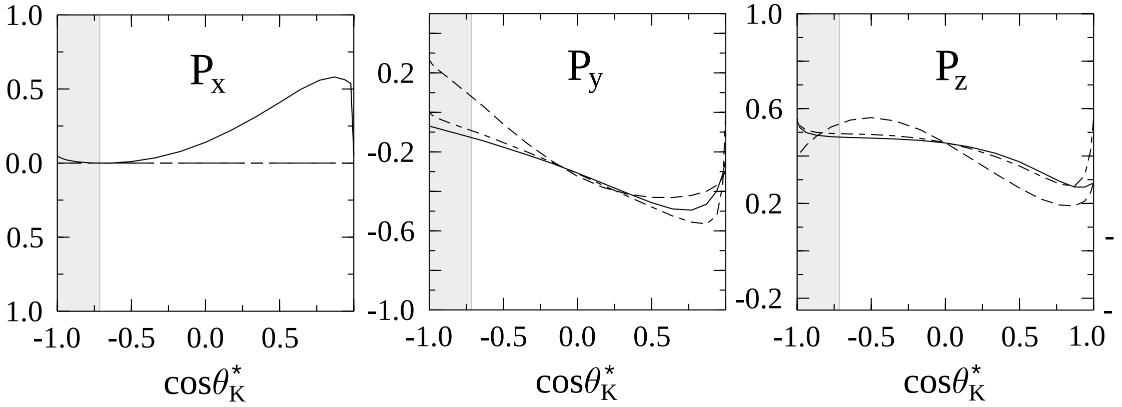

Figure 58: Electroproduction Regge exchange calculations for the three Λ polarization components at 6 GeV for W=2.2 GeV, Q^2=1.0 (GeV/c)^2 [24]. The solid curves are for the full calculation, the dashed curves are for K exchange only, and the dot-dashed curves are for K^* exchange only. The shaded portions of the plots correspond to where the calculation is extrapolated to higher t.

Results of recent 6 GeV calculations are presented in Fig. 58. The Λ polarization components in the $\vec{e}p \to e'K^+\vec{\Lambda}$ reaction are plotted against $\cos\theta_K^*$ for the fixed angle $\phi_K^* = 180°$. As the model has been developed for moderate momentum transfers, it is pushed to its limit at larger θ_K^*, where extrapolations to higher t are carried out. This is highlighted by the shaded portions of the plots.

At lower energies, only enough energy is available in the intermediate state to create K and K^* resonances. To fully test the idea of Regge-trajectory exchange, higher energies are necessary to create the higher-mass kaons in the intermediate state. Only through higher-energy studies can the notion of a trajectory exchange be more rigorously tested.

6.4 Monte Carlo Studies

For the 6 GeV simulation, the $ep \to e'K^+\Lambda$ reaction was generated by weighting the event kinematics and angular distributions by the calculated cross section based on the WJC model [19]. After selecting the beam energy, five quantities are necessary to completely characterize the $ep \to e'K^+\Lambda$ reaction in the laboratory system. These quantities are the scattered electron momentum p_e and scattering angles θ_e and ϕ_e. Also the center-of-mass angles of the electro-produced kaon θ^*_K and ϕ^*_K are generated. In addition to these quantities, the reaction vertex position is also generated at the target. At the present time, however, a point target is assumed. These events are thrown into GSIM, which uses the GEANT routines from the CERN libraries as a framework for the Monte Carlo simulation of the CLAS detector. The simulation properly included the known dead wires in the drift-chamber system, the known drift-chamber position resolution, and the known resolutions of the scintillators and calorimeters. The simulations properly accounted for in-flight K and Λ decays from their known life times. Radiative effects on the scattered electron were also modeled. The momentum, angles, and position of each particle at the target are reconstructed using RECSIS, the standard CLAS analysis software package. All simulations were performed at the maximum CLAS torus magnetic field setting of $0.9\mathrm{B}_0$.

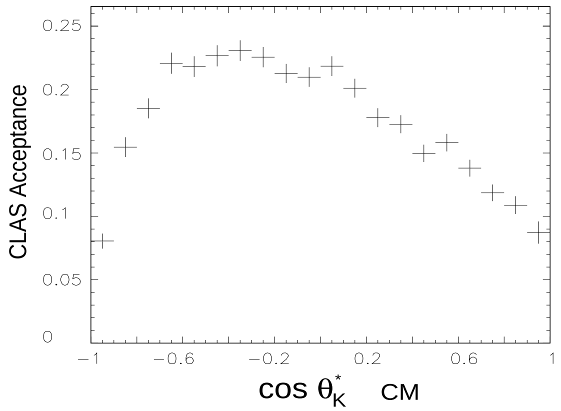

Figure 59: CLAS acceptance function for $ep \to e'K^+X$ summed over all Q^2 and W from 6 GeV Monte Carlo studies.

The CLAS acceptance for the $ep \to e'K^+X$ reaction, detecting only the scattered electron and electro-produced kaon is shown in Fig. 59 as a function of $\cos\theta^*_K$. The average acceptance of CLAS over all Q^2 and W for the $e'K^+$ two-body final state is roughly 20%.

The momentum and angles of the nucleons from the $p\pi^-$ and $n\pi^0$ Λ-decay branches are generated isotropically in the Λ rest frame. The main purpose of modeling the Λ decays is to evaluate the CLAS acceptance function of the three-body $e'K^+p$ final state in terms of $\cos\theta_p^{RF}$ for all three directions of the Λ-spin vector (x,y,z). The determination of this acceptance function is highlighted in Fig. 60. The three different plots represent the CLAS acceptance function for each of the three Λ-spin direction axes. The average acceptance of CLAS for $ep \to e'K^+pX$ over all Q^2 and W is roughly 5%.

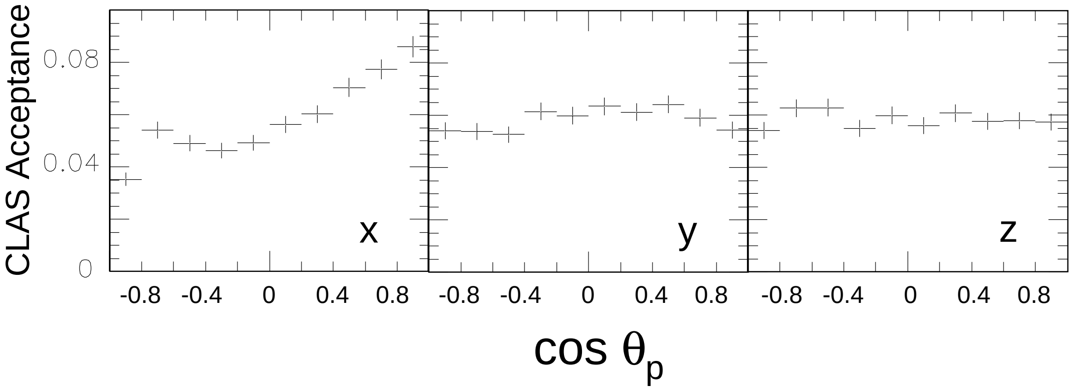

Figure 60: CLAS acceptance function for $ep \to e'K^+pX$ summed over all Q^2 and W from 6 GeV Monte Carlo studies. The three different columns correspond to the three different spin polarization axes (x,y,z) for the Λ.

6.5 Statistical Errors

The 6 GeV data set will span a range of Q^2 from 1.5 to 6 (GeV/c)^2 and W from 1.6 to 3.0 GeV. Keeping with the binning choices of E93-030 and E99-006, we have selected bins in W of 0.2 GeV and bins in Q^2 of 0.5 (GeV/c)^2 for estimates of statistical precision. The expected counting rates in each bin are given by:

$$RATE = \mathcal{L} \cdot \Gamma_v \cdot \sigma_v(Q^2, W) \cdot \Delta Q^2 \cdot \Delta W \cdot ACC. \tag{18}$$

In this expression, $\mathcal{L}$ is the beam-target luminosity, $\sigma_v(Q^2, W)$ is the total virtual photon cross section integrated over all hadronic CM angles ($d\Omega_K^*$), ΔQ^2 and ΔW are our chosen bin sizes, and ACC is the CLAS acceptance for the final state of interest.

To estimate the counting rates for this experiment, we have used the published $d\sigma_v/d\Omega_K$ electroproduction data from Bebek [25]. These data span Q^2 from 1.2 to 3.5 (GeV/c)^2, W from 2.1 to 2.7 GeV, and ϵ from 0.35 to 0.94. This data was limited to $\theta_K^* < 15°$. Using the t-dependence of the differential cross section from calculations of Bennhold allows us to estimate that these data contained ≈7.5% of the total events. With this factor, the total virtual photon cross section was determined. Our rate estimates have also included a scaling factor, applied uniformly to all bins, to force agreement of the calculated hyperon production rate bins over all Q^2/W with that determined from analysis of 5.56 GeV CLAS data. For our estimates, we have assumed flat acceptances for the $e'K^+$ and $e'K^+p$ final states of 20% and 5%, respectively.

Table 9 highlights our expected counts per 100 hours of running in each of our Q^2/W bins at a luminosity of 5×10^{33} cm^{-2}s^{-1}. The total predicted production rate of Λ hyperons detected through the $e'K^+p$ final state over all Q^2/W bins is 79/hour. Analysis of 5.56 GeV CLAS data shows this number to be 76±8/hour.

For the differential cross section measurements, we can determine how long we should run to achieve a given statistical error if we want at least 10 bins in θ_K^*/ϕ_K^* for each Q^2/W bin. From Table 9, our average $e'K^+$ rate over all Q^2/W bins is 9/hr. To achieve a 3% error in each $Q^2/W/d\Omega_K^*$ bin, requires 9000 counts in each Q^2/W bin, or with the given production rates, about 1000 hours of running at a single torus magnetic field setting.

Table 9 also allows us to estimate the statistical precision of our Λ polarization measurements. Each polarization component and its associated statistical error can be defined as:

$$P_\Lambda = \frac{2}{\eta\alpha} \cdot \frac{N_+ - N_-}{N_+ + N_-}, \qquad \sigma_{P_\Lambda} = \frac{2}{\alpha\eta\sqrt{N_0}} \cdot \left(1 - \frac{1}{4}\alpha^2 P_\Lambda^2\right)^{1/2}. \tag{19}$$

In this expression, η is the electron beam polarization and α is the Λ weak-decay asymmetry parameter. The total number of Λ decay protons detected in each Q^2, W, and $d\Omega_K^*$ bin is $N_0 = N_+ + N_-$. The number of protons in the Λ rest frame going forward and backwards (relative to the coordinate being considered) is given by N_+ and N_-, respectively. Eq(19) also makes it very clear that the statistical uncertainty goes as $1/\eta$, the electron-beam polarization. Thus the *highest* possible beam polarization is important to reduce our measurement uncertainties.

W	Q^2	$e'K^+$	$e'K^+p$
1.7	2.0	3586	897
	2.5	1254	314
	3.0	491	123
	3.5	209	52
	4.0	94	24
	4.5	45	11
	5.0	23	6
	5.5	12	3
1.9	2.0	4123	1031
	2.5	1567	392
	3.0	642	161
	3.5	294	74
	4.0	138	35
	4.5	68	17
	5.0	34	9
	5.5	18	5
2.1	2.0	3868	967
	2.5	1574	394
	3.0	692	173
	3.5	322	81
	4.0	156	39
	4.5	77	19
	5.0	39	10
2.3	2.0	3124	781
	2.5	1337	334
	3.0	610	153
	3.5	290	73
	4.0	142	36
2.5	2.0	2219	555
	2.5	978	245
	3.0	453	113
	3.5	215	54
2.7	2.0	1371	343
	2.5	603	151
	3.0	271	68
2.9	2.0	684	171

Table 9: Expected counts per 100 hours of running in CLAS in each of our Q^2/W bins at 6 GeV for a luminosity of 5×10^{33} cm^{-2}s^{-1}. A simple quark model has been used to extrapolate from the existing electroproduction cross section data. Energies and momenta in GeV.

Our expected errors on the Λ polarization are shown in Table 10 for one particular binning scenario in Q^2, W, $\cos\theta_K^*$, and ϕ_K^*. In determining the statistical uncertainty for the polarization measurements, a total running time of 1000 hours has been assumed with a beam polarization of 70% and a luminosity of 5×10^{33} cm^{-2}s^{-1}. This run duration is compatible with the other experiments in the run group.

6.6 Systematic Errors

There are two primary sources of systematic uncertainties: uncertainties associated with determination of the kinematic variables, and uncertainties associated with conditions of the experimental apparatus. Furthermore, the systematic errors are expected to enter differently for the cross section measurements and the polarization measurements.

	Statistical Uncertainty						
$Q^2 \downarrow \backslash W \rightarrow$	1.7	1.9	2.1	2.3	2.5	2.7	2.9
2.0	±0.09	±0.08	±0.07	±0.10	±0.11	±0.15	±0.21
2.5	±0.15	±0.14	±0.14	±0.15	±0.17	±0.22	-
3.0	±0.24	±0.21	±0.21	±0.22	±0.25	±0.33	-
3.5	±0.38	±0.31	±0.30	±0.32	±0.37	-	-
Q^2 bins : 0.5 (GeV/c)^2, W bins : 0.2 GeV $d\Omega_p^{RF}$ bins = 1, $\cos\theta_K^*$ bins = 4, ϕ_K^* bins = 1							

Table 10: Expected Λ polarization statistical uncertainties at 6 GeV for a 40 day run at a luminosity of 5×10^{33} cm^{-2}s^{-1} and 70% electron beam polarization for a given choice of binning in Q^2, W, and $d\Omega_K^*$.

A list of the various sources of relative systematic errors for the cross section measurements, including a description of the error, an estimate of the expected size, and an estimate of the effect on the cross section are included in Table 11. The correlated errors are added linearly, and the uncorrelated subsets are added in quadrature.

Source of Error: Size of Effect	Size of Error in Cross Section	Sum
Geometrical Acceptance 20%	3%	4%
In-flight K-decay: 10-90%	1%	
Angle Measurement: 1 mrad	1-2.5%	5%
Momentum Measurement: 0.5%	1.5%	
Beam Energy: 0.3%	0.9%	
Electron ID Efficiency 1-5%	1-5%	5%
Kaon ID Efficiency 1-5%	1-5%	5%
Radiative Corrections: 10-25%	2%	2%
Total	10%	

Table 11: A list of the sources of relative systematic uncertainty for the cross section measurements at 6 GeV.

The effects of systematic errors come in slightly differently for the polarization components, and the effects are also somewhat different for each component. Since we measure each polarization component integrated over ϕ_K^*, there is no helicity-dependent component in P_y. In this situation it is not possible to extract the polarization component without knowledge of the CLAS acceptance function. On the other hand, there are no helicity-independent polarization components for P_x and P_z. In this case ratio methods are available in which the CLAS acceptance function cancels out, assuming the CLAS acceptance function is independent of the helicity of the electron beam. However, in this case, we have an uncertainty due to the electron-beam polarization.

Table 12 summarizes the sources and estimated individual absolute systematic uncertainties for the three polarization components. The total is the sum of each of the individual sources of uncertainty added in quadrature.

In the end we will also have a number of self-consistency checks with respect to the

Source of Uncertainty	σ_{P_x}	σ_{P_y}	σ_{P_z}
Beam Helicity	±0.30	±0.00	±0.030
Proton Acceptance	±0.00	±0.04	±0.00
Background (Σ^0, π^+ etc.)	±0.03	±0.03	±0.03
Angle	±0.015	±0.015	±0.015
Momentum	±0.025	±0.025	±0.025
Beam Energy	±0.010	±0.010	±0.010
Radiative Corrections	±0.015	±0.015	±0.015
Total	±0.055	±0.061	±0.055

Table 12: A list of the sources of absolute systematic uncertainty for each polarization component at 6 GeV.

polarization observables that will help us to better understand our systematic uncertainties. These checks include: *(i).* After integration over ϕ_K^*, the polarization components P_x^0, P_z^0, and P_y' must be zero, deviations from zero will indicate problems with acceptance or energy calibrations, *(ii).* We can also bin data on a CLAS sector-by-sector basis so that any sector dependencies can be determined and corrected, *(iii).* The results for P_y^0 must be independent of the helicity state of the electron beam, and *(iv).* For a given W and Q^2 bin at a given beam energy, the results must be independent of the magnetic field setting of the CLAS torus.

6.7 Summary

This proposal describes a new program to study exclusive kaon electroproduction with CLAS at 6 GeV using the $ep \to e'K^+Y$, $Y = \Lambda, \Sigma$ reaction. This proposal represents an extension of the strangeness production experiments currently included in the e1 run group program in Hall B (including experiments: E89-043, E93-030, E95-003, and E99-006) to 6 GeV. The large acceptance of CLAS will allow us to efficiently detect the $e'K^+$ and $e'K^+p$ final states over a range of Q^2 from 1.5 to 6 (GeV/c)^2 and W from 1.6 to 3 GeV.

We conclude this summary section with the following remarks:

- The CLAS detector has a sizeable two-body and three-body final-state acceptance for the $e'K^+$ and $e'K^+p$ reactions, respectively, that will enable study of the cross sections, single-polarization, and double-polarization observables over a much broader range of Q^2, W, and t at 6 GeV compared to 4 GeV.
- The CLAS spectrometer has a large and uniform acceptance in $\cos\theta_K^*$ and ϕ_K^* that allows for a reliable determination of the σ_T, σ_L, σ_{TT}, and σ_{TL} structure functions, along with a portion of the TL' and TT' response functions.
- We have attempted to stress the importance of performing this experiment with the highest possible electron-beam polarization available from the accelerator to achieve the smallest possible statistical uncertainties on the polarization measurements.
- Our detailed analysis of the existing 2.4, 4.0, and 5.56 GeV data, in conjunction with our detailed Monte Carlo simulations of CLAS at 6 GeV, has enabled us to provide

a reasonably accurate estimation of our expected statistical uncertainties for the requested run time.

- The data are expected to allow for increased understanding of the reaction mechanism for strange quark production. Additionally, the data are expected to to provide for a unique opportunity for the further development and probing of the different theoretical approaches to study the interaction. These studies will help to quantify the transition from non-perturbative to perturbative QCD.
- This proposal describes a new experimental program to study kaon electroproduction with CLAS at 6 GeV. The goals are to extend physics knowledge that will be gained in previously approved experiments at lower energies as well as to explore new physics accessible only at higher energies. The physics that we are hoping to study is of broad interest within the community.

References

[1] K.H. Hicks, M.D. Mestayer *et al.*, JLab Experiment E93-030.

[2] K. Dhuga, R.A. Schumacher *et al.*, JLab Experiment E95-003.

[3] L. Dennis, H. Funsten *et al.*, JLab Experiment E89-043.

[4] D.S. Carman, K. Joo, L. Kramer, B.A.Raue *et al.*, JLab Experiment, E99-006.

[5] S. Steininger *et al.*, Phys. Lett. B **391**, 446 (1997).

[6] N. Kaiser *et al.*, Nucl. Phys. A **612**, 297 (1997).

[7] P. Brauel *et al.*, Z. Phys. C **3**, 101 (1979).

[8] G. Niculescu *et al.*, Phys. Rev. Lett. **81**, 1805 (1998).

[9] J. Clemans and F.E. Close, Nucl. Phys. B **85**, 429 (1975).

[10] G. Knöchlein, D. Drechsel, L. Tiator, Z. Phys. A **352**, 327 (1995).

[11] D.B. Lichtenberg, Phys. Rev. **178**, 2197 (1969).

[12] S. Capstick and W. Roberts, Phys. Rev. D **58**, 74011 (1998).

[13] M.Q. Tran *et al.*, Phys. Lett B **445**, 20 (1998).

[14] D.P. Barber *et al.*, Z. Phys. C **7**, 17 (1980).

[15] T. Azemoon *et al.*, Nucl. Phys. B **95**, 77 (1975).

[16] C. Bennhold *et al.*, Preprint nucl-th/9711048, (1997).

[17] M.G. Sapozhnikov, Preprint hep-ex/9812025, (1998).

[18] J.C. David, C. Fayard, G.H. Lamot, and B. Saghai, Phys. Rev. C **53**, 2613 (1996); T. Mizutani, C. Fayard, G.H. Lamot, B. Saghai, Phys. Rev. C **58**, 75 (1998).

[19] R.A. Williams, C. Ji, and S.R. Cotanch, Phys. Rev. C **46**, 1617 (1992).

[20] K. Ackerstaff *et al.*, Eur. Phys. J. **C2**, 49 (1998).

[21] A. LeYaouanc *et al.*, Phys. Rev D **8**, 2223, (1973); Phys. Rev. D **9**, 1415, (1974); Phys. Rev. D **11**, 1272, (1975).

[22] J.W. Alcock *et al.*, Z. Phys. C **25**, 161 (1984); S. Kumano and V.R. Pandharipande, Phys. Rev. D **38**, 146 (1988).

[23] M. Guidal *et al.*, Nucl. Phys. A **627**, 645, (1997); M. Vanderhaeghen *et al.*, Phys. Rev. C **57**, 1454, (1998); M. Guidal *et al.*, Preprint hep-ph/9904511, (1999).

[24] Calculations by J.M. Laget, unpublished, (1998).

[25] C.J. Bebek *et al.*, Phys. Rev. D **15**, 3082 (1977).

7 High Q^2 ϕ-Meson Production

Spokespersons: W. Brooks[a] and H. Funsten[b]

[a]Jefferson Laboratory, Newport News, VA 23606
[b]The College of William and Mary, Williamsburg, VA 23187

This section describes a new experiment to study the data for evidence of a signal for the decreasing size of electro-produced $\phi(1020)$ mesons with Q^2 using CLAS. This proposal represents a 6 GeV extension to the approved Hall B experiment E93-022 studying $\phi(1020)$ polarization in exclusive electroproduction at 4 GeV.

7.1 Vector Meson Electroproduction

In vector meson (VM) electroproduction, the "bare" photon fluctuates in a time t^{lab}_{fluc} into a VM that diffractively scatters from the proton target. The t distribution of this meson is given by:

$$\frac{d\sigma}{dt} \propto e^{-b|t|}. \tag{20}$$

Here, the slope parameter b measures the transverse size of the interaction region R_{int}, the sum of the VM transverse size R^{VM}_T and the target size R^{hadron} (which is $\approx$1 fm). t^{lab}_{fluc} is related to Bjorken x_B, as asymptotically, $x_B \propto (t^{lab}_{fluc})^{-1}$. An increase in the virtual photon mass Q^2 should result in $R^{VM}_T(|Q^2|)$ "shrinking", along with a corresponding "hardening" or decrease of b.

Among the low-mass vector mesons, ϕ electroproduction best exhibits possible shrinking. The ϕ, an $s\bar{s}$ meson, has minimal q exchange with the target as its width is only 4 MeV. Furthermore, there is minimum overlap with other mesons.

This proposal represents an extension of the 4 GeV exclusive ϕ electroproduction experiment (E93-022) to 6 GeV in order to obtain the Q^2 dependence of transverse size of the ϕ $R^{\phi}_T(|Q^2|)$ as measured by b.

7.2 Models of Transverse-Size Shrinkage with Q^2

Two models have been suggested regarding the transverse-size shrinkage of the ϕ meson with Q^2.

1). Vector Meson Dominance model (VMD): The VMD model assumes that the longitudinal extent of the meson goes as:

$$R^{\phi}_{longitudinal}(|Q^2|) = ct^{lab}_{fluc}. \tag{21}$$

When transformed to the ϕ center-of-mass, this extent can be written as [1]:

$$R^{\phi}_T(|Q^2|) = c\frac{M_\phi}{M^2_\phi + |Q^2|}. \tag{22}$$

2). Quark model (QM): The QM assumes that the longitudinal extent of the meson is equivalent to the maximum transverse distance separating a quark pair which, when evaluated in the Breit frame, yields a transverse extent given by [2, 3]:

$$R_T^{\phi}(|Q^2|) = \frac{R^{hadron} M_{\phi}}{\sqrt{M_{\phi}^2 + |Q^2|}}. \tag{23}$$

From these two expression for the transverse size, the QM exhibits a less rapid fall off of b with Q^2.

The parameter b will depend strongly on several other factors, namely, the meson fluctuation distance and the expansion distance. For fluctuation distances $ct^{lab}_{fluc} >> R_{int}$, the incident photon remains hadronically "dressed", and b saturates to a maximum value of $b_{sat} \approx 7 \;\; \text{GeV}^{-2}$. This value is seen to be typical for hadronic diffractive scattering. As the fluctuation distance decreases below the transverse size of the interaction region R_{int}, b enters a transition region. In this region b_{trans}, the "bare" point-like photon component becomes increasingly predominant as ct^{lab}_{fluc} decreases, and the scattering becomes harder. Thus with b_{trans}, the magnitude of b decreases.

The expansion distance ct_{form} represents the distance over which a "shrunken" ϕ can expand back into a conventional hadron with size R^{hadron}. In the ϕ rest frame, t_{form} is given approximately by a typical $s\bar{s}$ multiplet-mass splitting $m_{\phi} - m_{\eta}$. For the kinematics of this proposed experiment, $ct_{form} \approx$3 fm.

7.3 Data Analysis Techniques

To determine the variation of b with Q^2, data should be analyzed at constant fluctuation times. For constant ct^{lab}_{fluc} and electron beam energy, Q^2 and W^2 are linearly related. This is shown in Fig. 61, which displays lines of constant fluctuation times in the Q^2 and W^2 plane available in data taken in a short CLAS run this spring at 5.56 GeV. Hence in making measurements of b versus Q^2, the kinematic variables W and Q^2 should be confined along lines of constant ct^{lab}_{fluc}.

7.4 Existing Data

Electromagnetic ρ meson production is presently the most extensive data set available for studies of the vector meson size [4]. In the data, two different regions of b exist. These regions correspond to long and short fluctuation distances ct^{lab}_{fluc} as detailed below.

1). For $ct^{lab}_{fluc} > 2.5$ fm ($x_B <\approx 0.1$) the virtual photon is completely "dressed" as a ρ meson, and b is saturated at a value b_{sat}. Variation of b with Q^2 is expected to be at a maximum.

2). For $ct^{lab}_{fluc} < 2.5$ fm ($x_B >\approx 0.1$) the value b decreases. For this situation the virtual photon becomes a "bare", point-like photon. One expects that as $t^{lab}_{fluc} \rightarrow 0$, the size parameter of the meson vanishes and

$$R_{int} \rightarrow R^{hadron}, \qquad b \rightarrow \frac{b_{max}}{4} \approx 1.6 \text{ GeV}^{-2}. \tag{24}$$

The ρ data supports this. In the b transition region, b varies between b_{sat} and the value of b characteristic of a point-like virtual photon.

The ρ data agrees with the quark model in both t^{lab}_{fluc} regions. In the b_{trans} region (2 above), $b_{\rho}^{Q^2 av}(t^{lab}_{fluc})$ varies with t^{lab}_{fluc} , and the $|Q^2|$ variation of b was determined at **constant** t^{lab}_{fluc} .

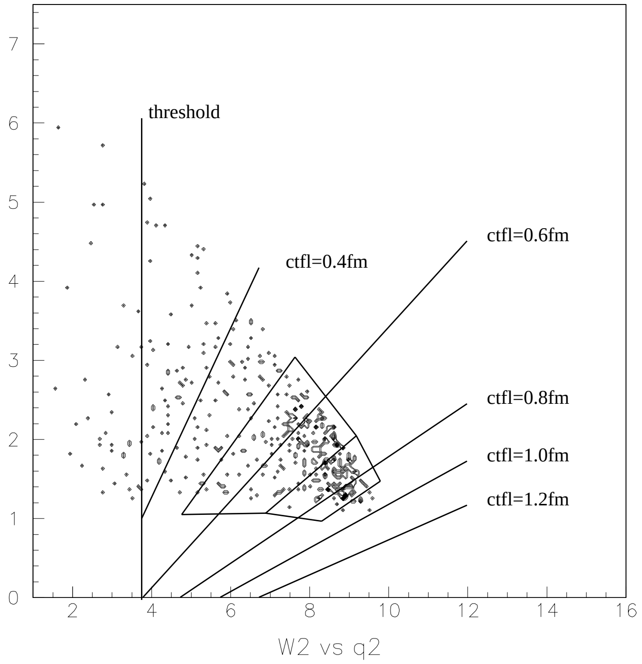

Figure 61: Phase space coverage of CLAS in Q^2 (y-axis) vs. W^2 (x-axis) from 5.56 GeV CLAS data showing lines of constant ct_{lab}^{fluc}.

Data from ω and ϕ mesons is sparse. What data does exist for the ω shows that b_ω exhibits the same decrease with t_{fluc}^{lab} as that for ρ mesons. There is no useful data on the b_ω variation with $|Q^2|$ at constant t_{fluc}^{lab} . For ϕ mesons, b_ϕ has approximately the same variation with t_{fluc}^{lab} as that for ρ production. The variation of b_ϕ with $|Q^2|$ cannot be determined.

7.5 Extension of ϕ Electroproduction to 6 GeV

For ϕ electroproduction the reaction $e + p \rightarrow e' + p' + K^+ + X$ will be used. From the $e' + p' + K^+ + X$ missing mass the K_{recon}^- is reconstructed. The ϕ meson is then reconstructed from the $e' + p' + X$ missing mass via a cut on the K_{recon}^-) mass.

The variation of $b_\phi(t_{fluc}^{lab}, |Q^2|)$ with Q^2 will be determined by analyzing data from two electroproduction and two photoproduction W^2, Q^2 regions, centered on lines of constant ct_{fluc}^{lab} to avoid variation of b with ct_{fluc}^{lab}. From analysis of the 5.56 GeV run, electroproduction regions centered on $ct_{fluc}^{lab} = 0.6$ and 0.8 fm are accessible as shown in Fig. 61.

These t_{fluc}^{lab} values correspond, in photoproduction, to $W^2 = 3.6$ (threshold) and 5.3 GeV^2 respectively, ($E_\gamma = 1.5$ and 2.4 GeV respectively). By combining photoproduction data [5] and electroproduction data, measurements of the Q^2 variation of b can be thus carried over a significant Q^2 range, $0 \rightarrow \approx 2$ (GeV/c)^2, at constant t_{fluc}^{lab} .

7.6 Estimation of Measurement Uncertainties

Scaling the 5.56 GeV data to a 40 day run results in ≈1500 reconstructed ϕ mesons in each of the two above W^2, Q^2 electroproduction regions. The 5.56 GeV data yielded a ϕ peak to (phase space + background) ratio of $\approx 2/1$.

A GSIM simulation was made of the reaction and yielded a 2% acceptance for the above kinematic cuts. Interpolating electro-phi production cross sections of Ref. [4] to the above kinematics, resulted in a simulated ϕ event rate only 20% less than the observed 5.56 GeV event rate. The simulation resulted in a flat t acceptance within $\approx$20% for $t > 2$ (GeV/c)^2. It yielded an uncertainty in the measured exponential slope parameter b of $\delta b/b \approx 8\%$.

The photoproduction data will result in >3000 reconstructed ϕs over a W^2 interval of 3.8 to 5.3 GeV^2 [5]. Dividing this into the two W^2, $Q^2 = 0$ regions, corresponding to the two above values of t^{lab}_{fluc} , yields an equivalent photoproduction statistical uncertainty in $\delta b/b$ of approximately the same as that for electroproduction, $\delta b/b =\approx 8\%$.

The expected relative electro/photo difference in b predicted by the VMD model, is :

$$\frac{\Delta b}{b} = \left(1 - \frac{b_{electro}}{b_{photo}}\right) \approx 50\% \text{ (VMD)},\ 30\% \text{ (QM)}. \tag{25}$$

(electroproduction was evaluated at Q^2=1.5 (GeV/c)^2 and $ct^{lab}_{fluc} = 0.8$ fm).

The above fluctuation times are in the transition region and may induce a possible dampening of Δb. The amount of dampening is uncertain; at its maximum, the above variations in b could be reduced by a factor of 2. A 40 day electroproduction run, together with the photoproduction data, can readily distinguish the difference in b between the QM and VMD predictions. Under maximum Δb dampening, the experiment can confirm the validity of the VMD prediction.

7.7 Possible Future Additional Measurements

7.7.1 L,T ϕ Polarization Measurements

CLAS will also permit determination of the σ_L and σ_T components of the ϕ through the decay angular distribution data of the K^+K^- final state. Asymptotically, $\bar{q}$ helicity = - q helicity, and the $q\bar{q}$ state is longitudinal. b, evaluated for the longitudinal components of the virtual photon and ϕ meson, should show preferential hardening with $|Q^2|$ relative to the transverse components. ρ electroproduction data analysis, affecting L,T separation by assuming s-channel helicity conservation, supports this idea.

7.7.2 Semi-Exclusive 6 GeV Measurements

Sensitivity of b to the transverse size of the ϕ meson can be increased by hardening the lower (proton) vertex. In other words, by analyzing a more inclusive reaction topology, $ep \to e'\phi X$, without the $e'pK^+$ missing mass cut. At 6 GeV, $M_X \leq\approx 2$ GeV/c^2.

7.7.3 Gluon Condensation

There have been indications of a gluon condensate, gg, with $r_{gg} << R^{hadron}$ [6]. A CLAS photo-ϕ experiment [7] will examine this effect that may appear as a sharp dip in $d\sigma/dt$ at $t = 2 \to 3$ (GeV/c)^2. The dip arises from the interference between (gg) q scattering at low values of t and (gg) qq scattering at high t. Although expressions of J. Arvieux and B. Pire, based on Cudell and Landshoff, and Nachtman, predict a $d\sigma/dt$ shape approximately independent of Q^2, ϕ electroproduction may indicate the possible dip moving to lower values of t with increasing $|Q^2|$.

References

[1] T.H. Bauer *et al.*, Rev. Mod. Phys. **50**, 261 (1978).

[2] C. Carlson, private communication

[3] L. Frankfurt, W. Koepf, and M. Strikman, Phys. Rev. D **54**, 3194 (1996).

[4] D.G. Cassel *et al.*, Phys. Rev. D **24**, 2803 (1981).

[5] D.J. Tedeschi, official CLAS approved project, G1 and subsequent runs.

[6] P.V. Landshoff and O. Nachtmann, Z. Phys. C **35**, 405 (1987); J. R. Cudell, Nucl. Phys. B **336**, 1 (1990).

[7] J.M. Laget *et al.*; see also Nucl. Phys. A **581**, 397 (1995).

8 Search for $J^{PC} = 1^{-+}$ Exotic Mesons

Spokespersons: I. Aznauryan[a], H. Funsten[b], and S. Stepanyan[a]

[a]Yerevan Physics Institute, Yerevan, Armenia, 375036
[b]The College of William and Mary, Williamsburg, VA 23187

8.1 Introduction

The gluon, the QCD gauge boson, carries color charge. It can have a component characterizing it as a force, and a component characterizing it as a constituent particle [1]. Thus it can act as a particle and experience a binding force to quarks arising from additional gluons interconnecting to the quarks. One thus expects a class of hadrons, known as hybrid mesons, comprised of a valence gluon bound to two quarks, $gq\overline{q}$. In addition, there are expectations for the existence of a gg glueball meson, and for the existence of hybrid baryons $gqqq$. QCD models have made a variety of predictions of the masses, widths, and decays of hybrid $gq\overline{q}$ states [1, 2, 3, 4, 5, 6]. The discovery of hybrids would be a strong confirmation of QCD, and important for understanding the non-perturbative structure of hadrons.

The detection of a state with the exotic quantum numbers $J^{PC} = 1^{-+}$will unambiguously indicate a hybrid. Although non-exotic hybrids (*i.e.* hybrids with conventional quantum numbers) exist, disentangling them from $q\overline{q}$ states with the same quantum numbers is difficult.

Most of the searches for exotics have used hadronic production, *i.e.* $\pi^- p$ and $p\overline{p}$ reactions, characteristically yielding high statistics data. J/ψ decays have been studied, but with considerably lower statistics. e^+e^- reactions have been used to search for exotic production via a 2γ process [7]. Although the results of these experiments have not been conclusive, there is a general indication of the possible existence of hybrid states.

8.2 Theoretical Predictions and Existing Data

8.2.1 Theory

Predictions have been made for hybrids in several different QCD models and have been presented in hadron spectroscopy workshop proceedings [8] and reviews [9]. All models, in general, predict $J^{PC} = 1^{-+}$ hybrids with masses at or below 2.0 GeV/c^2 [4, 5, 6, 10, 11]. Widths in the range $\Gamma \approx 50 \rightarrow 200$ MeV are favored. The predicted decay modes are uncertain. In some models, gluonic excitation does not transfer its spin to the relative orbital angular momentum of final-state mesons, and hybrid decay to two mesons consisting of s-wave quarks does not occur. However, other models [10, 12, 13, 14] predict such decay. It occurs through such effects as spurious bag CM motion [10], or through the sequential decay of the exotic hybrid into a non-exotic hybrid, and then into a conventional meson via mixing [14]. The non-exotic hybrid is mixed with a conventional meson that appears in the final state. In this description the $\pi\eta(\eta')$ have small constituent gluonic components. In general, branching ratios of $BR_{\eta\pi} \approx 0.1$ and $BR_{\eta\pi}/BR_{\eta'\pi} \approx 1/3$ are predicted.

There are only a few reports on the production mechanisms and the cross sections for hybrid production. In Ref. [15], a detailed description of photo and electroproduction mechanisms of $J^{PC} = 1^{-+}$ exotic hybrids is given. It is shown that the predominant electromagnetic production mechanisms of $J^{PC} = 1^{-+}$states can be estimated for forward scattering by using values of allowed hadronic couplings and VMD. The forward production of positive $J^{PC} = 1^{-+}$ (also $a_2(1320)$) proceeds predominantly via π^+ exchange because of the large πNN coupling. Electromagnetic production of neutral $J^{PC} = 1^{-+}$ mesons can go only through the C-odd ω and ρ exchanges, ω exchange being dominant at small momenta transfers because:

(a) the coupling constant $g_{\omega pp}$ is larger than $g_{\rho pp}$: $g_{\omega pp} \simeq 4 \cdot g_{\rho pp}$ [16]
(b) the coupling constant $g_{\rho\gamma}$ is larger than $g_{\omega\gamma}$: $g_{\rho\gamma} \simeq 3 \cdot g_{\omega\gamma}$.

Since spin-nonflip $g^V_{\omega pp}$ is much larger than spin-flip $g^T_{\omega pp}$, in the forward direction the $\hat{X}$ polarization equals that of the virtual photon. Production of the neutral $J^{PC} = 1^{-+}$ system is dominated at small momentum transfer by spin-nonflip natural parity exchange.

The flux tube description of the hybrid electroproduction mechanism and qualitative estimates of the relative cross sections are given in Ref. [17]. The conclusion is made that meson electroproduction by electro-excitation of an exchanged meson should readily produce hybrid mesons, and that exclusive hybrid meson production cross sections should be comparable to exclusive ordinary meson production cross sections.

In Ref. [18] there is an attempt to estimate $J^{PC} = 1^{-+}$hybrid meson photo and electroproduction cross sections. It is argued that the cross sections only weakly depend on the $\pi^+\gamma \rightarrow J^{PC} = 1^{-+}$ transition form factor, and peaks at energies near the threshold. The estimated photoproduction cross section is of order of 0.3 to 0.8 μb, and is large enough for experimental studies at JLAB.

8.2.2 Existing Data

Several experiments have examined the decay angular distribution of final state mesons in hadronic production in order to detect $J^{PC} = 1^{-+}$ exotic hybrid states. In most of the experiments, the final states $\eta\pi$ and $\eta'\pi$ were studied [19, 20, 21, 22, 23, 24]. In the E272 [21, 22, 23] final states, $\rho\pi^+$ and $D(1285)\pi^+$ were analyzed as well.

The most recent data on the existence of an exotic state has been reported by the E852 collaboration [25]. The $\eta\pi^-$ final state was studied in the interaction of negative pions with a hydrogen target at 18 GeV beam energy. A large asymmetry in the angular distribution of the decay products was observed. Partial wave analysis (PWA) of this data shows a clear $a_2(1320)$ sign in the $J^{PC} = 2^{++}$ wave and $J^{PC} = 1^{-+}$ resonance structure at M = 1.37 GeV/c^2, which is an exotic hybrid.

There are no reported electroproduction experiments, and photoproduction data of hybrids are sparse. There are two reported experiments on photoproduction of hybrids that are not necessarily J^{PC} exotics. Final state meson systems other than $\pi\eta(\eta')$ were observed. The first experiment was diffractive photoproduction of the $b_1\pi$ system [26]. There were two resonant structures for $m_{b_1\pi} \geq 1.5$ GeV/c^2. The first structure was interpreted as the $\omega_3(1670)$. The second had a centroid mass of 1.8 GeV/c^2 and a width $\leq$0.3 GeV, and was interpreted as a gluonic hybrid.

The second experiment was photoproduction of an isovector $\rho\pi$ meson system [27]. A resonant structure was observed at an invariant mass of ($\rho\pi$) 1.775 GeV/c^2. The structure can not be interpreted as a $\pi_2(1670)$ due to a significant mass shift ($\approx$100 MeV/c^2) and dominant $\rho\pi$ coupling. The angular distribution of the decay in the Gottfried-Jackson frame was consistent with $J^P = 1^-; 2^-; 3^+$.

8.3 Proposed Experiment

This experiment is based on the conditionally approved proposal E94-118. The experiment we propose is to look for electroproduction of an exotic hybrid from a hydrogen target, with isospin 1 and $J^{PC} = 1^{-+}$. In electromagnetic production, hybrids may be produced via vertices that do not exist in hadro-production. Electroproduction allows measurements of couplings to polarization states not accessible with either a pion or real photon beam. Furthermore, transition form factors can also be measured and studied.

We propose to use CLAS to search for exotic hybrids in the $\pi^+\eta(\eta')$ and $\pi^0\eta(\eta')$ decay channels at $E_e = 6$ GeV beam energy. The reactions to be studied are:

$$1)\ ep \rightarrow e'\hat{X}^+ n;\ \hat{X}^+ \rightarrow \pi^+\eta(\eta')$$

$$2)\ ep \rightarrow e'\hat{X}^0 p;\ \hat{X}^0 \rightarrow \pi^0\eta(\eta'),$$

where $\hat{X}^{\binom{+}{0}}$ are the charged/neutral $J^{PC} = 1^{-+}$exotic hybrid mesons. Measurements will be done in the hadronic mass range $W \geq$2.6 GeV and $Q^2 \geq 0.5$ (GeV/c)^2. The final-state mesons, π, η, η', will ensure the desired C parity of the decaying meson.

The ability of the Hall B CLAS spectrometer to detect multi-particle final states will allow determination of the J and P from the $W(\theta, \phi, \Phi)$ of the pseudoscalar decay. Here θ is the decay polar angle, ϕ is the angle between the decay and hadron CM planes, and Φ is the angle between the electron and hadron CM planes.

$W(\theta, \phi, \Phi)$ uniquely determines J and P since the relative orbital angular momentum of the two pseudoscalar mesons, characterizing $W(\theta, \phi, \Phi)$, is equal to J. $W(\theta, \phi, \Phi)$ also determines the polarization of the hybrid meson, *i.e.* the measurement is polarization "self analyzing". The C, J, P measurement will then identify a $J^{PC} = 1^{-+}$ exotic.

8.4 Acceptance Simulations

As noted above, the hybrid exotics will be studied via decay modes: $\pi^+\eta$, $\pi^+\eta'$, $\pi^0\eta$, and $\pi^0\eta'$. Reconstruction of π^0 and η mesons will be done by detection of their two photon decays, and η' reconstruction will be mainly by the $\rho\gamma$ decay mode. The final detected particles in the reactions (1) and (2) are:

(1) $\hat{X}^+ \Rightarrow \pi^+\eta$: $e'\ \pi^+\ \gamma\ \gamma$
$\quad\ \hat{X}^+ \Rightarrow \pi^+\eta'$: $e'\ \pi^+\ \pi^+\ \pi^-\ \gamma$
(2) $\hat{X}^0 \Rightarrow \pi^0\eta$: $e'\ p\ \gamma\ \gamma\ \gamma\ \gamma$
$\quad\ \hat{X}^0 \Rightarrow \pi^0\eta'$: $e'\ p\ \pi^+\ \pi^-\ \gamma\ \gamma\ \gamma$.

Realistic simulations have been performed using the standard simulation and reconstruction tools for CLAS.

Calculations of acceptances and resolutions for each of the four final states were made at W=3.0 GeV and Q^2=0.6 (GeV/c)^2 at 6 GeV beam energy and torus field setting at 1/2 strength with negatives bending outward. The obtained acceptance for the $\pi^+\eta$ final state was $A_{\pi^+\eta} \approx 11\%$. Acceptances for the other final states were: $A_{\pi^+\eta'} \approx 4\%$; $A_{\pi^0\eta} \approx 4.5\%$; and $A_{\pi^0\eta'} \approx 1\%$.

8.5 Cross Section and Counting Rates

There is no reported data on electromagnetic production of the $J^{PC} = 1^{-+}$ hybrid. However an upper limit on the $J^{PC} = 1^{-+}$photoproduction cross section can be estimated using existing data on $a_2(1320)$ ($J^{PC} = 2^{++}$) photoproduction, the $a_2(1320)$ radiative decay width, and measured upper limits for Primakoff $J^{PC} = 1^{-+}$ hybrid production [28]. Estimated upper limit of hybrid photoproduction cross section is $\sigma^{\gamma}_{\hat{X}}$=0.9 μb. This estimate is very close to that in Ref. [18] for an exotic mass around 1.4 GeV/c^2. Then $\hat{X}$ photoproduction cross section can be extended to electroproduction:

$$\frac{d^2\sigma_{ep\to\hat{X}^+n}}{dQ^2dW} = \Gamma_e \cdot F_\rho \cdot \sigma^{\gamma}_{\hat{X}}, \tag{3}$$

where Γ_e is the Mott cross section and F_ρ is a factor based upon $\gamma \to \rho$ VMD conversion. For W = 3.0 GeV and Q^2=0.6 (GeV/c)^2 at 6 GeV beam energy, and $\Gamma_e \cdot F_\rho = 8.4 \cdot 10^{-4}$, this yields a cross section of $\approx 7.6{\times}10^{-4}$ μb(GeV/c)$^{-3}$.

Table 13 shows the estimated count rates for ΔW =0.6 GeV and ΔQ^2=0.5 (GeV/c)^2 for one day of running at luminosity $L = 1 \times 10^{34}$ cm^{-2}s^{-1}.

Process	Decay Modes and Branching Ratios				Acc.	Counts
$ep \to e'\hat{X}^+$	$\hat{X} \to \eta\pi^+$	0.1	$\eta \to \gamma\gamma$	0.39	0.11	1040
$ep \to e'\hat{X}^+$	$\hat{X} \to \eta'\pi^+$	0.3 : 1.4†	$\eta' \to \pi^+\pi^-\gamma$	0.3	0.04	620
$ep \to e'a_2^+n$	$a_2^+ \to \eta\pi^+$	0.15 :	$\eta \to \gamma\gamma$	0.39	0.11	3600

† Using $BR(\hat{X}^+ \to \pi^+\eta') = 3 \cdot BR(\hat{X}^+ \to \pi^+\eta)$ and phase space factor for η' of 1.4.

Table 13: Count Rates for one day of running at $L = 1 \times 10^{34}$ cm^{-2}s^{-1}.

8.6 Background

Coherent and incoherent background for $\hat{X}$ identification will arise from multi-particle final state events. Incoherent background was estimated for the final states in reaction (1) using the CELEG code [29] as an event generator. In the deep inelastic region CELEG uses the Lund Monte Carlo program LEPTO [30]. Events from the above generator were simulated in the CLAS detector, and defined cuts for identifying an exotic meson were used to reconstruct the final states.

Using the branching ratios and CLAS acceptance, the resulting ratio of reconstructed $ep \to e'\hat{X}^+$ to background was estimated to be ≈4:1. A similar estimation for the $\pi^+\eta'$ final state of (1) resulted in an upper limit for the background contribution of $<$ 20%.

Coherent background arises from production of conventional mesons that decay to the specific final states in (1) and (2). However only a limited number of them, *i.e.* those with natural spatial and C parity (*i.e.* $J^{PC} = 0^{++}, 1^{-+}, 2^{++}, ...$) decay to $\pi\eta$ or $\pi\eta'$ final states. The decay angular distribution partial wave analysis that is necessary for the $J^{PC} = 1^{-+}$ exotics will permit additional identification of these conventional mesons.

Among the well known mesons in the mass range $m_M \geq$1.3 GeV/c^2, only the 2^{++} a$_2$(1320) has a large radiative width and branching ratio to $\pi\eta$. There are no known mesons with significant branching ratio to the $\pi\eta'$ final state (BR($a_2(1320) \rightarrow \pi\eta'$) < 1% [31]). Hence the $a_2(1320)$ appears to be the only other meson in this mass range having the final states of reactions (1) and (2). In previous experiments with π beams, the signature of exotics was found in accompaniment with the a_2 [19, 20, 24]. In Table 13 we show the estimated rate for $a_2^+(1320)$ electroproduction under the same kinematic conditions and decay meson systems as the exotic production. The estimated statistics will allow reliable analysis to determine the hybrid and $a_2(1320)$ meson properties.

8.7 Summary

This experiment will search for an $\hat{X}^{\overset{+}{0}}$, $J^{PC} = 1^{-+}$ exotic hybrid meson in electroproduction using the Hall B CLAS detector. The mass range of $\hat{X}^{+(0)}$ will be up to $\approx$2 GeV/c^2. The hybrid will be unambiguously reconstructed through the $\eta\pi^{+(0)}$ and $\eta'\pi^{+(0)}$ decay channels. In addition, the zero spin of the decay-channel mesons permit unique determination of the J and P of the exotic hybrid by measurement of the decay angular distribution, $W(\theta, \phi, \Phi)$. The polarization of the hybrid, and hence the electroproduction helicity amplitudes, can additionally be determined from $W(\theta, \phi, \Phi)$, giving a powerful tool in determining the production mechanism.

A 15 day run at a beam energy of 6 GeV will be required in order to get sufficient statistics for PWA. The number of reconstructed events in the $\eta\pi^+$ mode is expected to be $\approx$15,000. The background count rate is expected to be in order of 1/4 of the signal. CLAS will be used in its standard setting, the target will be liquid hydrogen, and the torus magnetic field will be set at half of its maximum value, with polarity such that negatives bend outward.

The full proposal (PR-94-118) was presented and conditionally approved by PAC-9 [32].

References

[1] D. Horn and J. Mandula, Phys. Rev. D **17**, 898 (1978).

[2] T.H. Burnett and S.R. Sharpe, Ann. Rev. of Nucl. Sci. **40**, 327 (1990).

[3] L.G. Landsberg, Phys. of Atomic Nuclei **57**, 42 (1994).

[4] N. Isgur, R. Kokoski, and J. Paton, Phys. Rev. Lett. **54**, 869 (1985).

[5] F. deViron and J. Weyers, Nucl. Phys. B **185**, 391 (1981).

[6] I.I. Balitsky, D.I. Dyakonov, and A.V. Yung, Z. Phys. C **33**, 265 (1986).

[7] Z. Li, Hadrons '91, S. Oneda and D.C. Peaslee, Eds., World Scientific, 726 (1992).

[8] Proc. of the 2nd Int. Conf. on Hadron Spectroscopy, 1987, Tsukuba, Japan;
Glueballs, Hybrids and Exotic Hadrons: Workshop, 1988, Upton, NY;
Hadron-89: Proc. of the 3rd Int. Conf. on Hadron Spectroscopy, 1989, Ajaccio, Corsica;
Hadron-91: Proc. of the 4th Int. Conf. on Hadron Spectroscopy, 1991, College Park, Maryland.

[9] L. Landsberg, Preprint of IHEP 91-180, Parts I and II, Protvino 1991.

S.-U. Chung, Nucl. Phys. A **473**, 511 (1988); Z. Phys. C **46**, 111 (1990).

[10] M. Chanowitz and S. Sharpe, Nucl. Phys. B **222**, 211 (1983).

[11] T. Barnes, F.E. Close, and F. deViron, Nucl. Phys. B **224**, 241 (1983).

[12] F. Close and H. Lipkin, Phys. Lett. B **196**, 245 (1987).

[13] S. Taun *et al.*, Phys. Lett. B **213**, 537 (1988).

[14] M. Tanimoto, Phys. Rev D **27**, 2648 (1983).

[15] I. Aznauryan, Z.Phys. C **68**, 459 (1995).

[16] O. Dumbrajs *et al.*, Nucl. Phys. B **216**, 277 (1983).

[17] N. Isgur, Preprint JLAB-THY-99-09 (1999).

[18] A. Afanasev and Ph. Page, Preprint JLAB-THY-97-46.

[19] D. Alde *et al.*, Phys. Lett. B **205**, 397 (1988).

[20] H. Aoyagi *et al.*, Phys. Lett. B **314**, 246 (1993).

[21] M. Zielinski *et al.*, Phys. Rev. D **30**, 1855 (1984).

[22] S. Cihangir *et al.*, Phys. Lett. B **117**, 119 (1982).

[23] T. Ferbel *et al.*, Proc. of the XVI-th Recontre de Moriond on New Flavors and Hadron Spectroscopy, Les Arcs - Savois, 373 (1981).

[24] G.M. Beladidze *et al.*, Phys. Lett. B **313**, 276 (1993).

[25] D.R. Thompson *et al.*, Phys. Rev. Lett. **79**, 1630 (1997).

[26] M. Atkinson *et al.*, Z. Phys. C **34**, 157 (1987).

[27] G. Condo *et al.*, Phys. Rev. D **43**, 2787 (1991).

[28] M. Zielinski, Z. Phys. C **34**, 255 (1987).

[29] CELEG Event Generator, CLAS-Note 89-004, (1989).

[30] LEPTO version 6.1, The Lund Monte Carlo for Deep Inelastic Lepton-Nucleon Scattering, TSL/ISV-92-0065, 1992

[31] Review of Particle Properties, Phys. Rev. D **50**, 1174 (1994).

[32] I. Aznauryan, H. Funsten, and S. Stepanyan, JLab Experiment E94-118.

9 Forward Pseudoscalar Meson Electroproduction Above the Resonance Region

S.V. Boiarinov[a], D. Cords[b], A.P. Freyberger[b], F.J. Klein[b,†],
B.B. Niczyporuk[b,†], I. Strakovsky[c], and A. Yegneswaran[b]

[a]ITEP, Moscow, Russia, 117259
[b]Jefferson Laboratory, Newport News, VA 23606
[c]The George Washington University, Washington, DC 20052
(†Spokesperson)

9.1 Introduction

A principal motivation for studying exclusive reactions is that they provide a new class of observables, called off-diagonal parton distributions, for the internal structure of the nucleon. The internal structure of the nucleon has been studied through inclusive scattering of high-energy leptons in the deep inelastic scattering (DIS) limit. Polarized DIS measurements of $g_1(x, Q^2)$, or the relevant helicity densities $\Delta q(x, Q^2)$, have revealed that only about 30% of the nucleon's spin is carried by the quark's intrinsic spin. The quark helicity densities, $\Delta q(x, Q^2)$, are not only accessible through polarized DIS measurements, but also via exclusive electroproduction of pseudoscalar mesons. It has been shown that exclusive meson production at large Q^2 and small t factorizes into a hard scattering coefficient, a quark-antiquark distribution amplitude of the meson, and an off-diagonal quark (or gluon) distribution that describes the "soft" physics in the nucleon. Hence, the polarized parton densities can be probed in unpolarized exclusive reactions. It is clear that we should study exclusive reactions at low t, and at high Q^2 and W, in the region of validity of QCD factorization theorems, and also in the transition region where off-diagonal parton distributions provide important information about the non-perturbative structure of the nucleon. The comparison of the reactions $ep \to ep\pi^0$ and $ep \to en\pi^+$ is vital for better understanding of the soft part of a proton structure, since these reactions may proceed via different production mechanisms.

We propose to study exclusive electroproduction of π^+, π^0, and K^+ mesons at low t, for $Q^2 > 1.4$ (GeV/c)^2, and $W > 2.0$ GeV. In order to properly and fully carry out the physics program described in this proposal, we plan on acquiring data at several different beam energies between 4 and 6 GeV. Our W, Q^2, and t kinematical regions were chosen to obtain sufficient acceptance for at least four of these beam energies in order to extract the Q^2 and t dependence of the structure functions: σ_T, σ_L, σ_{TT}, and σ_{LT} in a model independent way.

As part of the overall proposal package we ask here *only* for the required beam time at 6 GeV. We assume that data at beam energies of 4.0, 4.5, and 5.0 GeV are going to be taken within the approved beam time of the current e1 program. In case no data are taken at a fifth beam energy of 5.5 GeV, we will require beam time for that energy in a future update of this proposal.

9.2 Physics Motivations

The structure of the nucleon revealed in hard processes is described by parton distributions. Traditionally, the internal structure of the nucleon has been studied (CERN, SLAC, DESY) through inclusive scattering of high-energy leptons in the DIS limit, *i.e.* at large Q^2, ν, and fixed Bjorken $x_B = Q^2/2m_p\nu$, where Q^2 and ν are the mass squared and energy of the virtual photon. For example, unpolarized DIS provided the first evidence that quarks carry only about 45% of the nucleon momentum via measurements of the structure function $F_1(x, Q^2)$, or the corresponding parton densities $q(x, Q^2)$. Recent measurements have focused on the leading-twist structure function $g_1(x, Q^2)$, which is roughly proportional to the inclusive spin asymmetry on a longitudinally polarized target. Polarized DIS measurements of $g_1(x, Q^2)$, or the relevant helicity densities $\Delta q(x, Q^2)$, have revealed that only about 30% of the nucleon's spin is carried by the quark's intrinsic spin [1].

Processes where at least one hadron is detected in the final state offer several distinct advantages over inclusive processes alone [2]. Particularly interesting is the chirally odd structure function $h_1(x, Q^2)$, or the appropriate transversity densities $\delta q(x, Q^2)$ [3, 4]. Together with $F_1(x, Q^2)$ and $g_1(x, Q^2)$, $h_1(x, Q^2)$ is necessary for a complete description of the quark structure of the nucleon in high-energy processes. The structure function $h_1(x, Q^2)$ has never been measured. Chirally odd quark distributions are difficult to measure because they are suppressed in totally inclusive deep inelastic scattering. However, the asymmetry for semi-inclusive leptoproduction of pions from a transversely polarized target contains a contribution from $h_1(x, Q^2)$ that is enhanced at low x. Another motivation for the measurement of $h_1(x, Q^2)$ is a sensitivity to the role of relativistic effects in the nucleon state, and a possible sensitivity [2] to gluon contributions to the spin of the proton.

Exclusive electroproduction of mesons from nucleons has become a field of growing interest [5, 6, 7] since a full factorization theorem has been proven [8, 9, 10]. It has been shown that exclusive meson production at large Q^2 and small t factorizes into a hard scattering coefficient, a quark-antiquark distribution amplitude of the meson, and an off-diagonal quark (or gluon) distribution that describes the "soft" physics in the nucleon. The proof of factorization applies when the virtual photon is longitudinally polarized. It has been also shown [8] that transverse polarization of the photon implies a power suppression in Q relative to the case of longitudinal polarization. The theorem applies to the production of mesons at all x_B. Therefore, off-diagonal (also called off-forward [9] or non-forward [10]) parton distributions allow the description of certain exclusive reactions in the framework of QCD.

For longitudinally polarized vector mesons, the relevant parton densities are the unpolarized ones, $q(x, Q^2)$. For transversely polarized vector mesons, the parton densities are the quark transversity densities, $\delta q(x, Q^2)$. The original hope [8] that $h_1(x, Q^2)$ may be measured via production of transverse vector mesons has, unfortunately, not come true because in hard scattering processes, such a transition is forbidden [11, 12]. For the pseudoscalar mesons, the relevant parton densities are the quark helicity densities, $\Delta q(x, Q^2)$, which are not suppressed at large x_B. Hence, the polarized parton densities can be probed in unpolarized collisions.

It is clear that the study of exclusive and semi-inclusive reactions provides a probe of nucleon structure complementary to purely inclusive studies. In particular, we should study exclusive reactions at low t, and at high Q^2 and W, in the region of validity of QCD factorization theorems, and also in the transition region where standard partonic models may no longer be valid. One can then probe the soft part of a proton in a novel way, and elucidate the transition between soft and hard scattering processes.

A measurement of the differential cross section $\sigma(t, W, Q^2)$ for the reactions $ep \to e' + \pi^+(K^+) + n(\Lambda)$ at beam energies of 4.0, 4.5, 5.0, 5.5, and 6.0 GeV has been proposed and discussed at two JLab workshops [13]. In this proposal, data will be collected simultaneously for π^+, π^0 and K^+ exclusive electroproduction using the CLAS detector at JLAB in the following kinematical region: $Q^2 > 1.4$ (GeV/c)^2 and $W > 2.0$ GeV. The reaction mechanism, which involves off-diagonal parton distributions, is sketched in Fig. 62.

In the following sections, existing data, detailed simulations, and reconstruction and analysis of meson electroproduction will be discussed.

9.3 Cross Section

The procedure of extracting a virtual photon cross section $\sigma_{\gamma_v p}$ from the observed electroproduction cross section is based on the one-photon approximation. In this procedure, electrons are regarded as providing a beam of virtual photons (flux Γ) of known polarization ϵ, mass squared Q^2, and energy ν. Electroproduction reactions can be described in terms of form factors that are generalizations of the form factors observed in elastic electron-proton scattering, or in terms of cross sections that are extensions of the photoproduction cross sections. The most general form of the differential cross section σ for the reactions

$$ep \to e' + \pi^+(K^+) + n(\Lambda), \quad ep \to e' + \pi^0 + p, \tag{26}$$

can be written in terms of four structure functions (unpolarized data) [14]:

$$\sigma_{\gamma_v p}(W^2, Q^2, t, \phi) \; = \; \sigma_T + \epsilon\sigma_L + \epsilon\sigma_{TT}\cos 2\phi + \sqrt{\epsilon(\epsilon+1)/2}\cdot\sigma_{LT}\cos\phi, \tag{27}$$

where σ_T, σ_L, σ_{TT}, and σ_{LT} are functions of the variables: Q^2, $W^2 = 2m_p\nu - Q^2 + m_p^2$, and $t \equiv (p_{\gamma_v} - p_{\pi,K})^2 - t_{min}$ (or θ^*, the angle between the virtual photon and the meson in the hadronic center-of-mass (CM) W). The dependence on the azimuthal angle ϕ (angle of the meson relative to the electron-scattering plane: $\phi \equiv \phi^*$) is shown explicitly in eq(27).

The term σ_T represents the cross section for transverse photons, σ_L represents the cross section for longitudinal photons, σ_{TT} is the interference between the transverse amplitudes, and σ_{LT} is the interference between transverse and longitudinal amplitudes. The terms σ_{TT} and σ_{LT} approach zero as $t \to 0$, and the terms σ_L and σ_{LT} vanish as $Q^2 \to 0$. In eq(27), the structure functions σ_T and σ_{TT} can be further decomposed into two parts: $\sigma_\perp$ corresponds to incident photons polarized perpendicular to the hadronic plane, and $\sigma_\parallel$ corresponds to photons polarized parallel to the hadronic plane: $\sigma_T = (\sigma_\parallel + \sigma_\perp)/2$, $\sigma_{TT} = (\sigma_\parallel - \sigma_\perp)/2$, and $\sigma_{LT} = 2Re(A_L A_\parallel^*)$.

In eq(27) we took explicitly into account the helicities of the virtual photon and ignored the helicities of the ingoing and outgoing nucleon [14]. By taking into account the nucleon spin, we can write: $\sigma_\parallel = |A_\parallel^N|^2 + |A_\parallel^F|^2$, $\sigma_\perp = |A_\perp^N|^2 + |A_\perp^F|^2$, $\sigma_L = |A_L^N|^2 + |A_L^F|^2$, and $\sigma_{LT} = 2Re(A_L^N A_\parallel^{N*} + A_L^F A_\parallel^{F*})$, where N and F refer to nucleon flip and non-flip amplitudes, respectively. In the t channel, the contributions to $A_\perp^{N,F}$ come only from natural parity exchange, and contributions to $A_\parallel^{N,F}$ and $A_L^{N,F}$ come only from unnatural parity exchange. Using a transversely polarized target one obtains six more structure functions that are the imaginary parts of products of non-flip and flip amplitudes $Im(A_i^N A_j^{F*})$.

The “inverse” reaction to $\gamma p \to \pi^+ n$ is the $\pi^+ n \to \rho^0 p$. Good quality data [15] exist only for the reaction $\pi^- p \to \rho^0 n$ at 17.2 GeV. The measured differential cross section, for the above reaction, as a function of $\sqrt{t}$ shows a behavior one would expect for one-pion exchange mechanism (spin-flip amplitude) which vanishes at $t = 0$. The most interesting observation for the $\pi^- p \to \rho^0 n$ reaction is the presence of strong polarization effects [16], *i.e.* a large left-right polarized target asymmetry (presence of non-flip amplitudes) in the low t region. A sizable asymmetry was also observed [17] in π^+ photoproduction from a polarized target at 5 and 16 GeV. A typical value of the asymmetry is about -0.5 in both experiments. This is very surprising since, according to general belief, this region should be dominated by one-pion exchange and should, therefore, show little or no polarization effects.

Determination of the pion form factor from electroproduction data requires the extraction of that part of the cross section which contains the spin-flip amplitudes, *i.e.* $|A_{\parallel}^F|^2$ and $|A_L^F|^2$.

9.4 Simulation

We have used the SDA Package [18] to simulate the $ep \to e'\pi^+(K^+)n(\Lambda)$ and $ep \to e'\pi^0 p$ reactions, and to reconstruct the events accepted in the CLAS detector. In order to estimate rates we have used the following form for the differential cross sections [20]:

$$\frac{d^2\sigma}{dQ^2 dW} = \frac{\alpha W \sqrt{(W^2 + Q^2 - m_p^2)^2 + 4m_p^2 Q^2}}{\pi(1-\epsilon)(s - m_p^2)^2 Q^2} \cdot \frac{d\sigma_{\gamma_v p}(W, Q^2, \theta^*, \phi^*)}{d\Omega_{\pi,K}}, \tag{28}$$

where the first term is a flux Γ of virtual photons, the second term, $\sigma_{\gamma_v p}$, represents the four structure functions as shown by eq(27), and s is the center-of-mass energy squared $s = m_p^2 + 2m_p E_{beam}$. In our simulation we have used the measured cross section $\sigma_{\gamma_v p}$ at $Q^2 < 1$ (GeV/c)^2 [21], and extrapolated to higher Q^2 values with a simple pole form: $\sim (1 + Q^2/0.462)^{-2}$.

A sample of 1.6 M events was generated in the Q^2 range from 1.2 to 3.2 (GeV/c)^2 and in W range from 2.05 to 2.15 GeV for 5 beam energies: 4.0, 4.5, 5.0, 5.5, and 6.0 GeV. Realistic trajectories of charged particles traversing the CLAS magnetic field were simulated, including multiple scattering and the drift cell spatial resolution of 250 μm. For the purpose of the present study, both the scattered electron and the meson had to be detectable in the trigger scintillation counters and in all layers of the drift chambers in a given sector. Additionally, we required that the outgoing electron was within the acceptance of the Ĉerenkov and Shower Counters. These requirements provide optimal trajectory reconstruction for both charged particles, and also a good missing-mass resolution.

Hereafter, we refer to the number of generated events weighted by the cross section (see eq(28)) at a given luminosity as the number of produced events, N_{prod}. A fraction of the N_{prod} events that would have been accepted by the geometry of the CLAS detector is not observed because of reconstruction inefficiencies and various other losses like: decaying pions (kaons), secondary interactions, radiative corrections, missing-mass cuts, etc. These losses depend on the event kinematics and can be corrected for on an event-by-event basis [19]. In the present study, to account for these losses, we have introduced a constant global weight factor $w_g = N_{acc}/N_{obs} = 1.4$.

During the reconstruction process we assumed that opposite sectors of the CLAS detector were not perfectly aligned, but were rotated relative to each other randomly by an angle of 1 mrad. We also have assumed that each nominal beam energy is randomly off by 0.1%.

The W, Q^2, and t regions were chosen to obtain sufficient acceptance for at least 4 of the beam energies.

Rates. In Table 14, using eq(28), we show the expected rates of produced (N_{prod}) and fully reconstructed events (N_{obs}) at each beam energy per 100 hours of running with the CLAS detector at a luminosity $L = 1 \times 10^{34}$ cm^{-2}s^{-1}, for $\Delta W = 2.05 - 2.15$ GeV and $\Delta\Omega_\pi = 2\pi \int sin\theta^*_\pi d\theta^*_\pi = 0.377$ sr ($\theta^*_\pi < 20°$). The expected rates for neutral pion electroproduction are roughly the same, and for K^+ electroproduction are smaller approximately by a factor of 10. The analysis of the CLAS data taken at a beam energy of 4 GeV shows that the rates for semi-inclusive electroproduction of charged pions are approximately larger by a factor of 15.

9.5 Particle Identification

To identify scattered electrons we first determine the clusters in the Shower Counter. Negative tracks (potential electrons) that match these clusters are selected. These tracks are then checked to determine whether the deposited energy in the cluster agrees with the track momentum. For our kinematical conditions, outgoing mesons have momenta ranging from 2.0 to 3.5 GeV/c, and the outgoing charged mesons are identified using a missing-mass technique. Our preliminary analysis of 4 GeV CLAS data indicate that the background under the missing-mass peak of the neutron is only about a few percent. The momenta of recoil protons for π^0 electroproduction are less than 0.8 GeV/c, and therefore will be identified via Time-of-Flight technique.

9.6 Analysis of Reconstructed Events

From the reconstructed (observed) events N_{obs}, we extract the Q^2 and t (or θ^*) dependence of the structure functions: σ_T, σ_L, σ_{TT} and σ_{LT} in a model independent way. The procedure consists of fitting the form of the differential cross section in eq(28) to the measured cross sections in a given kinematical bin $\Delta Q^2 \Delta W \Delta t$. The structure functions $\sigma_T + \epsilon\sigma_L$, σ_{TT}, and σ_{LT}, can be isolated experimentally using the ϕ dependence of the cross section at a given beam energy. A separation of σ_T and σ_L requires data collected at different beam energies.

The measured cross section $(\partial\sigma_{\gamma_v p}/\partial\vec{k})_m$ has been obtained from $N_{obs} \pm \sqrt{N_{obs}}$ in each bin $\Delta\vec{k} = \Delta Q^2 \Delta W \Delta\theta^* \Delta\phi^*$ in the following way:

$$\left(\frac{\partial\sigma_{\gamma_v p}}{\partial\vec{k}}\right)_m = \frac{N_{obs}(\Delta\vec{k}) \cdot w_g(E_b)_m}{A(\Delta\vec{k}, E_b) \cdot L_m(E_b) \cdot F_m(\Delta W, \Delta Q^2, E_b) \cdot \Delta\vec{k}_m}. \tag{29}$$

The average acceptance $A_m(\Delta\vec{k}, E_b)$ in each bin $\Delta\vec{k}$ and at each beam energy has been determined by generating at random 400 events/bin. These events were transformed into the lab system with a random rotation of the electron-scattering plane around the beam direction, and were checked to determine if the outgoing electron and meson both lie within the geometry of the CLAS detector [19]. In Table 15, as an example, we show the acceptance as a function of the CM angles (θ^*_π,ϕ^*_π) for $\Delta W = (2.05 - 2.15)$ GeV, $\Delta Q^2 = (2.0 - 2.2)$ (GeV/c)^2 and $E_{beam} = 4.5$ GeV. The measured flux $F_m(\Delta W, \Delta Q^2, E_b)$, in eq(29), was obtained by averaging over all events observed in each bin of $\Delta W \Delta Q^2$, and for given beam energy. In

Fig. 63 we show, as an example, the derived differential cross sections as a function of ϕ^* and E_{beam} for one bin k of size $\Delta W \Delta Q^2 \Delta t$.

To extract the four structure functions from the measured cross sections in a bin k, as shown in Fig. 63, we used the following functional form in the χ^2 minimization procedure:

$$f(\phi^*)_k = \sum_i \left(P_1 + P_2 \cdot \epsilon_i + P_3 \cdot \epsilon_i \cdot cos2\phi^* + P_4 \cdot \sqrt{\epsilon_i(\epsilon_i+1)/2} \cdot cos\phi^* \right), \qquad (30)$$

where the index i runs over the different beam energies.

The four parameters (P_1, P_2, P_3, and P_4) are determined from the fit. The virtual photon polarization ϵ_i was evaluated at the center of the ΔW and ΔQ^2 bins. Data with $A(\Delta\vec{k}, E_b) <$ 2% were excluded from the fit, see Table 14. The Q^2 dependence of the four structure functions and their statistical errors, derived from the fits, are summarized in Fig. 64 for pions, and in Fig. 65 for kaons (see full circles with error bars). The dashed or solid curves in Figs. 64 and 65 represent the input to the Monte Carlo simulation. The full squares (σ_L) and full stars (σ_T) in Fig. 64 represent the currently available data [22] for pions. The full stars ($\sigma_L + \epsilon\sigma_T$) in Fig. 65 represent available data [23] for kaons. The fitting procedure also includes the expected systematic errors in determining the luminosity $L_m(E_b)$ of $\leq 2\%$ and a global correction $w_g(E_b)_m$ of $\leq 2\%$; *i.e.* uncorrelated systematic errors at each beam energy setting. In addition to the above, we introduced a correlated systematic error (common to all beam energies) of about 3%. The successful σ_L and σ_T separation was possible, in the above kinematical regions, once sufficient data were collected for at least 4 of the 5 beam energies.

9.7 Summary

A challenging problem in particle physics is to understand the transition from the "current" quarks and gluons appearing in the QCD Lagrangian to the degrees of freedom of low-energy QCD. One could take the approach that anything that can be calculated by pQCD can be called a hard process. All the rest would be soft. Soft interactions are usually understood as the interactions of hadrons at a relatively small scale (low Q^2 in *ep* interactions or low p_T in hadron-hadron interactions). The problem, however, is that what we calculate and what we measure are not the same. Soft interactions are not easily disentangled from hard ones.

That said, let us summarize here what we can measure in a model independent way.

Stage 1. Analyze the existing e1 data taken at beam energies 4 GeV and 4.5 GeV. (At present, only 20% of our required 4 GeV data and only 40% of our required 4.5 GeV data have been acquired.) Extract the Q^2 and t dependences of the structure functions: $\sigma_T + \epsilon\sigma_L$, σ_{TT}, and σ_{LT}, and identify remaining issues.

Stage 2. Take remaining data at beam energies 4.0 and 4.5 GeV, and new data at 5.0 GeV within the approved beam time of the current e1 program. Extract the Q^2 and t dependences of the structure functions: $\sigma_T + \epsilon\sigma_L$, σ_{TT}, and σ_{LT}.

Stage 3. Take new data at a beam energy 6.0 GeV (from this proposal package) and try to disentangle all structure functions: σ_T, σ_L, σ_{TT}, and σ_{LT}.

Stage 4. In case no data at our fifth beam energy of 5.5 GeV are acquired, we will require beam time at 5.5 GeV in a future update of this proposal.

To complete our experiment we need at least 10 days of beam time at each energy setting assuming a luminosity of 5×10^{33} cm^{-2}s^{-1} and using CLAS in a standard configuration (normal field: $B/B_0 = +87\%$).

Since the charged particles (electrons and mesons) are detected mainly at low polar angles, it is of great importance that the CLAS detector is fully operational in the forward direction. It is also very important that data at different beam energies are collected with the identical running conditions: *i.e.* beam current, beam position, target, magnetic field settings, trigger logic, and threshold settings.

We want to emphasize that it is crucial to acquire data at beam energies of 4.0 and 4.5 GeV as well as 5.5 and 6.0 GeV, as these mark the energy endpoints for a large fraction of the W, Q^2 bins. Otherwise the structure functions cannot be accurately determined over the proposed kinematical range due to acceptance problems.

9.8 Conclusions

We have shown that using the CLAS spectrometer at JLAB, and with beam energies between 4 and 6 GeV, we can obtain good quality electroproduction data that will improve our understanding of the nucleon structure as well as the hadronic properties of the photon. We emphasize the importance of studying both the Q^2 and t dependencies of the various structure functions for π^+, π^0 and K^+ exclusive electroproduction. The comparison of $ep \to ep\pi^0$ and $ep \to en\pi^+$ reactions is vital for better understanding of the soft part of a proton structure since these reactions may proceed via different production mechanisms.

In the future we wish to measure asymmetries for exclusive and semi-inclusive meson electroproduction on a transversely polarized target. Technically, it is a challenging task to operate CLAS with the strong transverse magnetic field of a polarized target.

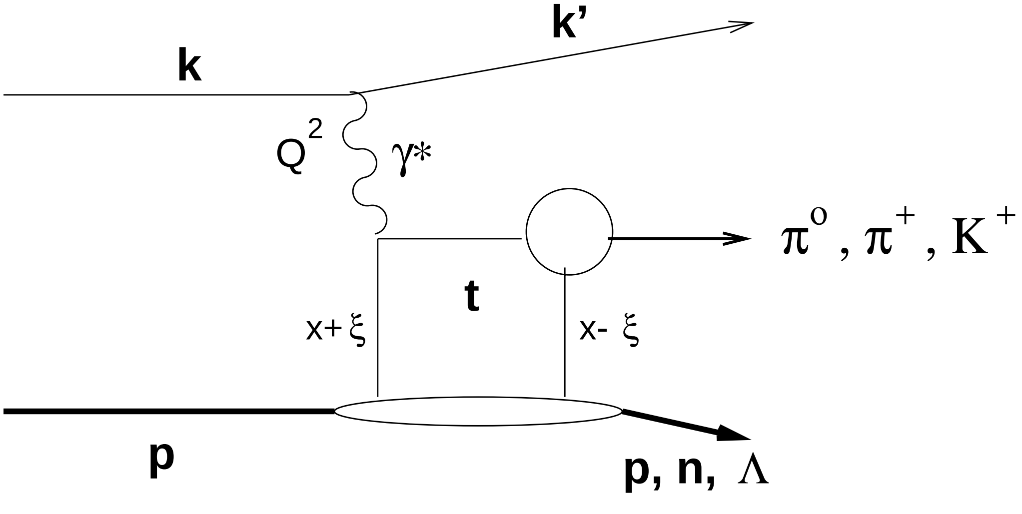

Figure 62: The diagram for the electroproduction of pseudoscalar mesons with quark exchange mechanism at $Q^2 = -q^2 = -(k-k')^2$ and at small momentum transfer $t = (p-p')^2$. The exchanged quarks carry the momentum fractions $x+\xi$ and $x-\xi$, where ξ is fixed to be $\xi = (p-p')\cdot q/2m_p\nu$ by kinematics, where p and p' are the four vectors of the incoming and outgoing baryons respectively.

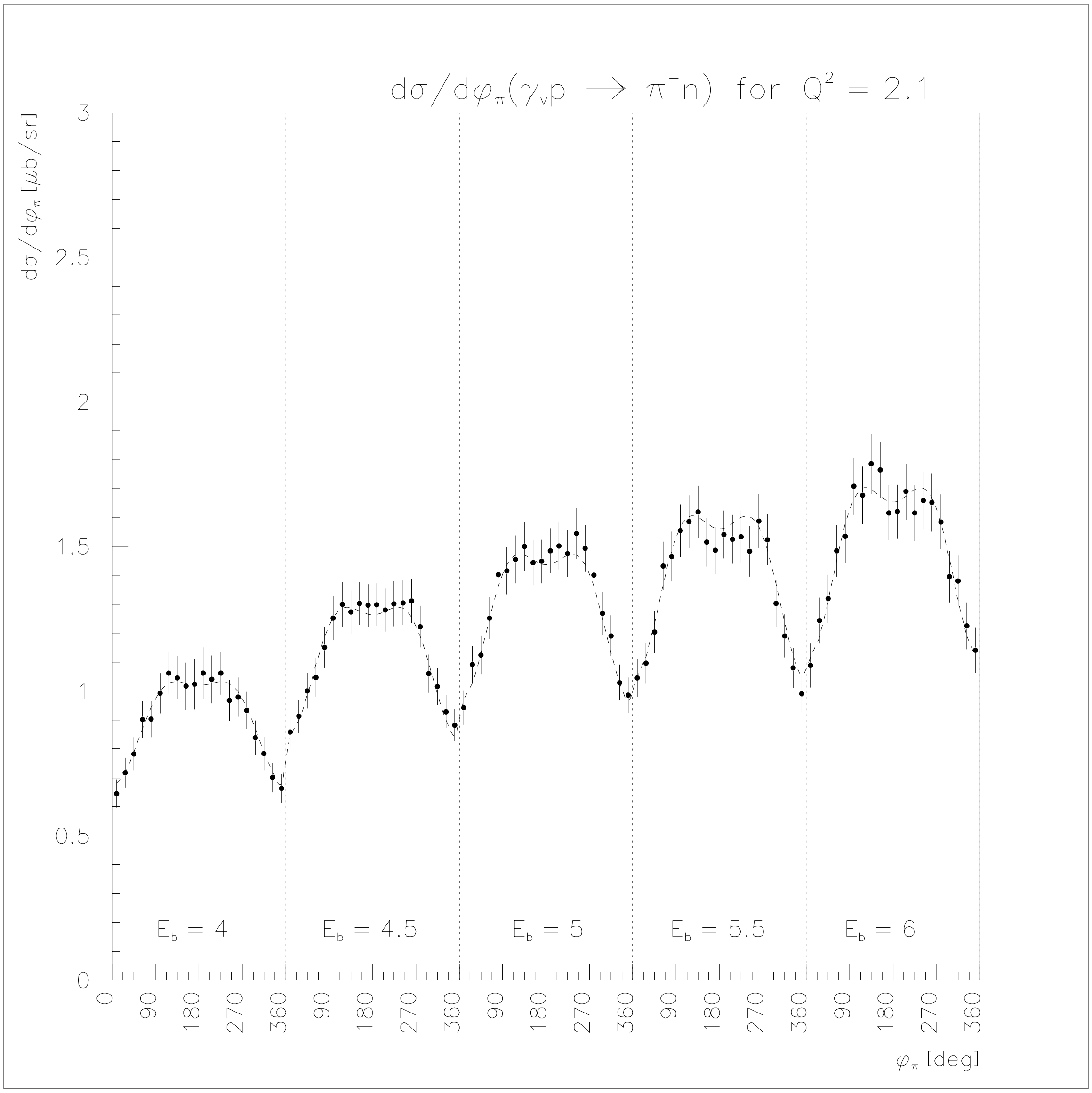

Figure 63: An example of the derived differential cross section as a function of ϕ^* and E_{beam} for $Q^2 = 2.1$ (GeV/c)^2.

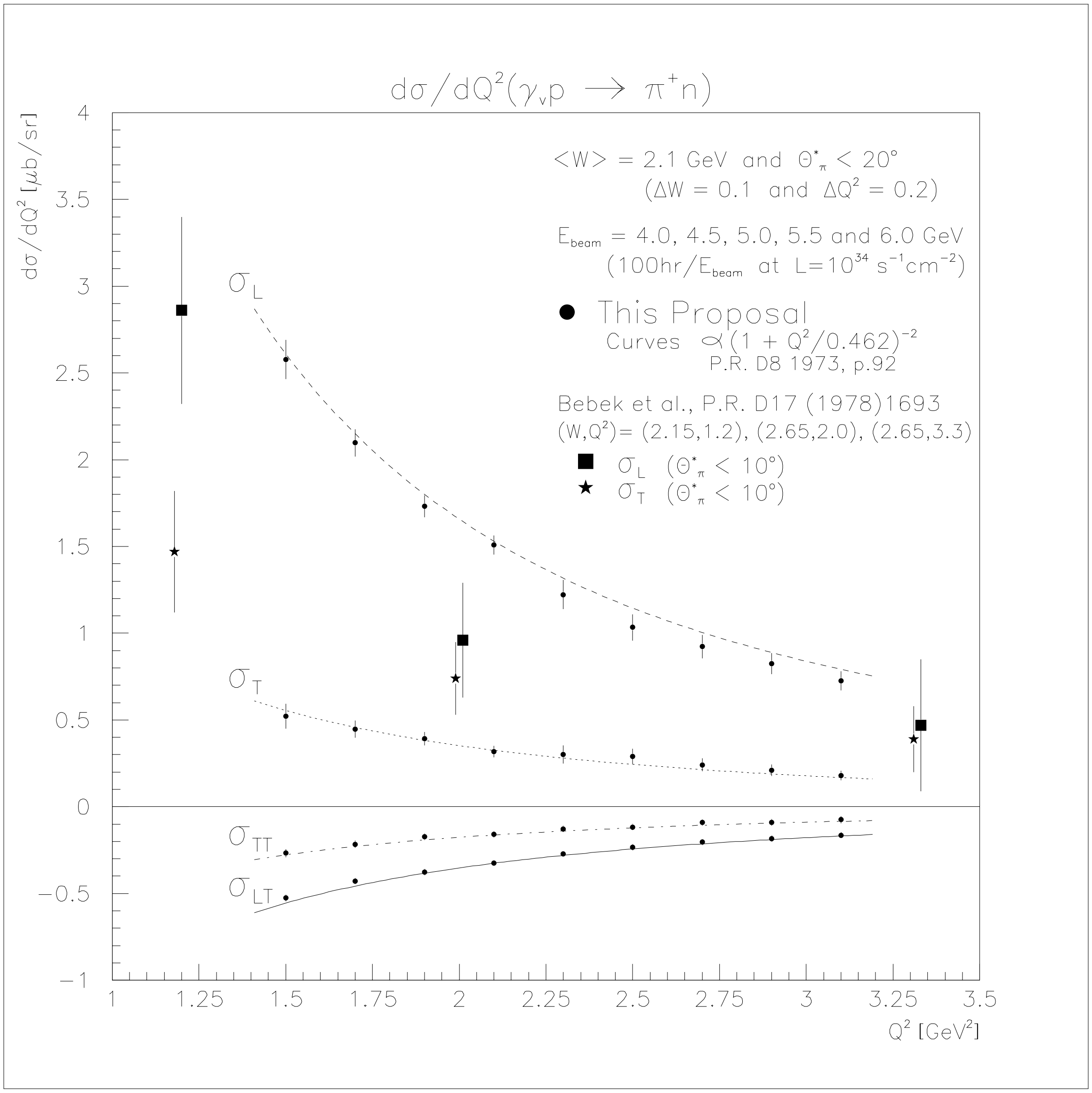

Figure 64: The Q^2 dependence of the four structure functions and their statistical errors, derived from fits, for pions. Existing data [22]: σ_L (boxes) and σ_T (stars).

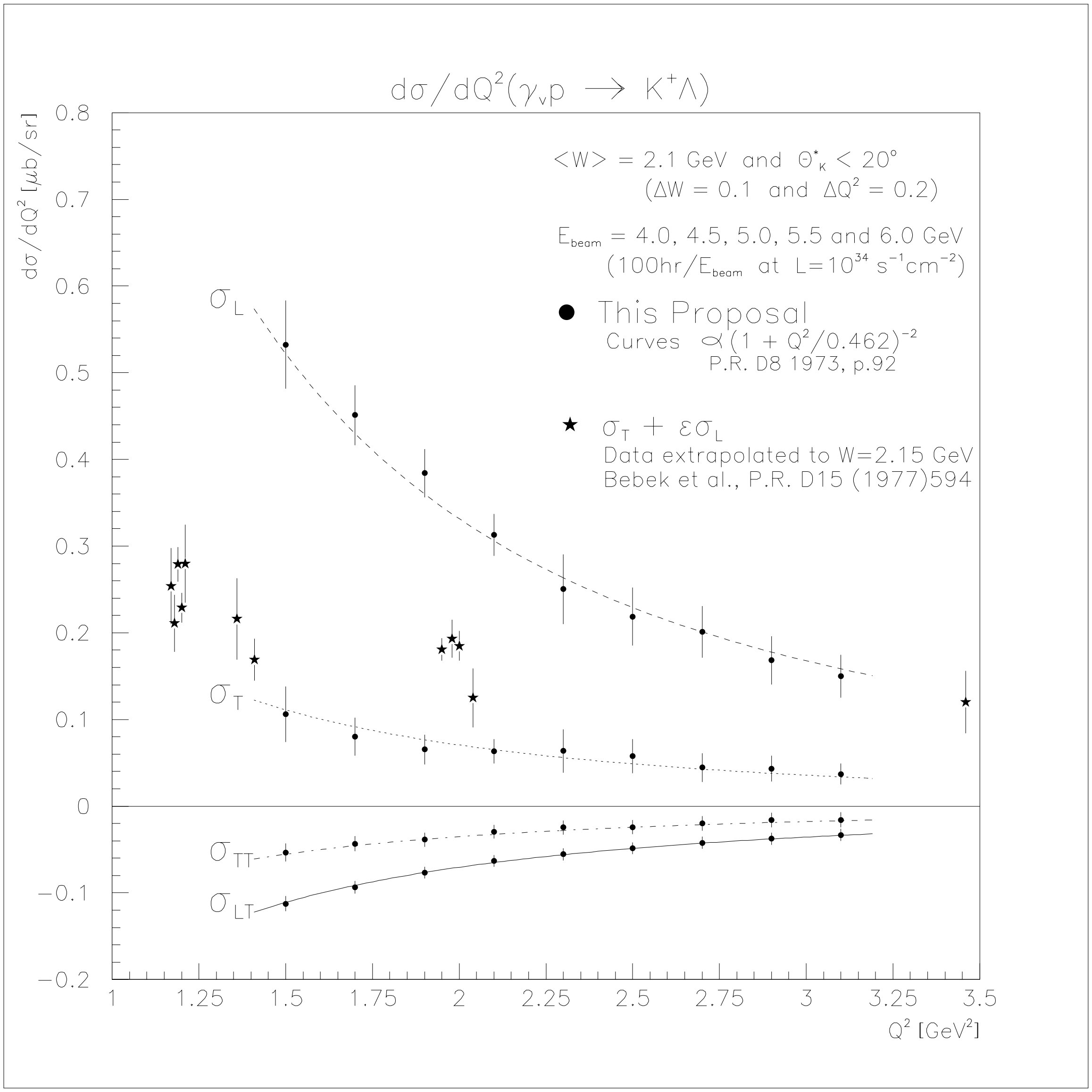

Figure 65: The Q^2 dependence of the four structure functions and their statistical errors, derived from fits, for kaons. Existing data [23]: $\sigma_L + \epsilon\sigma_T$ (stars).

	$E_b = 4.0$	$E_b = 4.5$	$E_b = 5.0$	$E_b = 5.5$	$E_b = 6.0$
ΔQ^2	N_{prod}	N_{prod}	N_{prod}	N_{prod}	N_{prod}
$(\mathrm{GeV/c})^2$	N_{obs}	N_{obs}	N_{obs}	N_{obs}	N_{obs}
1.4 - 1.6	36349	43455	49217	53913	
	13226	13547	11511	6677	
1.6 - 1.8	23494	28537	32698	36107	38980
	8946	10395	10073	8091	5059
1.8 - 2.0	15564	19372	22451	25049	27130
	5968	7566	7755	7283	5957
2.0 - 2.2	10527	13480	15805	17756	19441
	3918	5440	5999	5975	5343
2.2 - 2.4	7262	9545	11399	12926	14175
	2552	3987	4533	4692	4511
2.4 - 2.6		6881	8325	9571	10511
		2855	3494	3738	3678
2.6 - 2.8		5011	6196	7182	8012
		2017	2645	2942	3016
2.8 - 3.0		3682	4670	5472	6144
		1419	1994	2311	2457
3.0 - 3.2		2734	3541	4219	4779
		974	1487	1792	1960

Table 14: Expected rates of produced (N_{prod}/100hr) and reconstructed (N_{obs}/100hr) π^+ mesons using the CLAS detector at a luminosity of 1×10^{34} cm^{-2}s^{-1} for $\Delta W = (2.05 - 2.15)$ GeV and $\Delta\Omega_\pi = 0.377$ sr ($\theta^*_\pi < 20°$).

$\Delta\phi^*_\pi$ [°]	$\Delta\theta^*_\pi$ [°] 0 - 5	$\Delta\theta^*_\pi$ [°] 5 - 10	$\Delta\theta^*_\pi$ [°] 10 - 15	$\Delta\theta^*_\pi$ [°] 15 - 20
0 - 18	0.72	0.70	0.67	0.68
18 - 36	0.67	0.69	0.64	0.63
36 - 54	0.68	0.66	0.57	0.51
54 - 72	0.64	0.54	0.53	0.48
72 - 90	0.64	0.59	0.48	0.45
90 - 108	0.64	0.55	0.45	0.39
108 - 126	0.68	0.52	0.43	0.39
125 - 144	0.70	0.58	0.46	0.41
144 - 162	0.64	0.60	0.52	0.44
162 - 180	0.63	0.66	0.60	0.42
180 - 198	0.67	0.61	0.57	0.41
198 - 216	0.66	0.60	0.56	0.41
216 - 234	0.64	0.55	0.44	0.34
234 - 252	0.64	0.55	0.49	0.36
252 - 270	0.63	0.52	0.50	0.45
270 - 288	0.67	0.59	0.52	0.43
288 - 306	0.67	0.61	0.54	0.46
306 - 324	0.69	0.63	0.53	0.56
324 - 342	0.73	0.69	0.66	0.59
342 - 360	0.68	0.71	0.66	0.70

Table 15: An example of the acceptance as a function of the CM angles (θ^*_π,ϕ^*_π) for $\Delta W = (2.05 - 2.15)$ GeV, $\Delta Q^2 = (2.0 - 2.2)$ (GeV/c)^2 and $E_{beam} = 4.5$ GeV.

References

[1] S.D. Bass, TUM/T39-99-03, Preprint hep-ph/9902280, (1999).

[2] J.M. Niczyporuk and E.E.W. Bruins, Phys. Rev. D **58**, 91501 (1998).
J.M. Niczyporuk, S.B. thesis, MIT, 1977, and references therein (available at http://www-hermes.desy.de/∼dilys/pub/97-LIB/nicz.97.018.ps.gz).

[3] R.L. Jaffe and X. Ji, Phys. Rev. Lett. **71**, 2547 (1993).

[4] Xiangdong Ji, Phys. Rev. D **49**, 114 (1994).

[5] M. Vanderhaeghen, M. Guidal, and J.M. Laget, Phys. Rev. C **57**, 1454 (1998).

[6] L. Mankiewicz, G. Piller, and A. Radyushkin, TUM/T39-98-33, Preprint hep-ph/9812467, (1998).

[7] S.J. Brodsky, M. Diehl, P. Hoyer, and S. Peigne, SLAC-PUB-8015, Preprint hep-ph/98122277, (1998).

[8] J.C. Collins, L. Frankfurt, and M. Strikman, Phys. Rev. D **56**, 2982 (1997).

[9] X. Ji, Phys. Rev. Lett. **78**, 610 (1997); Phys. Rev. D **55**,7114 (1997).

[10] A.V. Radyushkin, Phys. Rev. D **56**, 5524 (1997).

[11] P. Hoodbhoy and X. Ji, Phys. Rev. D **58**, 054006 (1998).

[12] M. Diehl, T. Gousset, and B. Pire, Phys. Rev. D **59**, 034023 (1998).

[13] B.B. Niczyporuk, JLAB-PHY-99-05, Preprint hep-ph/9904506, (1999); B.B. Niczyporuk at "Workshop on CEBAF at Higher Energies", CEBAF, Newport News, April 14-16, 1994.

[14] A. Bartl and W. Majerotto, Nucl. Phys. B **62**, 267 (1973).

[15] G. Grayer, B. Hyams *et al.*, Nucl. Phys. B **75**, 189 (1974).

[16] H. Becker, G. Blanar *et al.*, Nucl. Phys. B **151**, 46 (1979).

[17] C.C. Morehouse, M. Borghini *et al.*, Phys. Rev. Lett. **25**, 835 (1970).

[18] B.B. Niczyporuk, "Standard Data Analysis (SDA) Package" (unpublished), CEBAF-PR-91-004 (1991).

[19] B.B. Niczyporuk, CEBAF-PR-89-040 (1989).

[20] R.G. Roberts, "The Structure of the Proton", Cambridge University Press, 1990.

[21] C.N. Brown, C.R. Canizares *et al.*, Phys. Rev. D **8**, 92 (1973).

[22] C.J. Bebek, C.N Brown *et al.*, Phys. Rev. D **17**, 1693 (1978).

[23] C.J. Bebek, C.N Brown *et al.*, Phys. Rev. D **15**, 594 (1977).